

Electronic Thesis and Dissertation Repository

---

1-22-2015 12:00 AM

## Investigating the Binding of Peptidyl-Prolyl Isomerase Pin1 to a Multi-Site Phosphorylated Substrate Modeled After Phosphatase CDC25C

Michelle K. Dubinsky  
*The University of Western Ontario*

Supervisor  
Dr. David Litchfield  
*The University of Western Ontario*

Graduate Program in Biochemistry  
A thesis submitted in partial fulfillment of the requirements for the degree in Master of Science  
© Michelle K. Dubinsky 2015

Follow this and additional works at: <https://ir.lib.uwo.ca/etd>

---

### Recommended Citation

Dubinsky, Michelle K., "Investigating the Binding of Peptidyl-Prolyl Isomerase Pin1 to a Multi-Site Phosphorylated Substrate Modeled After Phosphatase CDC25C" (2015). *Electronic Thesis and Dissertation Repository*. 2660.  
<https://ir.lib.uwo.ca/etd/2660>

This Dissertation/Thesis is brought to you for free and open access by Scholarship@Western. It has been accepted for inclusion in Electronic Thesis and Dissertation Repository by an authorized administrator of Scholarship@Western. For more information, please contact [wlsadmin@uwo.ca](mailto:wlsadmin@uwo.ca).

INVESTIGATING THE BINDING OF PEPTIDYL-PROLYL ISOMERASE PIN1 TO A  
MULTI-SITE PHOSPHORYLATED SUBSTRATE MODELED AFTER PHOSPHATASE  
CDC25C

(Thesis format: Monograph)

by

Michelle K. Dubinsky

Graduate Program in Biochemistry

A thesis submitted in partial fulfillment  
of the requirements for the degree of  
Master of Science

The School of Graduate and Postdoctoral Studies  
The University of Western Ontario  
London, Ontario, Canada

© Michelle K. Dubinsky, 2015

## Abstract

Pin1 is a human protein classified as a peptidyl-prolyl *cis/trans* isomerase. The protein regulates the conformation of phosphorylated protein substrates by rotating the peptide bond between phosphorylated serine/threonine residues that precede proline residues. Structurally, Pin1 consists of an N-terminal WW domain and a C-terminal PPIase domain. The PPIase domain catalyzes *cis/trans* isomerization of peptide bonds in substrate proteins that contain the aforementioned consensus motif. We hypothesize that Pin1 binding is positively impacted when two phospho-acceptor sites on peptides derived from mitotic phosphatase CDC25C, a known Pin1-interacting protein, are phosphorylated. Using nuclear magnetic resonance and fluorescence polarization, binding affinities of CDC25C peptides to Pin1 were calculated. The results indicate that doubly-phosphorylated peptides bound to Pin1 have lower dissociation constants and consequently greater binding affinities, than complexes containing non- or singly-phosphorylated peptides, at the equivalent residues. This suggests that Pin1 has two independent phospho-binding sites that when bound, increase substrate binding affinity.

## Keywords

Pin1, protein, peptidyl-prolyl isomerase, isomerization, peptide, binding, CDC25C, phosphorylated serine/threonine-proline, NMR, fluorescence polarization

## Co-Authorship Statement

Dr. Brian Shilton provided the Arg14Ala and Arg14Ala Cys113Asp Pin1 plasmids used in this thesis.

Dr. Melanie Bailey provided the GST-Pin1 plasmids used in this thesis.

Kristina Jurcic of the Department of Biochemistry and Jasmine Wang of the Department of Chemistry performed MALDI Mass Spectrometry.

## Acknowledgments

Thank you very much to my supervisor Dr. David Litchfield and my committee members Dr. Brian Shilton and Dr. Chris Brandl for all of the assistance and support throughout my time at Western. Your guidance through experimental interpretations and suggestions helped me learn and grow as a scientist.

Thank you to the Litchfield lab members and all of the Pin1 group members for feedback and ideas. The foundations for this work were laid by Dana Onica and my Pin1 studies would not have been the same without Brendan Innes and Dominic Leblanc. I would especially like to thank Rachel Mah for her tireless protein purifications, Michelle Gabriel for helpful suggestions and Stephanie Zukowski for being such a wonderful editor.

Thank you so much to Andrew Maciejewski, and the Choy lab for being so patient with an NMR newbie. In addition, I would like to thank Liliana Santamaria-Kisiel and the Shaw Lab for training and use of the NMR facility, Kristina Jurcic and Jasmine Wang for running my samples on the MALDI and the Li lab members Rakesh Joshi and Courtney Voss for help with FP. A huge thank you goes out to Lee-Ann Briere in the BICF for being so patient and teaching me about every instrument in the facility.

Last, but certainly not least, I would like to thank my family and friends for constant encouragement. Thank you all for listening to my science rants and being so understanding about my common evenings and weekends in the lab. To Adam, thank you for your support and superior formatting skills.

# Table of Contents

|   |      |
|---|------|
| Abstract.....   | ii   |
| Co-Authorship Statement.....                                      | iii  |
| Acknowledgments.....  | iv   |
| Table of Contents.....  | v    |
| List of Tables.....   | viii |
| List of Figures.....  | ix   |
| List of Appendices.....   | x    |
| List of Abbreviations.....  | xi   |
| 1. Introduction.....  | 1    |
| 1.1 Peptidyl-prolyl isomerases.....                               | 2    |
| 1.2 Introduction to Pin1.....                                     | 4    |
| 1.3 Pin1 in the cell.....   | 4    |
| 1.4 Role of Pin1 in pathogenesis.....                             | 6    |
| 1.4.1 Decrease of Pin1 in neurodegeneration.....                  | 6    |
| 1.4.2 Pin1 overexpression in cancer.....                          | 7    |
| 1.5 Pin1 as a therapeutic target.....                             | 8    |
| 1.6 Structural features of Pin1.....                              | 9    |
| 1.7 Pin1 catalytic mechanism.....                                 | 9    |
| 1.8 Binding models.....   | 14   |
| 1.9 CDC25C and Pin1 as a system for this study.....               | 17   |
| 1.10 Objectives and hypothesis.....                               | 18   |
| 2. Materials and Methods.....                                     | 23   |
| 2.1 Expression and purification of recombinant Pin1 proteins..... | 23   |

|       |  |    |
|-------|--|----|
| 2.1.1 | Hexa-histidine tagged proteins.....  | 23 |
| 2.1.2 | GST tagged proteins.....   | 25 |
| 2.2   | Human CDC25C peptides.....   | 28 |
| 2.3   | Peptidyl-prolyl isomerization activity assays.....                                 | 28 |
| 2.4   | Amino acid analysis .....  | 30 |
| 2.5   | Analytical ultracentrifugation .....   | 30 |
| 2.5.1 | Sedimentation velocity.....  | 30 |
| 2.6   | Circular dichroism spectropolarimetry .....  | 31 |
| 2.7   | Pin1-peptide NMR titrations .....  | 33 |
| 2.8   | Fluorescence polarization experiments .....  | 34 |
| 2.9   | Pin1 crystallization.....  | 35 |
| 2.10  | X-ray crystallography data collection and structure refinement .....               | 35 |
| 3.    | Results .....  | 36 |
| 3.1   | Protein purification and activity.....   | 36 |
| 3.2   | Peptide addition to Pin1 does not cause global conformational changes .....        | 40 |
| 3.3   | Pin1 stability does not change with peptide addition.....                          | 47 |
| 3.4   | Pin1 interacts with a phosphorylated CDC25C peptide.....                           | 50 |
| 3.5   | Pin1 does not bind to a non-phosphorylated peptide with high affinity .....        | 58 |
| 3.6   | The number of phosphorylation sites affects Pin1-CDC25C peptide interactions ..... | 64 |
| 4.    | Discussion .....   | 68 |
| 4.1   | Pin1-CDC25C interactions .....   | 69 |
| 4.2   | Effects of peptides on Pin1 global conformation.....                               | 70 |
| 4.3   | Protein stability did not change when peptides were added .....                    | 70 |
| 4.4   | Pin1 has a higher affinity for phosphorylated peptides.....                        | 71 |
| 4.5   | Two phosphorylation sites further increase Pin1-peptide binding affinities .....   | 74 |

|      |   |     |
|------|---|-----|
| 4.6  | Peptide binding to individual Pin1 domains .....  | 75  |
| 4.7  | The WW domain of Pin1 acts as the main binding domain.....  | 76  |
| 4.8  | $K_d$ values compared to literature values.....   | 77  |
| 4.9  | The distance between phosphorylated residues impacts binding.....                                     | 80  |
| 4.10 | Pin1 binding to phosphate moieties .....  | 81  |
| 4.11 | Effects of molecular crowding on Pin1 binding .....   | 82  |
| 4.12 | Pin1 binding model .....  | 82  |
| 4.13 | Future directions for the present work .....  | 84  |
| 4.14 | Summary .....   | 86  |
|      | References.....   | 88  |
|      | Appendices.....   | 100 |
|      | Appendix A: Crystal structure of C113D Pin1 construct shows a residue change in the active site ..... | 100 |
|      | Curriculum Vitae .....  | 105 |



## List of Tables

|   |    |
|---|----|
| Table 1 Cdc25 derived peptides synthesized to test binding affinities to Pin1 protein <i>in vitro</i> . ..  | 41 |
| Table 2 Fluorescence polarization experimental results of the human CDC25C- derived peptides synthesized to test binding affinities to Pin1 protein <i>in vitro</i> . ..... | 67 |
| Table 3 Peptides used in the literature compared to the 2xP peptide used in the present study...  | 79 |

## List of Figures

|   |    |
|---|----|
| Figure 1 The cis-trans isomerization reaction catalyzed by Pin1. ....   | 3  |
| Figure 2 Surface covered ribbon representation of the x-ray crystallography reference structure of Pin1. ....   | 11 |
| Figure 3 Illustrative representation of Pin1 binding models. ....   | 16 |
| Figure 4 Purified recombinant Pin1 protein construct sequences. ....  | 26 |
| Figure 5 Purified recombinant Pin1 protein and peptidyl-prolyl isomerase activity. Purified recombinant Pin1 protein and peptidyl-prolyl isomerase activity. ....     | 38 |
| Figure 6 Pin1 peptidyl prolyl isomerization assay sample curve. ....  | 39 |
| Figure 7 Sedimentation velocity experiments of Pin1 with CDC25C-derived peptides. ....  | 46 |
| Figure 8 Secondary structure and thermal stability analysis of Pin1 and Pin1-peptide complexes. ....  | 49 |
| Figure 9 $^1\text{H}$ - $^{15}\text{N}$ HSQC NMR spectra of Pin1 and Pin1-2xP complex with the changing residues plotted and mapped to the 3D structure of Pin1. .... | 55 |
| Figure 10 Pin1-2xP complex intensity changes seen by NMR and their locations mapped to the surface of Pin1. ....  | 57 |
| Figure 11 $^1\text{H}$ - $^{15}\text{N}$ HSQC NMR spectra and chemical shift data for Pin1 and the Pin1-0xP complex. ....   | 61 |
| Figure 12 Pin1-0xP complex intensity changes observed by $^1\text{H}$ - $^{15}\text{N}$ HSQC NMR and their locations mapped to the surface of Pin1. ....              | 63 |
| Figure 13 Fluorescence polarization experiments of Pin1-peptide complexes and their binding constants. ....   | 66 |

## List of Appendices

|   |     |
|---|-----|
| Appendix A Crystal structure of C113D Pin1 construct shows a residue change in the active site<br>..... | 100 |
| Table A1 Pin1 R14A C113D crystallographic data collection and refinement parameters. ....               | 101 |
| Figure A2 Pin1 C113D refined crystal structure. ....  | 103 |
| Figure A3 Plot of select WW domain residues displaying peak chemical shift changes. ....                | 104 |

## List of Abbreviations

|           |  |
|-----------|--|
| °C        | degrees Celsius                                    |
| 3D        | three-dimensional                                  |
| A         | absorbance   |
| A $\beta$ | amyloid beta                                       |
| AD        | Alzheimer's disease                                |
| APP       | amyloid precursor protein                          |
| AUC       | analytic ultracentrifugation                       |
| CD        | circular dichroism                                 |
| CDC25C    | cell division cycle 25 (isoform C)                 |
| cm        | centimeter   |
| CyPs      | cyclophilins                                       |
| DMSO      | dimethyl sulfoxide                                 |
| DSS       | 4,4-dimethyl-4-silapentane-1-sulfonic acid         |
| DTT       | dithiothreitol                                     |
| EDTA      | ethylenediaminetetraacetic acid                    |
| FID       | free induction decay                               |
| FKBPs     | FK-506 binding proteins                            |
| FP        | fluorescence polarization                          |
| x g       | relative centrifugal force                         |
| GST       | glutathione-s-transferase                          |
| HEPES     | 4-(2-hydroxyethyl)-1-piperazineethanesulfonic acid |
| HBS       | HEPES buffered saline                              |
| HPLC      | high-performance liquid chromatography             |
| HSQC      | heteronuclear single quantum coherence             |
| IPTG      | isopropylthio- $\alpha$ -D- $\beta$ -galactoside   |
| ITC       | isothermal titration calorimetry                   |
| MALDI     | matrix-assisted laser desorption/ionization        |
| mg        | milligram  |
| min       | minute   |

|                       |  |
|-----------------------|--|
| mL                    | millilitre   |
| mM                    | millimolar   |
| $\mu$ M               | micromolar   |
| $\mu$ g               | microgram  |
| MRE                   | mean residue ellipticity   |
| MWCO                  | molecular weight cut-off   |
| NHS                   | N-hydroxysuccinimide   |
| nm                    | nanometer  |
| NIMA                  | never in mitosis gene A  |
| NMR                   | nuclear magnetic resonance   |
| OD                    | optical density  |
| PBS                   | phosphate buffered saline  |
| PEG                   | <i>polyethylene</i> glycol   |
| Pin1                  | protein interacting with NIMA-1                                    |
| PMSF                  | phenylmethanesulfonyl fluoride                                     |
| PP2A                  | protein phosphatase 2A   |
| RNA                   | ribonucleic acid   |
| s                     | second   |
| SDS                   | sodium dodecyl sulphate  |
| SDS-PAG               | sodium dodecyl sulphate polyacrylamide gel                         |
| SDS-PAGE              | sodium dodecyl sulphate polyacrylamide gel electrophoresis         |
| SPARC                 | SickKids Proteomics, Analytics, Robotics & Chemical Biology Centre |
| Suc-AEPF- <i>p</i> NA | Succinyl-AEPF- <i>p</i> Nitroaniline                               |
| sw                    | sedimentation coefficient  |
| TEV                   | tobacco etch virus   |
| V                     | volts  |

# 1. Introduction

Cell homeostasis is a key feature involved in the maintenance of healthy cells; therefore signalling pathways that respond to external stimuli in the changing environment are tightly regulated. An extensive network of cellular proteins is implicated in these signal transduction cascades, including protein kinases that phosphorylate substrate proteins, and other proteins that elicit responses through modifications of substrate proteins pre- or post-phosphorylation<sup>1</sup>. One such modification is the isomerization of peptide bonds<sup>2-5</sup>.

Peptide bonds have been shown to exhibit partial double bond characteristics and can therefore exist in one of two conformations: *cis* or *trans*<sup>6</sup>. Isomerases are enzymes that catalyze the interconversion of peptide bond isoforms; further, isomerization is a mechanism for higher-order regulation<sup>7-10</sup>. The majority of peptide bonds occur in *trans* in proteins, as *trans* isomers tend to be more stable due to the separation of large functional groups in space, which disables steric hindrance<sup>11</sup>. In contrast, the bonds preceding a proline (Pro) residue often appear in the *cis* conformation as a result of the restrictive cyclic structure of Pro and the symmetry of the carbon atoms within the ring<sup>12</sup>. The phenomenon of *cis* bond isomers occurs in approximately 30% of peptides and 10% of proteins, compared to their corresponding *trans* isomers<sup>13</sup>. The interconversion between the two peptide bond isoforms is a slow process if un-catalyzed, hence the utility of peptidyl-prolyl isomerases (PPIase), a specific class of isomerase, that increases the rate of bond interconversion for peptide bond conformations proximal to Pro residues.

## 1.1 *Peptidyl-prolyl isomerases*

There are three families of PPIases: cyclophilins (CyPs), FK506-binding proteins (FKBPs) and parvulins. Several members of these protein families have been identified as targets for the development of immunosuppressive drugs including CyPs and FKBP, which have been identified as the targets of cyclosporin and rapamycin respectively. Similar to parvulins, both the CyPs and the FKBP are able to catalyze peptidyl-prolyl isomerization; however their sequences and structures show no noticeable similarities. Each of the three enzyme families has a different recognition motif for residues preceding a proline<sup>14-18</sup>. The parvulin family, so named because of the small size of the proteins, has two protein sub-classes: the non-Pin1 parvulins and the Pin1-like parvulins. The non-Pin1 sub-class can isomerize the peptide bond between a non-phosphorylated residue preceding a Pro, while the Pin1-like parvulins isomerize the peptide bond between a phosphorylated residue preceding a Pro<sup>17</sup> (**Figure 1**). Mechanistically, Pin1 has a proline-directed function that acts on phosphorylated serine/threonine (pSer/Thr) substrates<sup>19</sup> and its phosphorylation-dependence is what makes Pin1 unique amongst its class of enzymes<sup>20</sup>.

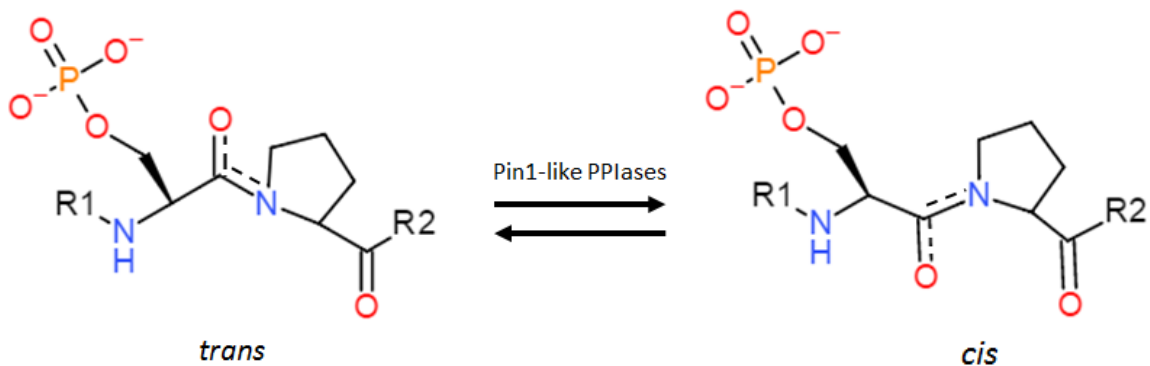


**Figure 1 The *cis-trans* isomerization reaction catalyzed by Pin1.**

*Cis-trans* isomerization is a slow process if uncatalyzed. Peptidyl-prolyl isomerases accelerate this process. Pin1 is a phosphorylation-dependent PPIase with a proline-directed function that acts on phosphorylated Ser/Thr substrates preceding a Pro residue. The other PPIases, Cyps, FKBP and non Pin1-like parvulins, isomerize the peptide bond between a non-phosphorylated residue preceding a Pro.



## 1.2 Introduction to Pin1

Pin1 is a peptidyl-prolyl isomerase that catalyzes the interconversion between *cis* and *trans* isomers of a peptide bond. It specifically binds to phosphorylated substrates preceding a Pro residue and regulates their isomeric conformation. The enzymatic isomerization function of Pin1 was originally discovered after the protein was observed to interact with the protein encoded by Never in Mitosis gene A (NIMA), a protein kinase involved in the regulation of mitosis. The protein interaction was identified using a yeast two hybrid screen and many similar proteins have since been identified in other eukaryotic organisms and some prokaryotes<sup>21</sup>. The Pin1 homolog in yeast, ESS1, was discovered in 1989<sup>22</sup> before the discovery of Pin1 in humans, by the Hunter lab in 1996<sup>21</sup>. Human Pin1 is an essential protein<sup>23</sup> and contains 45% sequence identity to its yeast homolog, which is known to be an essential protein for growth in yeast<sup>22</sup>. A role for Pin1 was first identified in mitotic regulation, but it is now known that Pin1 catalyzes the isomerization of proteins involved in many different cellular processes, including apoptosis, cell cycle progression, cell survival and proliferation, DNA repair, stress responses and transcription<sup>8,24-30</sup>.

## 1.3 Pin1 in the cell

The activity of Pin1 can be regulated post-translationally, through phosphorylation by protein kinases, and by oxidation. The reduction and oxidation of Pin1 has been studied in relation to its role in Alzheimer's disease<sup>31</sup>. Ser residues 16 and 65 can both be phosphorylated, to decrease substrate binding or to increase protein stability by reducing the occurrence of further modifications on the site<sup>19,32</sup>. Pin1 is

localized *in vitro* to the nucleus and the cytoplasm, with the former being its predominant location<sup>21,33</sup>.

To date, Pin1 is the only known peptidyl-prolyl *cis/trans* isomerase that functions as a phosphorylation-directed enzyme<sup>34</sup>. It regulates conformational changes for many substrate proteins involved in signalling pathways that mediate cancers and neurodegenerative diseases<sup>26,35-39</sup>. For example, Pin1 interacts with Cyclin D1, a protein that forms a complex with cyclin-dependent kinases and functions as a regulatory subunit in the G1 to S phase transition of the cell cycle<sup>40</sup>. Once bound, Cyclin D1 transcription is increased because Pin1 can promote upstream signalling factors. This includes Jun N-terminal kinases, which generate phosphorylated c-Jun to stimulate further transcription of Cyclin D1. Cyclin D1 is also unable to exit the nucleus and therefore unable to be targeted to the proteasome for degradation<sup>41</sup>. Other Pin1 interacting proteins that regulate Cyclin D1 transcription are  $\beta$ -catenin and NF $\kappa$ B<sup>42,43</sup>. Pin1 disables the re-generation of  $\beta$ -catenin and targets it to the nucleus where it can promote the transcription of other genes. The p65/RelA binding site located on NF $\kappa$ B undergoes isomerization by Pin1 and the conformational change detaches NF $\kappa$ B from an inhibitor enabling nuclear targeting. Once in the nucleus, NF $\kappa$ B aids in promoting Cyclin D1 transcription. E2F transcription as well as cell cycle progression is regulated by Cyclin D1 and is positively controlled by Pin1. This feedback mechanism is used in cancerous tumours from mouse models by the proteins Her2/Neu and Ras to stimulate continuous cell growth in mammary epithelial cells<sup>44</sup>. For this purpose, the inhibition or down regulation of Pin1 could effectively target cancers evading multiple pathways. In addition to the above-mentioned example,

previous studies have also identified a variety of other cellular proteins that interact with Pin1 including: Akt<sup>45</sup>, Bcl-2<sup>46</sup>, Cdc25<sup>47</sup>, P53<sup>48</sup> and Tau<sup>49</sup>.

#### *1.4 Role of Pin1 in pathogenesis*

Pin1 is implicated in two well-studied, yet diverse diseases: Alzheimer's disease (AD) and cancer. This is not surprising due to the known proteins and pathways in which Pin1 has been associated. The protein induces opposing effects in AD and cancer, based on its expression and amount of enzymatic activity.

##### *1.4.1 Decrease of Pin1 in neurodegeneration*

Various studies have implicated Pin1 in neurogenesis<sup>50</sup>. Pin1 knockout mice have shown prognostic AD markers<sup>51</sup> and decreases in cellular Pin1 protein levels contribute to AD through effects on the Tau protein and the amyloid precursor protein (APP)<sup>52</sup>.

Tau is implicated in AD because when the protein is inactivated, microtubule stabilization is affected. Pin1 interacts with Tau after Tau is phosphorylated on residues Thr212 and Thr231<sup>49,53</sup>. Following this, pThr231 becomes dephosphorylated by PP2A, a phosphatase that acts to specifically dephosphorylate *trans* conformational bonds, and Tau can begin to stabilize microtubules. In the neurons, when Tau becomes hyperphosphorylated through a lack of Pin1 and PP2A function, neurofibrillary tangles can form<sup>53</sup>. These tangles are common occurrences in the process of neurodegeneration.

A second common occurrence in neurodegenerative disorders is the formation of senile plaques in the brain. These plaques are composed of insoluble amyloid- $\beta$  (A $\beta$ ) peptides, which are generated from APP<sup>54</sup>. Pin1 interactions with the binding motif pThr668-Pro of APP help to regulate the amount of A $\beta$  peptides generated. Once Pin1 is

bound to APP, the peptidyl-prolyl isomerization is increased by over 1000-fold<sup>54</sup>. The *cis* isoform of APP is responsible for the increase of insoluble A $\beta$  peptides which can accumulate into plaques in the brain<sup>55</sup>. Pin1 is accountable for the *cis* to *trans* conversion of APP and if Pin1 is down-regulated, the pathogenic *cis* isoform of APP becomes dominant<sup>54</sup>.

#### 1.4.2 *Pin1 overexpression in cancer*

The effects of Pin1 in cancer are contrasting to those of AD. For one, Pin1 is down-regulated in AD and its depletion leads to cell death<sup>56</sup>, while the protein is up-regulated in cancer and postulated to promote tumour growth<sup>19</sup>. Pin1 has a role in many forms of cancer including breast<sup>57</sup>, cervical<sup>58</sup>, colon<sup>59</sup>, liver<sup>60</sup>, lung<sup>61</sup>, oral squamous<sup>62</sup>, head and neck cancers<sup>63</sup> and prostate cancer<sup>64</sup> (see <sup>65</sup> for a general overview). Upon further characterization, Pin1 overexpression has been implicated as a marker for poor prognosis and a higher likelihood of recurrence in prostate cancer<sup>64</sup>. Cancerous tumours displayed overexpression of Pin1 at the mRNA as well as the protein level<sup>41</sup>.

Pin1 has been well studied in tumours generated through the dysregulation of Her2/ Neu or Ras protein-implicated pathways<sup>44,66,67</sup>. Using mouse models, studies have shown that Pin1 overexpression increases the oncogenic effects of Neu and Ras, whereas mice lacking Pin1 do not exhibit such effects. These proteins affect E2F, a transcription factor, which leads to an increase in Cyclin D1 and Pin1 in cells<sup>44,68</sup>.

Overall, in the context of cancer Pin1 inhibits tumour suppressors by changing the conformation of a substrate so that its activator cannot bind<sup>69</sup>. In addition, Pin1 stabilizes the extensively studied tumour suppressor p53, a key protein that stimulates apoptosis

under cell stress conditions<sup>70</sup>. Pin1 has therefore been recognized as a potential therapeutic target because of its diverse implications in disease.

### *1.5 Pin1 as a therapeutic target*

Pin1 was originally revealed to regulate key players in mitosis, but through further characterization Pin1 has been presented in many other complex processes<sup>26,71,72</sup>. The phosphorylation-specific nature of Pin1 adds an increased level of regulation in relation to Pro-directed enzymes, such as kinases, needed for cellular processes<sup>73</sup>. Of note is the association of Pin1 with proteins involved in cancer, and Alzheimer's disease. As a result, Pin1 is a potential candidate for the development of targeted therapeutics. The other PPIase protein families, cyclophilins and FKBP, both have drug associations that act in an inhibitory manner to decrease protein activity<sup>74,75</sup>. The compound juglone, a naturally occurring compound, was isolated as a parvulin family inhibitor. This molecule was able to inhibit Pin1 and other parvulins, through an interaction with Cys113. Unfortunately, the lack of specificity towards Pin1 and the potential for off-target effects on cellular proteins (including RNA polymerases) disabled juglone from becoming a therapeutic agent for cancer treatment<sup>76</sup>. Therefore, targeted therapeutics towards Pin1 have been focused on the active site Cys residue, the hydrophobic pocket or the phosphate binding loop<sup>72,77,78</sup>. Structure-based inhibitor design is a commonly used method, but many of the isolated compounds contained phosphate moieties to increase their binding affinity, which in turn decreased their cell membrane permeability. To circumvent this setback, work in the Litchfield lab used phage display to identify peptide sequences that inhibit Pin1. The screen was directed towards identifying cyclic peptides that would inhibit the PPIase domain of the protein, to decrease its function and

potentially act as a cancer therapeutic. The cyclic peptides were shown to bind with a high affinity to Pin1, potentially due to their rigidity, and the cyclic peptides may also have the ability to evade proteolysis<sup>79</sup>. In order to generate potent inhibitors, it is important to understand the mechanism by which Pin1 binds to its substrates and the corresponding affinities. With Pin1 having two domains for binding, and knowing that Pin1 substrates may themselves have multiple binding sites increases complexity within the *in vitro* system.

## 1.6 Structural features of Pin1

Pin1 is a small 18.4 kDa protein, consisting of 163 amino acids in length<sup>21</sup>. It has two diverse structural domains, as determined by X-ray crystallography<sup>45</sup>: an N-terminal type IV WW domain, so named for its conserved tryptophan residues located at amino acid positions 11 and 34, and a C-terminal PPIase enzymatic domain<sup>74,80</sup>. The domains are separated by a flexible linker of ten residues in length, between residues 1-39 of the WW domain and residues 50-163 of the isomerase domain (**Figure 2**)<sup>81</sup>. Both domains recognize similar motifs containing phospho-Ser/Thr-Pro<sup>82</sup>. Proline-directed binding and isomerization are both well-known mechanisms for post-phosphorylation regulation and have been extensively studied<sup>73,83,84</sup>.

The secondary structure of Pin1 consists of three anti-parallel  $\beta$ -sheets in the WW domain, which contains a hydrophobic area on its surface. The PPIase domain has four  $\alpha$ -helices and three anti-parallel  $\beta$ -sheets in its secondary structure. Two characterized regions are also located in the PPIase domain: a proline binding pocket and a phosphate binding loop<sup>85</sup>. These known structural areas are located on opposing sides of the active site of the protein, which is centered on Cys residue 113 (**Figure 2** - bottom panel). Other

active site amino acids include His 59, His 157 and Ser 154<sup>86</sup>. These residues arrange into a pocket in which a substrate peptide bond can enter (1PIN structure and **Figure 2**)<sup>45</sup>. The proline binding pocket is a hydrophobic groove with conserved leucine (Leu), methionine (Met) and phenylalanine (Phe) residues (Leu122, Met130 and Phe134). The phosphate binding loop contains positively charged residues that can interact with a negatively charged phosphate moiety. Lys63, Arg68 and Arg69 are the central amino acids coordinating this binding<sup>87</sup>.

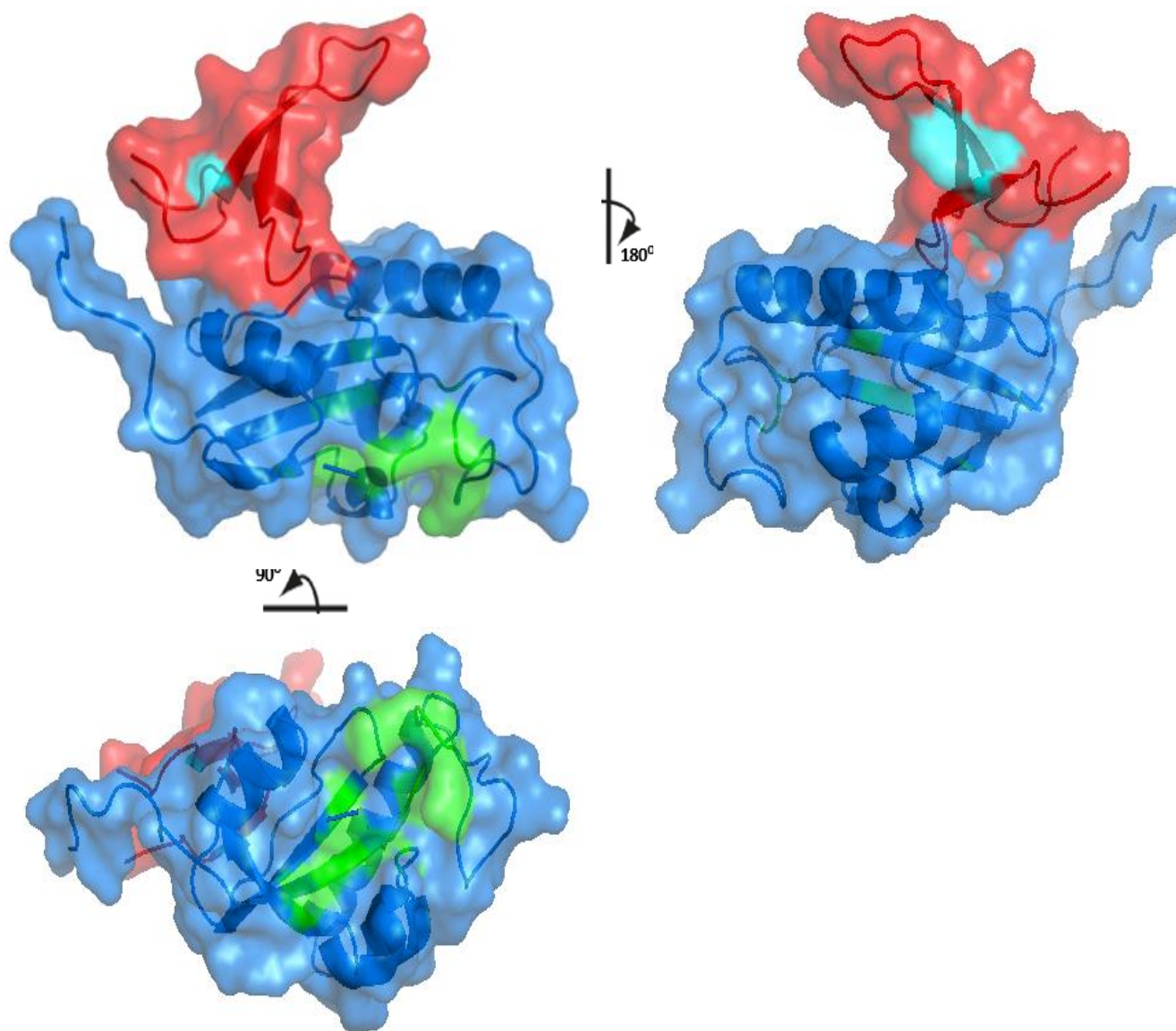


**Figure 2** Surface covered ribbon representation of the x-ray crystallography reference structure of Pin1.

Pymol-generated image of the surface and ribbon structure of Pin1, using the R14A Pin1 crystal structure (Protein Data Bank Code 1PIN). The WW domain, residues 1-39, is visible in red with the characteristic Trp11 (left panel) and Trp34 (right panel) coloured in cyan. This domain has three anti-parallel  $\beta$ -sheets. The PPIase domain, residues 50-163, is coloured in blue and is comprised of four  $\alpha$ -helices and three anti-parallel  $\beta$ -sheets. The left panel image is rotated along the vertical axis by  $180^\circ$  to show the right panel. The bottom surface view is shown by rotating the left panel image along the horizontal axis by  $90^\circ$ . The protein active site, located in the isomerase domain, is coloured in green and is composed of amino acid residues (H59, L60, L61, V62, K63, R68, R69, A85, I89, C113, L122, S154, I156 and H157) centered on the catalytic Cys113.



In binding, the WW domain of Pin1 is known to bind to substrates with a higher affinity than the PPIase domain. The residues from this domain involved in substrate binding are: Arg17, Tyr23 and Trp34. This domain enhances substrate specificity when a binding motif is located on a peptide<sup>88</sup>. The WW domain of Pin1 has been shown to have a ten-fold higher binding affinity for a known Pin1 substrate, Pintide (WFYpSPR-NH<sub>2</sub>) compared to the PPIase protein domain<sup>88</sup>. The WW domain has a high affinity for most substrates and it is therefore thought to be responsible for substrate targeting and recognition whereas, the PPIase domain alone is usually unable to bind known substrates, but takes on the role of catalyzing imide bond isomerization<sup>89</sup>.

Many of the Pin1-interacting proteins have one binding site identified, whereas some may contain multiple binding sites. In the latter case, these sites are separated by approximately 19 amino acid residues within the protein sequence<sup>29,52</sup>. This separation is intriguing and may be related to the spacing between the two domains in Pin1. The downstream binding site could bind to the WW domain and the upstream site could bind and/ or undergo isomerization by the PPIase domain. One such example of the multiple binding sites occurs in the protein Tau, a protein found in neural tissues, and another is CDC25C, a mitotic initiator protein. In the aforementioned proteins, there are two Pin1 binding sites separated by 19 amino acids<sup>24,52</sup>.

Studies conducted by Smet *et al.*<sup>90</sup> used peptides derived from the protein Tau. One of the peptides contained two phosphorylation sites separated by two amino acids. Another contained three phosphorylation sites, the two previously mentioned and the third separated by 16 residues. The first and third phosphorylated residues are each part of a Pin1 binding motif. Results show that two Pin1 binding motifs on a peptide increase

the protein-peptide binding affinity but decrease the peptide isomerization rate<sup>90</sup>. From this work, two unresolved questions arose: does cooperativity occur between peptide binding motifs interacting with Pin1, and do the two Pin1 domains cooperate during substrate binding?

### 1.7 *Pin1 catalytic mechanism*

Based on structural studies, Ranganathan *et al.*<sup>45</sup> proposed that the catalytic mechanism of Pin1 involves covalent binding, where Pin1 binds to a ligand and adopts a tetrahedral intermediate conformation<sup>45</sup>. The phosphorylated residue on the substrate fits into the binding pocket for isomerization and the peptide bond is shifted by 90 degrees to move the carbonyl oxygen away from the active site of Pin1. With this movement, the side chain of residue Cys113 of Pin1 can enter the protein active site. His59, another residue located in proximity to the active site, deprotonates Cys113 priming it for a nucleophilic attack on the carbonyl carbon atom of the substrate. The carbonyl oxygen of the substrate is negatively charged and can be modulated by His157. The intermediate species is then abolished allowing for the discharge of the substrate<sup>45</sup>.

In 2000, this mode of substrate catalysis was questioned when the structure of a Pin1 homologue in *Arabidopsis thaliana* was determined by solution-state NMR<sup>91</sup>. The Cys113 equivalent residue in the plant organism exhibited minimal motion when bound to a ligand. This finding contradicted previous reports of covalent binding<sup>92</sup>. Using an approach comprising mutagenesis and peptidyl-prolyl isomerization activity assays, the Litchfield lab displayed that a non-covalent mechanism was likely the mode of binding used for Pin1-substrate interactions<sup>77</sup>. A unigenic evolution study conducted by Behrsin *et al.* invalidated the nucleophilic tendencies of Cys113<sup>77</sup>. In this paper, the Cys residue

was mutated to a Ser in order to retain nucleophilic tendencies; however, this mutation disabled Pin1 catalytic activity. On the other hand, when the residue was mutated to an Asp catalytic activity was only reduced. The enzymatic activity of Pin1 is therefore mediated by factors such as charge<sup>77</sup>.

Continued efforts to elucidate the catalytic mechanism of Pin showed that the two His residues located near the binding pocket, His59 and His157, are needed to increase protein stability<sup>86</sup>. These residues, previously thought to engage in hydrogen bonding, were mutated into Leu residues. This revealed that proton donors were not required for binding. The His59Leu mutation caused the protein to become inactive, but when His157Leu was introduced in conjunction with His59Leu, protein catalytic activity was restored. Further, a different isomerization mechanism was suggested in 2008 because of the negative charge surrounding the Pin1 active site Cys<sup>86</sup>.

Most PPIases use the bond-distortion mechanism for substrate catalysis, which is similar to that hypothesized for Pin1. The active site environment results in a low pKa for Cys113. Consequently, at neutral pH the partial negative charge on cysteine enables the stabilization of the carbonyl group on the substrate. The substrate carbonyl group exhibits double-bond rigidity and if a resonance structure were to form, the peptide bond to be isomerized would become rigid and impact *cis/trans* changes<sup>93</sup>.

## 1.8 *Binding models*

Pin1 is able to bind to phosphorylated motifs through both of its structural domains. The domains can bind concurrently or separately to specific protein substrates that contain the sequence motif pSer/Thr-Pro. For this reason, the mode of binding for

Pin1 to substrates remains unknown. To date, there are four potential binding mechanisms modeled for Pin1 binding and peptidyl-prolyl isomerization (**Figure 3**). The catalysis-first binding model begins with the PPIase domain binding to a *cis* isomer to isomerize the bond and convert it into *trans*. From there the WW domain, known to bind preferentially to *trans* isoforms, can favourably bind to the substrate<sup>94</sup> (**Figure 3A**). A second model is the multimeric model in which Pin1 is part of a complex of proteins. Since the WW domain binds preferentially to most substrates, it is likely that the domain binds a protein as part of the complex. This leaves the enzymatic domain free to isomerize a ligand<sup>36</sup> (**Figure 3B**). The sequential model for Pin1 binding suggests that the WW domain binds to its target sequence first. Then, the PPIase domain is able to bind, at the same site or an adjacent site, for isomerization (**Figure 3C**). This model seems preferential in the case of Pin1 interactors containing multiple binding motifs. Some examples of proteins with greater than one Pin1 target sequence include: CDC25C, CK2 and Tau<sup>35</sup>. The simultaneous binding model is the fourth method recently proposed in the literature. This method involves multi-phosphorylated substrates that can be bound by both Pin1 domains independently yet synchronously to increase substrate affinity<sup>95</sup> (**Figure 3D**).

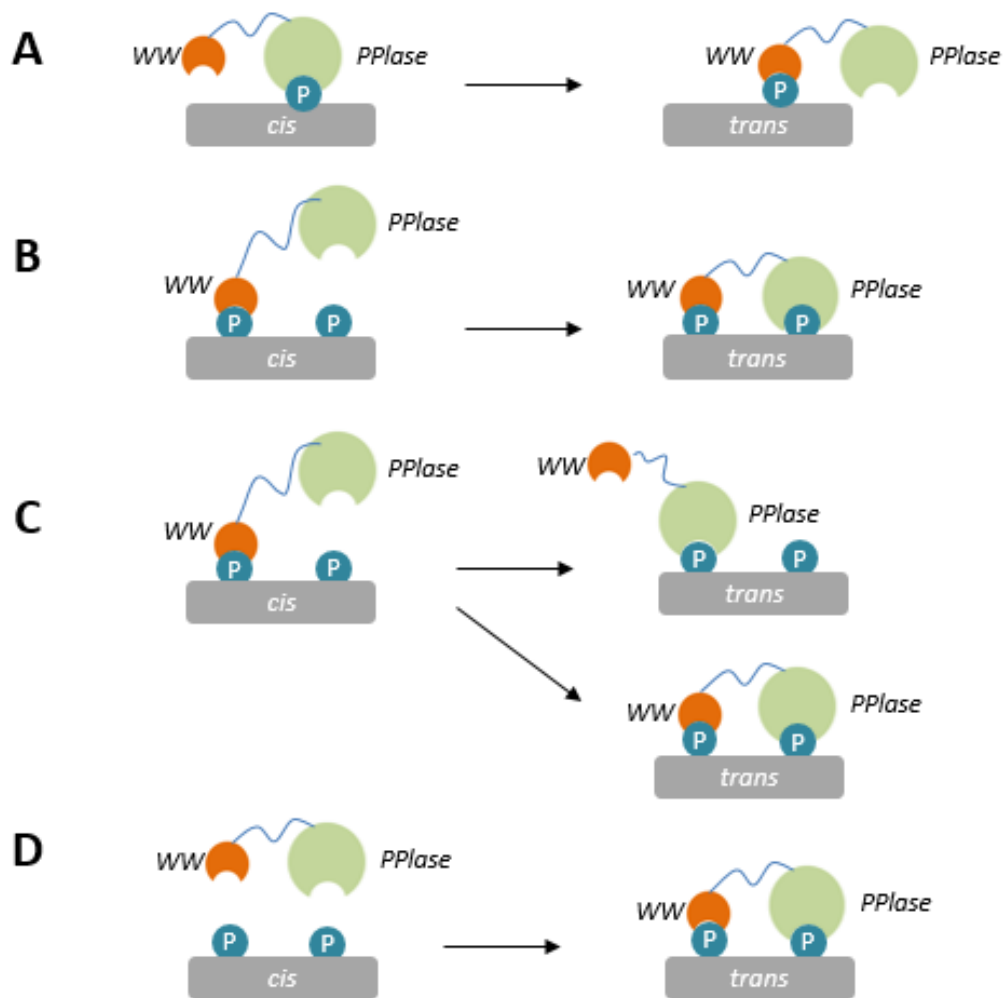


**Figure 3 Illustrative representation of Pin1 binding models.**

**A)** The catalysis-first binding model: The PPIase domain of Pin1 binds to a pSer/Thr-Pro motif in the *cis* isoform to isomerize the peptide bond. The WW domain can then preferentially bind to the *trans* substrate.

**B)** The multimeric binding model: Pin1 is involved in a protein complex through WW domain interactions. The PPIase domain is able to isomerize a substrate in close proximity.

**C)** The sequential binding model: The WW domain of Pin1 can first bind to a pSer/Thr-Pro motif and then the PPIase domain is able to bind to the substrate, at the same site or an adjacent site, for isomerization.

**D)** The simultaneous binding model: Both Pin1 domains can bind to a substrate containing multiple pSer/Thr-Pro binding motifs. Each domain may have a low affinity for the site, but together this binding can increase the affinity.

Pin1 itself is phosphorylated which can act to inhibit its isomerization capabilities<sup>96</sup>. In other cases, Pin1 phosphorylation has no effect on its interaction with proteins involved in key regulatory processes<sup>45-48,61,97</sup>. One such example of a Pin1-interacting protein is human CDC25C. Through the interaction between Pin1 and CDC25C, Pin1 is associated with eukaryotic entry into mitosis. Once Pin1 isomerization occurs on its substrate CDC25C, the substrate then dephosphorylates CDC2 which can form an active complex with Cyclin B. The activated protein complex stimulates a decrease in mitotic entry<sup>98</sup>.

### *1.9 CDC25C and Pin1 as a system for this study*

In order to elucidate the roles of Pin1 with respects to function and pathogenesis, researchers began to look at protein interactions. Many proteins known to be implicated in diverse cellular processes were found to associate directly or indirectly with Pin1<sup>24,44,67,69,99-103</sup> and a few undergo conformational changes upon interaction<sup>8,23,24,35</sup>. The association between human CDC25C and Pin1, discovered in 1998<sup>23</sup>, was later shown to affect the conformation of the Pin1 substrate<sup>24</sup>. CDC25C is a phosphatase with considerable sequence similarity between the human and *Xenopus* forms and is required for mitotic initiation. Many post-translational modifications affect this protein to regulate its function in the triggering of mitotic events. In order to initiate mitosis, CDC25C is activated by hyper-phosphorylation<sup>103</sup>. In contrast to CDC25C, most phosphatases act to reverse the process of phosphorylation and generate opposing effects. In the case of CDC25C, Pin1 binding to the phosphorylated residues Thr48 and Thr67, in the regulatory N-terminus of the protein, affects the conformation of CDC25C and enables subsequent dephosphorylation<sup>24</sup>. This two-step process is initiated by the phosphorylation of specific

Ser/Thr residues preceding a Pro and concluded with substrate catalysis by Pin1.

Phosphorylation followed by Pin1 isomerization depicts one of many tightly regulated mechanisms for the well-known and controlled cellular process of mitosis<sup>24</sup>.

To date, the literature describes studies that have used peptides containing one phosphorylation site to monitor Pin1 binding<sup>8,23,49,56,94,95</sup>. Using peptides containing two phosphorylation sites has been presented by Smet *et al.*<sup>90</sup> to increase the binding affinity of Pin1 towards the peptide, but there is a decrease in isomerization activity<sup>90</sup>. In the present work, peptides comprising two different pThr-Pro motifs seem to interact with both domains of Pin1 because each domain has an affinity for a phosphate group. The peptides chosen are derived from human CDC25C protein, because it is a Pin1-interacting protein that is naturally phosphorylated at multiple sites.

This work utilizes peptides derived from the sequence of human CDC25C to investigate binding interactions with Pin1. Previous studies have shown that the binding of CDC25C to Pin1 requires the full length isomerase, as the individual protein domains decrease binding affinities. Some peptides have also shown no detectable binding to the PPIase domain of Pin<sup>88,95,104,105</sup>.

### *1.10 Objectives and hypothesis*

The use of doubly-phosphorylated peptides to elucidate binding mechanisms by the protein Pin1 is a novel application. This study tests the hypothesis that doubly-phosphorylated substrates bind more strongly to Pin1, if the phosphorylation sites are located on Thr residues preceding a Pro and when the recognition motifs are spaced apart in the peptide sequence. Many studies examined the substrate specificity of Pin1 using

singly phosphorylated peptides as well as peptides composed of shorter sequence lengths<sup>90,104,106,107</sup>. This approach will give insights into the binding of Pin1 to a specific and known interacting protein, human CDC25C. It also highlights binding affinities of the protein-peptide complexes, based on the number of peptide phosphorylation sites.

This work was conducted to assess the overall global changes induced by phosphorylated-peptide binding to Pin1. The changes can give insights into binding locations of the peptides onto Pin1 and substrate affinities when bound. The goal of this project is to investigate the relationship between the peptidyl-prolyl isomerase Pin1 and how it binds to phosphorylated substrates and aims to determine whether a singly-phosphorylated substrate or a doubly-phosphorylated substrate has a lower dissociation constant and therefore a stronger binding affinity to the protein. This knowledge can lead to the generation or improvement of Pin1 inhibitors to decrease protein overexpression and its subsequent effects in cancer. Using peptides derived from the human protein CDC25C, known to promote the initiation of mitosis, changes to Pin1 have been assessed through the use of analytical ultracentrifugation (AUC) experiments, circular dichroism (CD) spectropolarimetry, nuclear magnetic resonance (NMR) and fluorescence polarization (FP) experiments. To further explore the binding interactions of Pin1, X-ray crystallography experiments were conducted however this was not chosen as one of the methods to pursue (See **Appendix**).

Analytical ultracentrifugation is a technique that determines native state stoichiometries of proteins and protein subunits in solution. Conformational changes in macromolecules can also be identified by an optical detection system that measures the concentration gradient of the sample within a cell<sup>108</sup>. Protein sedimentation analysis



occurs in real-time. The experiments were conducted using sedimentation velocity to detect molecules tumbling together in solution and to determine molecular mass and shape<sup>109</sup>. These experiments addressed global changes in Pin1 upon phospho-peptide binding.

The next technique used was circular dichroism spectropolarimetry. This method observes peptide backbone amide bonds and aromatic side chains by measuring the differences between left and right handed circularly polarized light. Only chiral molecules will display differences in the directionality of polarized light passing through. The chromophores associated with protein amides can align into arrays and when aligned, the optical transitions produced are split into many transitions of different wavelengths and intensities<sup>110</sup>. Secondary structural elements have distinct CD spectra as a result of these transitions. Alpha-helical secondary structures show a strong positive peak at 193 nm whereas  $\beta$ -sheets have a weaker positive peak at 195 nm. Both structural elements exhibit large negative curves between 208 and 250 nm in a CD spectrum<sup>111</sup>. The CD experiments conducted assessed changes in the secondary structure of Pin1 with the addition of peptides. Protein and protein-peptide complexes were then tested by thermal melting, as secondary structural features can be denatured by high temperatures<sup>112</sup>. The stability of Pin1 and Pin1-peptide complexes was tested before moving onto binding studies.

Following CD, nuclear magnetic resonance using  $^1\text{H}$ - $^{15}\text{N}$  heteronuclear single quantum coherence (HSQC) was used for peptide titration experiments. NMR affects atomic nuclei because they exhibit magnetism when subjected to a magnetic field<sup>113,114</sup>. A separate magnetic field that is orthogonal to the force applied by the magnet must be

applied to the atoms, with both fields having the same frequency<sup>115</sup>. This enables a magnetization when atomic nuclei are in thermal equilibrium<sup>116</sup>. Short pulses from a transversely oscillating magnetic field are applied to a sample to obtain free induction decay (FID) information. The FID is generated from the voltage induced by the absorption of energy<sup>116</sup>.

Atomic nuclei generate resonant frequencies that are dependent on the location of each nucleus within a magnetic field. The chemical environment surrounding a nucleus will affect which frequencies are absorbed<sup>115</sup>. The location of a nucleus, and therefore the corresponding resonant frequency, is critical information for the analysis of protein structure<sup>116</sup>. NMR gives insights into the Pin1 protein residues affected upon peptide addition.

HSQC experiments relate nitrogen atoms and amide protons, characteristic of 19 amino acid peptide bonds excluding proline. Each amide in the backbone of a protein, and side chains containing protons bound to nitrogen atoms, generate a peak in an HSQC spectrum<sup>117</sup>. Hydrogen nuclei have the largest gyromagnetic ratios and are the most sensitive atoms to use for NMR<sup>118</sup>. The relaxation time associated with an experimental series is increased to obtain the most information from one experiment<sup>115</sup>. The Pin1 backbone amino acids are located in an HSQC spectrum and changes in Pin1 can be seen in the spectra of Pin1 with increasing amounts of peptide.

Fluorescence polarization is a technique that uses a fluorophore to detect potential interactions in solution. A ligand is labeled with a fluorescent marker and once the ligand is excited it will emit light at a given wavelength. This light can be easily detected if

mobile in solution, but when the ligand is bound by another molecule its mobility will decrease. An increased amount of emitted light will be polarized upon binding, compared to that of the free ligand, indicative of a protein interaction<sup>119</sup>. The polarization of fluorescent light can be measured quantitatively to determine dissociation constants for Pin1-peptide complexes.

## 2. Materials and Methods

### 2.1 Expression and purification of recombinant Pin1 proteins

#### 2.1.1 Hexa-histidine tagged proteins

To generate recombinant proteins, histidine-tagged wild type Pin1 (His-Pin1), Arg14Ala Pin1 (R14A Pin1) and Arg14Ala Cys113Asp Pin1 (R14A C113D Pin1) constructs (**Figure 4**) were cloned into pProEX-HTA plasmids and expressed in BL21 DE3 *Escherichia coli* (*E.coli*) cells. These plasmids were a generous gift from Dr. Brian Shilton. Colonies were picked and grown to an optical density (OD)<sub>600</sub> of ~ 0.6 in Luria-Bertani medium supplemented with 100 µg/mL ampicillin (Roche) at 37 °C with shaking at 200 rpm. Once the desired OD<sub>600</sub> was reached, protein expression was induced with 0.6 mM isopropylthio- $\alpha$ -D- $\beta$ -galactoside (IPTG) (Roche) for three hours at 37 °C. Bacteria were pelleted by centrifugation at 4420 x g for 15 minutes (mins) and resuspended in a 4-(2-Hydroxyethyl) piperazine-1-ethanesulfonic acid (HEPES) buffer comprising 10 mM HEPES, 100 mM NaCl and 5 mM NaN<sub>3</sub>, pH 7.4 with protease inhibitors (1 mM phenylmethylsulfonyl fluoride (PMSF), 10 µg/mL pepstatin A and 10 µg/mL leupeptin) (Sigma). The cells were lysed using an EmulsiFlex-C3 pressure homogenizer (Avestin) at 15,000 psi and the cell debris was pelleted by centrifugation at 23 300 x g for 20 mins. The soluble fraction of lysate was loaded onto a 5 mL HisTrap HP nickel sepharose affinity column (GE Healthcare Life Sciences). The column was washed with 20 column volumes of HEPES buffer with an additional 10 mM imidazole, followed by 10 column volumes of HEPES buffer with 50 mM imidazole and all washes were collected. Histidine<sub>6</sub>-tagged Pin1 (His-Pin1) constructs were eluted using HEPES buffer with 500 mM imidazole in 15 1.5 mL fractions. Eluted fractions were monitored at

an absorbance (A) wavelength of 280 nm, using an ÄKTA FPLC system (GE Healthcare Life Sciences).

The protein concentration of the eluted fractions was determined by  $A_{280}$ , after pooling the fractions containing His-Pin1 protein, and analyzed by 15% SDS-PAGE gels using SDS-PAGE buffer (192 mM glycine (Bioshop), 25 mM Tris-base (Bioshop), 0.1% SDS (Bioshop) at a constant voltage of 150 V for 75 mins. A prestained BLUEye molecular weight marker (FroggaBio) was used for reference. Protein purity was assessed by staining with Coomassie R-250 Brilliant Blue (Bio-Rad). Tobacco Etch Virus (TEV) protease was added to the protein at a molar ratio of 1:25, along with 5 mM DTT and 1 mM EDTA. This solution was rotated at room temperature for 5 hours, followed by the addition of a second aliquot of TEV, DTT and EDTA. After rotation at room temperature overnight, the solution was spun down at 3724 x g to remove any precipitant and then dialyzed against 1 L of HEPES buffer for at least 6 hours at 4 °C. The solution was then loaded onto a 5 mL HisTrap column using HEPES buffer containing 10 mM imidazole, where the His-TEV would remain bound to the column while the un-tagged Pin1 protein would come off in the flow through. The flow through was then collected and purified wild type His-Pin1 was concentrated and dialyzed into 2x HEPES buffered saline (HBS) (280 mM NaCl, 50 mM HEPES, 12 mM Dextrose, 10 mM KCl, 1.5 mM  $\text{Na}_2\text{HPO}_4$ , pH 7.0) at 4 °C for 16 hours to remove imidazole. Purified R14A Pin1 and R14A C113D Pin1 were concentrated to greater than 18 mg/mL using an Amicon Ultra centrifugal filter tube (Millipore) and dialyzed into crystallization buffer (10 mM HEPES, 100 mM NaCl, 5 mM  $\text{NaN}_3$ , 5 mM DTT and 1 mM EDTA), containing 20% glycerol (Caledon), at 4 °C for 16 hours to remove imidazole. Where proteins were required for

different experimental procedures, the proteins were dialyzed against their respective buffers as indicated elsewhere. All protein concentrations were determined using the Bradford Protein Assay (Bio-Rad), before being flash frozen and stored at -80 °C.

### 2.1.2 *GST tagged proteins*

For NMR experiments, wild type Pin1 protein was expressed with a GST-tag (**Figure 4**) from a pGEX-KG vector in BL21 DE3 *E. coli* cells, courtesy of Dr. Melanie Bailey. Colonies were picked and grown to an optical density (OD)<sub>600</sub> of ~ 0.9 in M9 media supplemented with 1.0 g/L of 99% <sup>15</sup>NH<sub>4</sub>Cl (Cambridge Isotope Laboratories) and 100 µg/mL ampicillin (Roche) at 37 °C, shaking at 250 rpm. Once the desired OD<sub>600</sub> was reached, protein expression was induced with 0.6 mM IPTG (Roche) overnight at 16 °C. Bacteria were pelleted by centrifugation at 4420 x g for 15 mins and resuspended in cold phosphate buffered saline (PBS), pH 7.5, containing protease inhibitors (1 mM PMSF, 10 µg/mL pepstatin A and 10 µg/mL leupeptin) (Sigma). The cells were lysed using a pressure homogenizer (Avestin) at 15, 000 psi. Triton X-100 (Sigma) was added to 1% of the total volume and the solution was rotated for 15 min at 4°C. The cell debris was pelleted by centrifugation at 23 300 x g for 20 mins and the supernatant was incubated with glutathione cross-linked agarose beads (Sigma) while rotating for one hour at 4 °C. The beads were washed with two column volumes of cold PBS and then the protein was eluted in 12 fractions of 1.5 mL each, with 10 mM reduced glutathione (Sigma) in PBS, pH 7.5. Aliquots of washes and eluates were analyzed by visualization on a 15% SDS-PAGE.

|  |   |  |
|--|---|--|
| <b>Hexa-Histine Tag ( His )</b>              | MSYYHHHHHHDYDIPTT <b>ENLYFQ</b> G<br>↓<br>TEV recognition site  |  |
| <b>Glutathione S-transferase Tag ( GST )</b> | MSPILGYWKIKGLVQPTRLLEYLEEKYEEHLYERDEGDKWRNKKFELGLEFPNLPYYID<br>GDVKLTQSMAIIRYIADKHNMLGGCPKERAISMLEGAVLDIRYGVSRIRIAYSKDFETLKV<br>DFLSKLPPEMLKMFEDRLCHKTYLNGDHSVTHPDFMLYDALDVLVLYMDPMDCLDAFPKLVCFK<br>KRIEAIPQIDKYLKSSKYIAWPLQGWOATFGGGDHPPK <b>ENLYFQ</b> G<br>↓<br>TEV recognition site |  |
| <b>wild type Pin1</b>                        | <b>His</b> — MADEEKLP PGWEKRMSRSSGRVYVFNHITNASQWERPSGNSSSGGKNGQGEPARVRCSHL 60<br>LVKHSQRRPSSWRQEKITRTKEEALELINGYIQKIKSGEEDFESLASQFSDCSSAKARG 120<br>DLGAFSRGQMOKPFEDASFALRTGEMSGPVFTDSGIHILRTE 163  |  |
| <b>wild type Pin1</b>                        | <b>GST</b> — MADEEKLP PGWEKRMSRSSGRVYVFNHITNASQWERPSGNSSSGGKNGQGEPARVRCSHL 60<br>LVKHSQRRPSSWRQEKITRTKEEALELINGYIQKIKSGEEDFESLASQFSDCSSAKARG 120<br>DLGAFSRGQMOKPFEDASFALRTGEMSGPVFTDSGIHILRTE 163  |  |
| <b>R14A Pin1</b>                             | <b>His</b> — ----ALPPGWEK <b>A</b> MSRSSGRVYVFNHITNASQWERPSGNSSSGGKNGQGEPARVRCSHL 55<br>LVKHSQRRPSSWRQEKITRTKEEALELINGYIQKIKSGEEDFESLASQFSDCSSAKARG 115<br>DLGAFSRGQMOKPFEDASFALRTGEMSGPVFTDSGIHILRTE 158   |  |
| <b>R14A C113D Pin1</b>                       | <b>His</b> — ----ALPPGWEK <b>A</b> MSRSSGRVYVFNHITNASQWERPSGNSSSGGKNGQGEPARVRCSHL 55<br>LVKHSQRRPSSWRQEKITRTKEEALELINGYIQKIKSGEEDFESLASQFSD <b>D</b> SSAKARG 115<br>DLGAFSRGQMOKPFEDASFALRTGEMSGPVFTDSGIHILRTE 158  |  |

**Figure 4 Purified recombinant Pin1 protein construct sequences.**

His-Pin1 constructs contain an N-terminal hexa-histidine tag and a tobacco etch virus (TEV) cleavage recognition sequence for ease of purification and then to remove the His-tag. Three His-Pin1 proteins were purified: wild type full length Pin1 (His-Pin1), His-Arg14Ala Pin1 (R14A Pin1) and His-Arg14Ala Cys113Asp Pin1 (R14A C113D Pin1). R14A Pin1 is the full length Pin1 protein, with a deletion of the five N-terminal amino acids and a single residue substitution at residue 14 in the WW domain, to increase protein stability for crystallization. R14A C113D Pin1 is the R14A Pin1 sequence with an additional single residue substitution at residue 113 in the PPIase domain. A GST-Pin1 fusion protein was also generated. This construct contains an N-terminal GST protein sequence attached to a TEV cleavage recognition sequence and wild type full length Pin1.

TEV protease was added to proteins in a 1:20 ratio of TEV to protein, to remove the GST-fusion tag. This incubation was conducted twice, for 5 hours and then overnight, at room temperature with constant rotation. An overnight dialysis into TEV cleavage buffer (50 mM Tris-HCl, 10 mM EDTA, 5 mM NaN<sub>3</sub>, 20 mM β-mercaptoethanol, pH 8.0) at 4 °C was performed, preceding a TEV cleavage reaction where TEV and protein were mixed with 5 mM DTT and 1 mM EDTA. Next the sample was spun down at 3724 x g to remove any precipitation and followed by a buffer exchange, using a 10 mL stirred cell (Millipore) connected to a Nitrogen gas pressure supply, into a phosphate buffer containing 10 mM monobasic sodium phosphate, 5 mM NaN<sub>3</sub>, 20 mM β-mercaptoethanol, 300 mM NaCl and 15% glycerol (pH 6.5). The protein was loaded onto a 120 mL HiPrep 16/60 Sephacryl S-100 High Resolution gel filtration column (GE Healthcare) equilibrated with the final NMR phosphate buffer (50 mM phosphate buffer, 100 mM Na<sub>2</sub>SO<sub>4</sub>, 1 mM DTT, 5 mM EDTA, 5 mM NaN<sub>3</sub>, pH 6.6). Proteins were eluted from the column and collected into a total of 95 0.5 mL fractions. Aliquots of fractions were analyzed on 15% SDS-PAGE gels and stained with Coomassie R-250 Brilliant Blue (Bio-Rad) to assess purity. Fractions containing the appropriate pure protein were pooled and concentrated using a 15 mL Amicon centrifuge filter (3000 MWCO) (Millipore). Protein concentrations were determined using the Bradford Protein Assay (Bio-Rad). Protein purity and integrity was assessed by SDS-PAGE and matrix-assisted laser desorption/ionization (MALDI) mass spectrometry, while protein concentration was confirmed through amino acid analysis (SickKids Proteomics, Analytics, Robotics & Chemical Biology Centre (SPARC), Toronto). The final volume and concentration of the <sup>15</sup>N-labeled Pin1 NMR samples were 650 μL and 322 μM respectively, following the



addition of 10% D<sub>2</sub>O to provide the field frequency lock, 100 μM 2,2-dimethyl-2-silapentane-5-sulfonic acid (DSS) as an internal standard and 1.5 mM imidazole (pH 8.0) to act as an internal pH monitor throughout the experiments.

## 2.2 *Human CDC25C peptides*

All peptides derived from human CDC25C were synthesized by EZBiolab (Carmel, Indiana). Peptides were prepared to 95.1 – 96.6% purity, as determined by HPLC analysis conducted by EZBiolab. Peptide sequences contained 32 amino acids and were as follows: CPDVPRTPVGKFLGDSANLSILSGGTPKRSLD, CPDVPR<sub>p</sub>TPVGKFLGDSANLSILSGGTPKRSLD, CPDVPRTPVGKFLGDSANLSILSGG<sub>p</sub>TPKRSLD and CPDVPR<sub>p</sub>TPVGKFLGDSANLSILSGG<sub>p</sub>TPKRSLD (referred to as 0xP, 1xP #1, 1xP #2 and 2xP respectively). Peptides were resuspended in the buffers mentioned for each experiment. Any peptide modifications were confirmed by MALDI Mass Spectrometry (MALDI Mass Spectrometry Facility, one of the facilities within the London Regional Proteomics Centre, Ontario).

## 2.3 *Peptidyl-prolyl isomerization activity assays*

Peptidyl-prolyl isomerase activity for each of the purified Pin1 proteins was determined with a spectrophotometric assay using a Cary-100 spectrophotometer at 0 °C. Enzymatic assays were performed in Assay buffer (50 mM HEPES, 100 mM NaCl, 5 mM NaN<sub>3</sub>, pH 7.4), as described in Behrsin, *et al.* 2007 and Duncan, *et al.* 2011<sup>77,79</sup>. The protein substrate Succinyl-AEPF-*p*Nitroaniline (Suc-AEPF-*p*NA) (Bachem) was dissolved in trifluoroethanol with 0.3 M LiCl, to maximize the amount *cis*-proline,

producing a stock concentration of 20 mM. The chymotrypsin (Type II, Sigma) had a concentration of 50 mg/mL, dissolved in 1 mM HCl. Reactions were performed with increasing concentrations of substrate, added to assay buffer, to a total sample volume of 2 mL. This was incubated for at least 30 seconds before adding a final concentration of 1.25 mg/mL chymotrypsin to enable the depletion of *trans*-proline peptide. The rate of chemical isomerization was measured as an absorbance over time until the slope became linear. 0.5  $\mu$ M from a 20  $\mu$ M stock of Pin1 was then added to the sample and the rate of both the Pin1-catalyzed as well as the un-catalyzed isomerization was measured. The run continued until all of the protein substrate was consumed and the absorbance plot displayed a slope of zero.

Absorbance measurements were made at different wavelengths, depending on the increasing substrate concentration, with an extinction coefficient ( $\epsilon$ ) for *p*NA of 6026  $\text{cm}^{-1} \text{M}^{-1}$  at 405 nm, 3680  $\text{cm}^{-1} \text{M}^{-1}$  at 430 nm and 1380  $\text{cm}^{-1} \text{M}^{-1}$  at 445 nm, to stay within the responsive range of the spectrophotometer. For each assay, the rate of un-catalyzed chemical isomerization was subtracted from the total isomerization rate, of the catalyzed and un-catalyzed reactions, to determine the Pin1-catalyzed *cis-trans* isomerization. The rate against the substrate concentration was plotted to determine a  $k_{\text{cat}} / K_{\text{m}}$  value, by fitting the values to a modified Michaelis-Menten equation for competitive inhibition, where only the linear region of the curve is used due to low substrate concentrations. The equation used is:

$$\text{Rate} = (k_{\text{cat}} / K_{\text{m}}) * [\text{S}] [\text{E}]_{\text{T}}$$

where  $[S]$  is the substrate concentration,  $[E]_T$  is the enzyme concentration, the slope of the line gives the  $k_{cat} / K_m * [E]_T$ , and the  $k_{cat} / K_m$  is determined by dividing the slope by the final Pin1 protein concentration in the assay.

## 2.4 *Amino acid analysis*

Samples of soluble Pin1 protein, obtained from the GST-Pin1 construct, and 0xP and 2xP peptides were sent for quantitative amino acid analysis to the Peter Gilgan Centre for Research & Learning at the Hospital for Sick Children (SPARC Biocenter, Toronto). The protein samples were quantified by Bradford and Guanidine-hydrochloride assays, comparing the protein to BSA standards or measuring an absorbance reading at 280 nm, respectively. The protein and peptide samples were all to be used for NMR experiments.

## 2.5 *Analytical ultracentrifugation*

A Beckman Optima XL-A analytical ultracentrifuge (Biomolecular Interactions and Conformations Facility, University of Western Ontario) was used to perform these experiments, with an An60Ti rotor. All protein and peptide samples used were dialyzed into 2x HBS buffer and spun down at 13,000 rpm to remove aggregates before AUC data collection. The solvent densities used were calculated from published tables. The protein sample partial specific volumes were calculated based on their amino acid sequences<sup>120</sup>.

### 2.5.1 *Sedimentation velocity*

Two sector cells with quartz windows were used to complete the sedimentation velocity experiments. Data were collected for the wild type Pin1 protein at a

concentration of 15  $\mu\text{M}$  and a speed of 45,000 rpm. Scans of all cells were taken every ten minutes, and averaged over three readings.

Data analysis was performed using the Origin 6.1 software (Microcal) and SVEDBERG<sup>121</sup>. Sedimentation coefficients ( $s_w$ ) were calculated using the method of sedimentation time derivative. Values were averaged from three separate sedimentation velocity runs and were then corrected to standard values for experiments conducted at 20  $^{\circ}\text{C}$  and in pure water ( $s_{w_{20,w}}$ ). The frictional coefficient ( $f$ ) of 1.399153 used in the experiments was calculated from the measured  $s_{w_{20,w}}$  according to the following equation:

$$f = [M * [(1 - \tilde{v}\rho)] / (N * s_{w_{20,w}})]$$

where  $M$  is the molecular mass of the protein,  $\tilde{v}$  is the partial specific volume of the protein,  $\rho$  is the density of the buffer and  $N$  is Avogadro's number.

## 2.6 *Circular dichroism spectropolarimetry*

Circular dichroism experiments were conducted using a Jasco J-810 spectropolarimeter with a Peltier temperature controlled system (Biomolecular Interactions and Conformations Facility, University of Western Ontario). A cell with a path length of 1 mm was used after Pin1 protein, obtained from the GST-Pin1 construct, and protein-peptide solutions were dialyzed into a 10 mM sodium phosphate buffer (100 mM  $\text{Na}_2\text{SO}_4$ , 5 mM  $\text{NaN}_3$ , 5 mM EDTA and 1 mM DTT, pH 6.6) and spun down to remove precipitants.

CD spectra were collected for recombinant Pin1 proteins used for NMR experiments. The protein concentration was 48  $\mu\text{M}$  and the CD experiments were conducted at 25  $^{\circ}\text{C}$ , scanning from 180 - 250 nm in 1 nm steps, and at a scanning speed of 50 nm/min. When a protein-peptide sample was measured, either 0xP or 2xP peptide was added at two equivalents of the protein. The ellipticity values were generated from averaging readings taken between one and four seconds at each wavelength and then averaged over ten separate scans of each sample. The software supplied by Jasco was used for data collection, and then plotted using Excel (Microsoft). The observed ellipticity values, given in millidegrees, were converted to mean residue ellipticity (MRE) values in  $\text{degree}\cdot\text{cm}^2\cdot\text{dmol}^{-1}$  as the units. This conversion is achieved using the equation:

$$\Theta_{\text{mre}} = (\Theta_{\text{obs}} * \text{MRW}) / (10 * l * c)$$

where  $\Theta_{\text{mre}}$  is the mean residue ellipticity,  $\Theta_{\text{obs}}$  is the observed ellipticity value in millidegrees, MRW is the mean residue weight which is calculated based on the molecular weight of the protein divided by the number of residues within the protein,  $l$  is the path length of the CD cuvette in centimeters and  $c$  is the protein concentration in  $\text{g}\cdot\text{mL}^{-1}$ .

Recombinant Pin1 was also analyzed with melting curves. The protein, at a concentration of 48  $\mu\text{M}$ , was melted by increasing the temperature at a rate of 1 $^{\circ}\text{C}$ /minute using the Peltier system. The curve ranged from 20 to 90  $^{\circ}\text{C}$ . When a protein-peptide sample was measured, either 0xP or 2xP peptide was added at two equivalents of the protein. Ellipticity values were obtained by averaging the readings taken over an eight second time frame at 228 nm. The observed ellipticity values, given in millidegrees,

were converted to mean residue ellipticity values in degree\*cm<sup>2</sup>\*dmol<sup>-1</sup> as the units. The resulting curves were plotted in Excel (Microsoft).

## 2.7 *Pin1-peptide NMR titrations*

All <sup>1</sup>H-<sup>15</sup>N HSQC NMR experiments were conducted on a Varian Inova 600 MHz spectrometer with pulse field gradient triple resonance probes, at 25 °C. 0xP and 2xP peptides were unlabeled and prepared as 2 mM stock solutions in NMR buffer. The peptides underwent an overnight dialysis at 4 °C to ensure buffer compatibility with the protein solutions. The concentration of the peptide solutions were determined by amino acid analysis (SPARC Biocentre, Toronto). The peptides were titrated separately into solutions of uniformly labeled <sup>15</sup>N- Pin1 (322 μM) in increments of 0.25 molar equivalents, until a final peptide concentration of 2 molar equivalents was reached. The sample was mixed at each addition and equilibrated in the magnet for a minimum of 10 mins prior to data acquisition. <sup>1</sup>H and <sup>15</sup>N chemical shift assignments for Pin1 were transferred from Jacobs *et al.*, BMRB 5305<sup>122</sup>. Chemical shift perturbations observed in the <sup>1</sup>H-<sup>15</sup>N HSQC spectra between the free and complexed states of the protein were quantified using the equation:

$$\Sigma\Delta\delta = 0.5(|\Delta\delta(^1\text{H})|) + 0.125 (|\Delta\delta(^{15}\text{N})|)$$

where  $\Delta\delta$  is the chemical shift change.

The combined chemical shift changes were calculated for the entire Pin1 protein, based on the above equation from Duncan *et al.*, 2011<sup>79</sup>. The chemical shift changes observed, were mapped to Pin1 using the coordinates from the 1PIN crystal structure.

## 2.8 *Fluorescence polarization experiments*

All peptides were fluorescently labeled with NHS-Fluorescein (Pierce Biotechnology, Inc.) following the manufacturer's protocol. Peptides were dissolved at 150  $\mu$ M in 50 mM borate buffer, pH 8.5. Briefly, NHS-Fluorescein (1 mg in 100  $\mu$ L DMSO) was added in a 15-fold molar excess to the peptide. The reaction was incubated at room temperature for one hour and excess label was consumed with a 30-fold molar excess of ethanolamine, pH 8.5. Peptides were dialyzed into 2x HBS (280 mM NaCl, 50 mM HEPES, 12 mM Dextrose, 10 mM KCl, 1.5 mM Na<sub>2</sub>HPO<sub>4</sub>, pH 7.0) and labeling was confirmed using MALDI Mass Spectrometry (MALDI Mass Spectrometry Facility, part of the London Regional Proteomics Centre, Ontario). Peptides were stored in the dark during all of the labeling and subsequent steps.

Fluorescence polarization assays were read using an Envision 2103 multi-plate reader (PerkinElmer). Optimal dilutions for each peptide were determined with the use of a reference peptide to give off a fluorescent signal within range of the detector. These dilutions were confirmed and used in all future experimentation. Individual reactions were conducted in duplicate, in a 35  $\mu$ L volume, using a 384-well black plate (Corning). The protein was serially diluted from a concentration of 800  $\mu$ M and 30  $\mu$ L of protein was added to each well. Finally, 5  $\mu$ L of 150  $\mu$ M peptide was added to each well before a 1 min incubation time with agitation (500 rpm) at room temperature. Before reading the assay, the plate was spun for 1 min at 100 x g and incubated for an additional 10 mins at room temperature. Analysis was performed using Prism 5 (GraphPad Software, Inc.) by subtracting the buffer sample polarization and the polarization associated with non-specific binding between the protein and the fluorescent tag. The data was then fit to a

non-linear regression for one-site, specific binding as a function of protein concentration.

The equation used for data fitting was as follows:

$$y = B_{\max} * x / (K_d + x)$$

where  $B_{\max}$  is the maximum specific binding value in fluorescence polarization units and  $K_d$  is the dissociation constant ( $\mu\text{M}$ ).

## 2.9 *Pin1* crystallization

Arg14Ala Pin1 and Arg14Ala Cys113Asp Pin1 constructs were crystallized by hanging drop vapour diffusion over three days in 2.3 and 2.4 M ammonium sulphate, 1% (v/v) polyethylene glycol 400 (PEG400) and 100 mM HEPES at 5 °C, pH 7.8.

## 2.10 *X-ray crystallography data collection and structure refinement*

Electron diffraction data was collected using a laboratory source in the Macromolecular Crystallography Facility (part of the London Regional Proteomics Centre, Ontario). The data was processed using IMOSFLM<sup>123</sup> and Scala<sup>124</sup>. Structure solution and refinement was done by molecular replacement in PHENIX<sup>125</sup> using the PDB file 2ITK<sup>107</sup>, after ligand removal, as the starting model for the Arg14Ala Cys113Asp Pin1 structure, and the PDB file 4QIB<sup>126</sup> as the model for the refinement.



## 3. Results

### 3.1 Protein purification and activity

Recombinant Pin1 proteins were purified in order to examine binding interactions between Pin1 and CDC25C-derived peptides. Various His-Pin1 recombinant protein constructs were purified by affinity purification using nickel columns where His-tagged proteins were eluted with imidazole. To remove the His-tags, eluted proteins were incubated with TEV using a reducing agent to stabilize protease activity. Since the TEV also contains a His-tag, the cleaved Pin1 was separated from His-TEV and any un-cleaved His-Pin1 by passing the reaction mixture over another nickel column (**Figure 5A**). Following the removal of the tags using TEV protease, the proteins were dialyzed into their final storage buffers. A wild type Pin1 construct was also fused to a GST-tag (GST-Pin1) and purified first using affinity chromatography, then TEV cleavage and a gel filtration step (not shown). None of the proteins used in the experiments described in the following sections contained tags.

To determine the isomerization activity of the purified proteins, a peptidyl-prolyl isomerization activity assay was performed using Suc-AEPF-*p*NA as a substrate, containing a *para*-Nitroaniline (*p*NA) on the C-terminus. The substrate peptide is added to the assay buffer to determine a baseline absorbance at 405 nm. Chymotrypsin is then added to remove all of the *trans* isomers of the substrate, releasing *p*NA which can be detected spectrophotometrically. Following the *trans*-peptide cleavage, the absorbance curve flattens and generates a positive slope, representing the un-catalyzed chemical isomerization rate of the substrate. From there, recombinant Pin1 is added to the reaction mixture and the absorbance curve shows a linear slope while the peptide is still in excess.

This slope depicts the catalyzed isomerization rate generated by Pin1 in addition to the un-catalyzed chemical isomerization rate. The substrate continues to be depleted by Pin1 as well as chymotrypsin, until it has all been utilized. The absorbance value at the point of Pin1 addition is subtracted from the absorbance value at the end of the curve to calculate the concentration of peptide within the system when protein is added. The slope of the un-catalyzed isomerization is subtracted from the slope of both the catalyzed and un-catalyzed isomerizations, to determine the enzymatic peptidyl-prolyl isomerization rate of Pin1 (**Figure 6**). This process is repeated to calculate the isomerization rate of Pin1 using increasing substrate concentrations and the data is graphed as the Pin1 isomerization rate, in mM/s units, as a function of *cis*-peptide concentration. The linear slope from this plot, in  $s^{-1}$  units, is divided by the concentration of protein in the assay to obtain a specificity constant or  $k_{cat}/K_m$  value in  $mM^{-1} * s^{-1}$  units (**Figure 5B**).

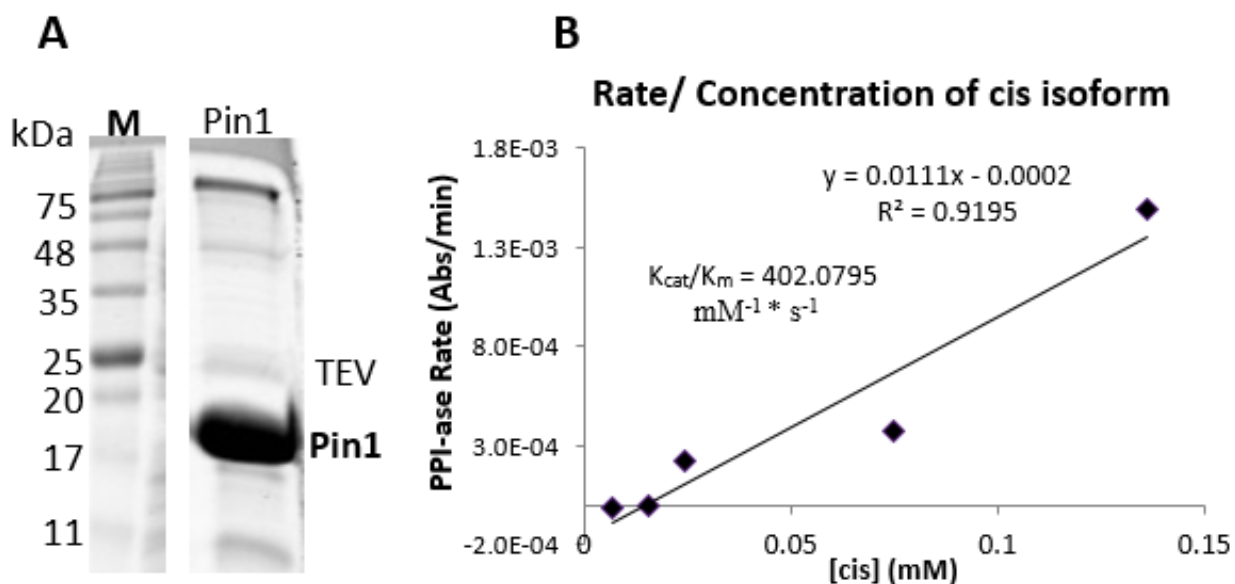


**Figure 5 Purified recombinant Pin1 protein and peptidyl-prolyl isomerase activity.**

(A) SDS-PAGE of purified wild type His-Pin1 protein. Pin1 is approximately 18 kDa and the His-TEV protein runs at a higher molecular weight on a polyacrylamide gel, depicted by the band labeled TEV in the figure. Other His-Pin1 constructs were purified using a similar affinity purification protocol (gels not shown).

(B) Peptidyl-prolyl isomerase assay analysis of a wild type Pin1 construct. The assay is conducted with increasing amounts of substrate to determine an isomerization rate. The  $k_{cat}/K_m$  value is representative of the activity of the Pin1 enzyme.

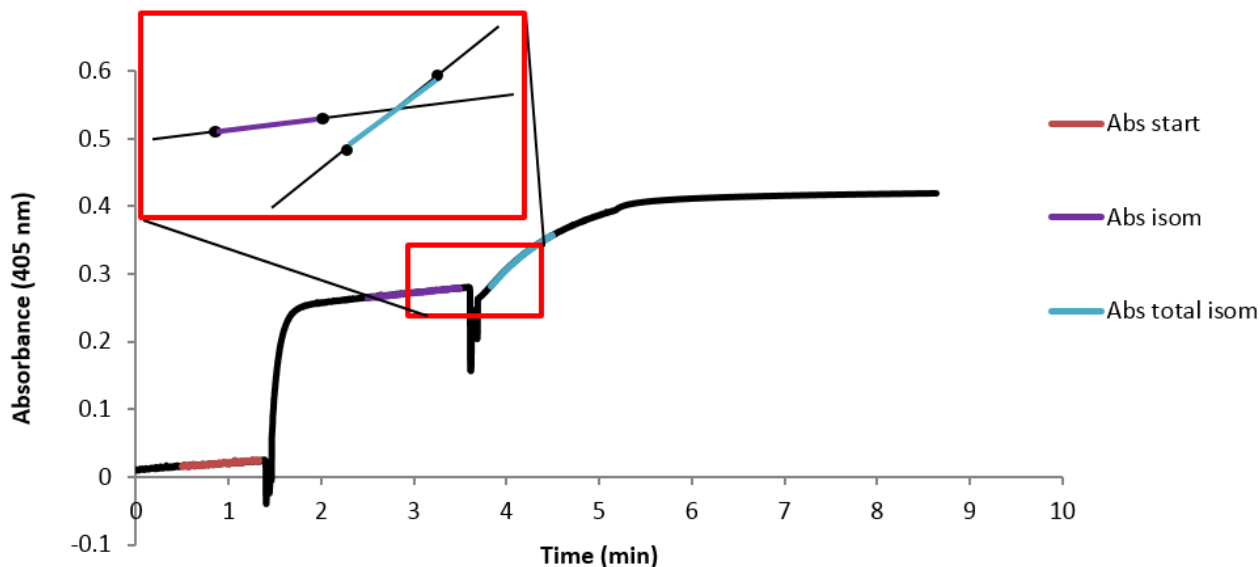


**Figure 6 Pin1 peptidyl-prolyl isomerization assay sample curve.**

The peptidyl-prolyl isomerization activity of purified Pin1 proteins is determined spectrophotometrically. The peptide Succinyl-AEPF-*p*Nitroaniline (Suc-AEPF-*p*NA) is used as a Pin1 substrate in the assay, and when released the *p*NA, located on the C-terminus of the peptide, can be detected spectrophotometrically. The substrate peptide is added to the assay buffer to determine a baseline absorbance at 405 nm (Abs start). Chymotrypsin is then added, seen by the rapid absorbance increase, to remove all of the *trans* isomers of the substrate. Following the *trans*-peptide cleavage, the absorbance curve flattens and generates a positive slope, representing the un-catalyzed chemical isomerization rate of the substrate (Abs isom). Recombinant Pin1 is added to the reaction and the initial rate of the absorbance curve is measured by fitting a line to the curve, immediately after the point at which Pin1 is added (Abs total isom). This slope represents the catalyzed isomerization rate generated by Pin1 in addition to the un-catalyzed chemical isomerization rate. The absorbance value upon Pin1 addition is subtracted from the final absorbance value of the curve to calculate the concentration of peptide when protein is added. The **inset** shows an expanded portion of the assay curve. Abs isom, the slope of the purple region of the curve, is subtracted from Abs total isom, the slope of the blue region of the curve, to determine the peptidyl-prolyl isomerization rate of Pin1. This process is repeated to calculate the isomerization rate of Pin1 using increasing substrate concentrations. The data is graphed as the Pin1 isomerization rate ( $s^{-1}$ ) when divided by the Pin1 concentration, as a function of *cis*-peptide concentration (mM).

### *3.2 Peptide addition to Pin1 does not cause global conformational changes*

Peptides for this study were synthesized with sequences designed from a known Pin1 substrate, CDC25C (**Table 1**). The peptides depict a portion of the CDC25C protein where there are two phospho-threonine sites in the sequence, 19 amino acids apart, at residues 48 and 67<sup>127</sup>. The non-phosphorylated (0xP), both of the singly-phosphorylated (1xP #1 and 1xP #2) and the doubly-phosphorylated (2xP) CDC25C-derived peptides were used for these experiments (**Figure 7**). Results were generated through the use of analytical ultracentrifugation, a technique that can determine native state stoichiometries of protein subunits and detect conformational changes in macromolecules. The ultracentrifuge contains an optical detection system that can measure the concentration gradient of the enclosed sample within a centrifuge cell<sup>108</sup>. Sedimentation analysis is completed in solution while observing real-time changes, minimizing the risk of protein interactions with resins or other surfaces. The experiments were conducted using sedimentation velocity to detect molecules tumbling together in solution. This technique is used to determine molecular mass and shape in solution when applying a centrifugal force. At given time intervals, scans at various radial distances measure the concentration of a solution based on an absorbance at 280 nm. The rate at which molecules move and sedimentation occurs is measured over time<sup>108,109</sup>.

**Table 1** Cdc25 derived peptides synthesized to test binding affinities to Pin1 protein *in vitro*.

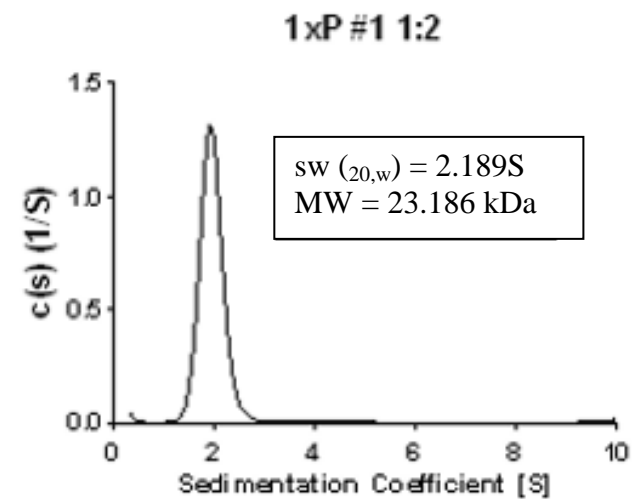
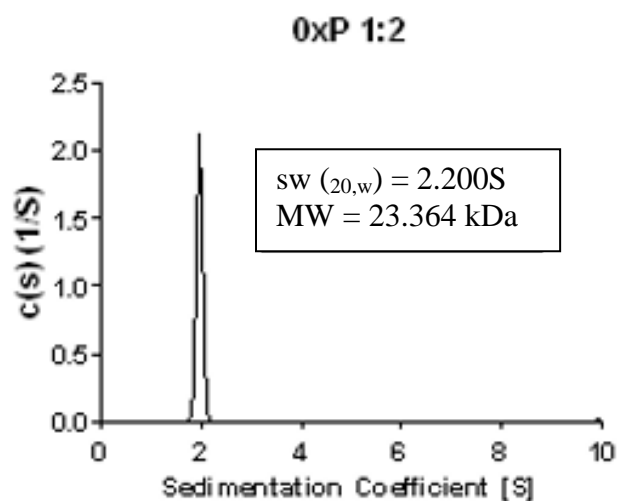
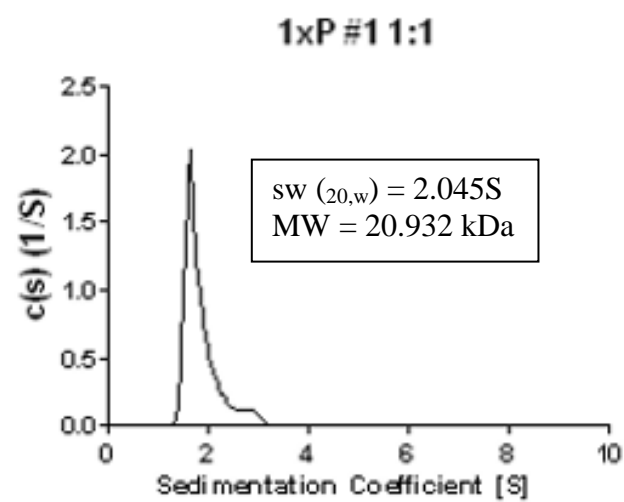
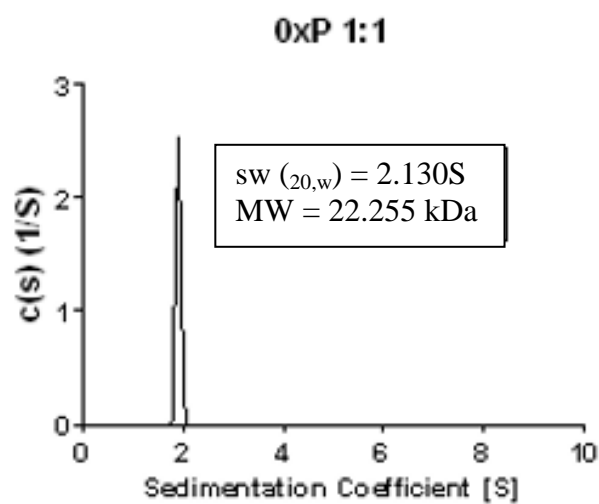
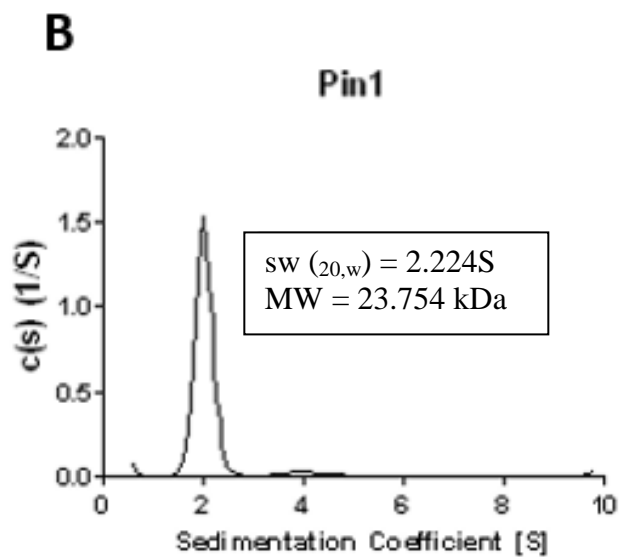
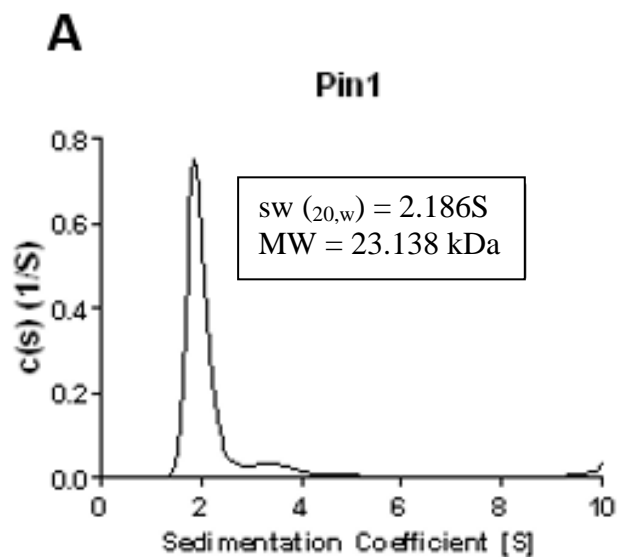
The phosphorylation sites all occur on Thr residues and are depicted in red.

| <u>Human Cdc25 peptide sequence</u>                      | <u>Phosphorylation Site</u> | <u>Shorthand Title</u> |
|--|-----------------------------|------------------------|
| CPDVPRTPVGKFLGDSANLSILSGGTPKRSLD                         | None                        | 0xP                    |
| CPDVPR <p style="color: red;">p</p> T                    | Site #1                     | 1xP #1                 |
| CPDVPRTPVGKFLGDSANLSILSGG <p style="color: red;">p</p> T | Site #2                     | 1xP #2                 |
| CPDVPR <p style="color: red;">p</p> T                    | Sites #1 and #2             | 2xP                    |

Data was collected using wild type Pin1 and each of the CDC25C-derived peptides, in triplicate, at a rotor speed of 45,000 rpm. After each experiment, the values of sedimentation coefficients observed ( $s_w$ ) were calculated, averaged and corrected for temperature effects as well as buffer effects ( $s_{w_{20,w}}$ ). A frictional ratio of  $f/f_0 = 1.399153$  was used for each experiment. Pin1 was mixed with each peptide at molar ratios of 1:1 and 1:2 equivalents of protein to peptide. The experiments resulted in a consistent molecular weight and sedimentation coefficient for the control reaction of Pin1 alone, within error (**Figure 7, first plot in each panel**). Each graph shows the sedimentation coefficient distribution ( $c(s)$ ), in 1/Svedbergs (1/S), of each protein or complex as a function of sedimentation coefficient, in Svedbergs (S). When mixed with the non-phosphorylated peptide, the Pin1-peptide complex gives a narrowed peak and a slight decrease in sedimentation coefficient at a ratio of 1:1, but this value increases back to original levels at a ratio of 1:2, whereas the peak stays narrow (**Figure 7A**). The Pin1-1xP #1 complex displays an increasing sedimentation coefficient as the amount of peptide in the sample is increased (**Figure 7B**). The peaks however exhibit the same trend as that observed for 0xP, a narrowing when peptide is added. The singly-phosphorylated site #2 peptide set of experiments generated the largest sedimentation coefficients. The coefficient decreases when peptide is added to Pin1 and then increases when more peptide is added. The peaks observed for Pin1 and the 1:1 ratio of protein to peptide are similar in width, but the peak narrows with an increase in peptide (**Figure 7C**). The sedimentation coefficients and narrow peaks for the 2xP peptide set of experiments display no change when peptide is added to the protein (**Figure 7D**). This is indicative of a folded, homogeneous sample in solution. The sedimentation coefficients

of all the protein-peptide complexes fall within range of the control protein alone samples, where the  $sw_{20,w}$  values are 2.05 – 2.25 S. It is important to note that the molecular weights (M) are calculated based on sedimentation coefficients, where  $sw$  is approximately  $M^{2/3}$ , indicating that the masses are subjected to a larger standard error<sup>109</sup>. Taken together, the changes occurring when the CDC25C-derived peptides are mixed with wild type Pin1 are minimal and there are therefore no large global conformational changes seen with peptide addition.





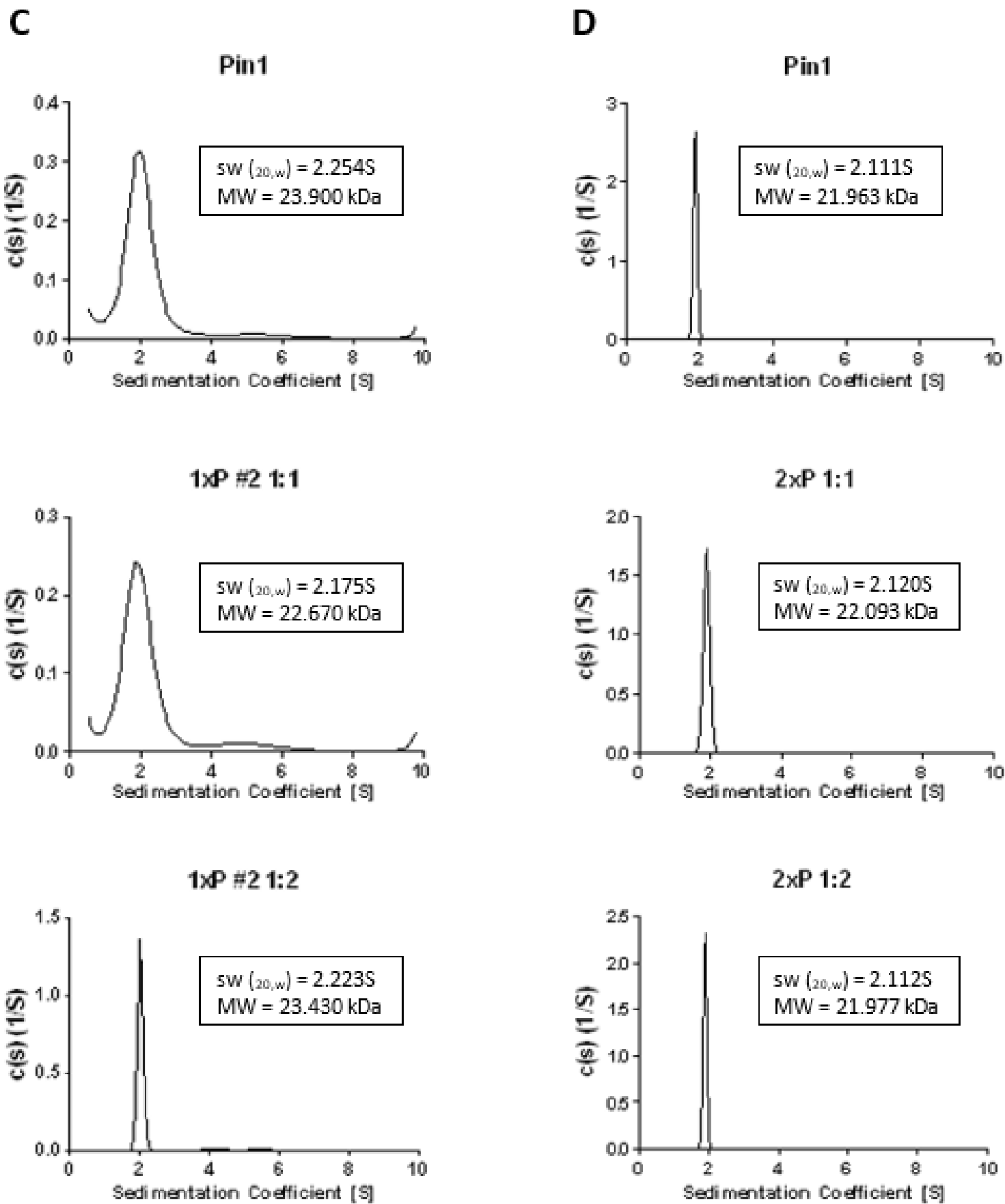


**Figure 7 Sedimentation velocity experiments of Pin1 with CDC25C-derived peptides.**

The non-phosphorylated 0xP peptide (**A**), singly-phosphorylated peptides at site #1 (**B**) and site #2 (**C**) and the doubly-phosphorylated 2xP peptide (**D**) were each mixed with Pin1 (15  $\mu$ M) in either a 1:1 or 1:2 ratio of protein to peptide. The sedimentation velocity experiments were conducted at a speed of 45,000 rpm and scans of all cells were taken every ten minutes, and averaged over three readings. Sedimentation coefficients ( $s_w$ ) were calculated using the method of sedimentation time derivative. Values were averaged from three separate sedimentation velocity runs and were then corrected to standard values for experiments conducted at 20 °C and in pure water ( $s_w(20,w)$ ). The frictional coefficient ( $f$ ) used in the analysis was 1.399153. Protein alone was used as a control in each experiment and is shown in the first graph of each panel.

### 3.3 *Pin1 stability does not change with peptide addition*

Pin1 protein alone, as well as protein with either 0xP or 2xP peptide were examined using circular dichroism. CD spectropolarimetry is a technique used to observe peptide backbone amide bonds and aromatic side chains by measuring the differences between left and right handed circularly polarized light in chiral molecules<sup>110</sup>. Protein amides have chromophores that can align into arrays, and when aligned, the optical transitions produced can be split into many transitions with different wavelengths and intensities associated to each. Secondary structural elements have distinct CD spectra as a result of these transitions<sup>111</sup>. The protein and protein-peptide complexes in the present study show similar  $\alpha$ -helical and  $\beta$ -sheet secondary structures, defined by the large negative curves between 212 and 250 nm (**Figure 8A**). The positive trends occurring from 180 to 208 nm which depict  $\alpha$ -helices with a strong peak at 193 nm and  $\beta$ -sheets with a weaker peak at 195 nm<sup>111</sup>, indicate that there may be some variation in secondary structure between the samples, because none of the plots have the same mean residue ellipticity values at each wavelength (not shown).

The stability of each complex was then tested by thermal melting, as secondary structural features can be denatured by high temperatures<sup>112</sup>. CD can be used to follow protein and protein-peptide stability by examining a specific wavelength and the spectral changes occurring in response to temperature. The melting temperatures for Pin1 and the protein-peptide complexes remain the same, starting to melt at 50 °C and unfolding until 60 °C when the protein is denatured (**Figure 8B**). There are visible transitions in the thermal denaturation profiles due to the loss of secondary structural elements. Observing the same thermal melting profiles for each of the samples is indicative of a constant

stability. The CDC25C-derived peptides therefore do not seem to have any major effect on Pin1 protein stability in solution.

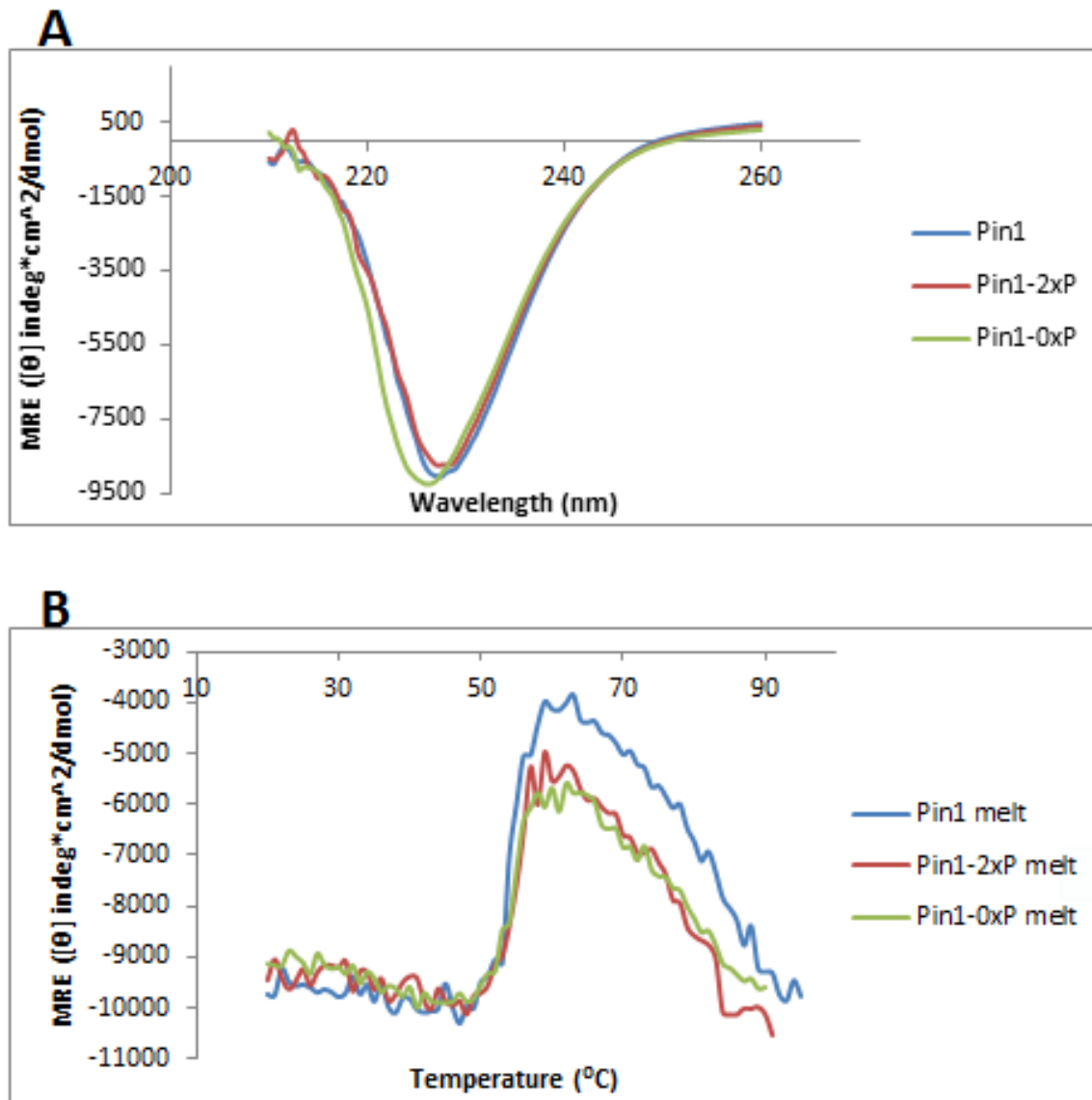


**Figure 8 Secondary structure and thermal stability analysis of Pin1 and Pin1-peptide complexes.**

(A) Circular dichroism spectropolarimetry analysis of Pin1 and Pin1 with either 0xP or 2xP peptide. The spectra were collected from 260 to 180 nm in a 10 mM sodium phosphate buffer (pH 6.6) with 100 mM  $\text{Na}_2\text{SO}_4$ , 5 mM  $\text{NaN}_3$ , 5 mM EDTA and 1 mM DTT at 25  $^{\circ}\text{C}$ , at a rate of 50 nm/min. The depicted spectra are the average of 10 accumulations, corrected for buffer effects based on protein concentration and path length. All spectra were collected in a 1.0 mm cuvette. The x-axis of the plot shows the wavelength while the y-axis of the plot shows mean residue ellipticity (MRE). (B) Thermal denaturation curves were constructed by monitoring changes in ellipticity at 228 nm from 20 to 90  $^{\circ}\text{C}$  in the above sodium phosphate buffer, at a rate of 1  $^{\circ}\text{C}/\text{min}$ . The overlaid spectra are corrected for buffer effects and take protein concentration and path length into account. The x-axis of the plot shows temperature while the y-axis of the plot shows mean residue ellipticity (MRE).

### 3.4 *Pin1 interacts with a phosphorylated CDC25C peptide*

Pin1 protein as well as the Pin1-0xP and the Pin1-2xP complexes were tested for (not shown), binding interactions through the use of  $^1\text{H}$ - $^{15}\text{N}$  HSQC NMR titration experiments. NMR has been used as a tool to investigate protein structures<sup>128</sup> and is based on the premise that atomic nuclei exhibit magnetism when subjected to a magnetic field<sup>113,114</sup>. Resonance occurs when nuclei are re-oriented from their natural equilibrium states by the magnetic field applied. For NMR, a torque or separate magnetic field that is orthogonal to the torque applied by the magnet must be applied to the atoms with both fields having the same frequency<sup>115</sup>. The strength of the second magnetic field is proportional to the resonant frequency of a sample, and determines the amount of magnetization when atomic nuclei are in thermal equilibrium<sup>116</sup>. Short pulses of a transversely oscillating field are applied to a sample in order to obtain free induction decay information, based on the voltage induced by the absorption of energy. The oscillations are visible in the time domain of the FID, and when a Fourier transform is performed on the data, a spectrum is generated in the frequency domain<sup>116</sup>.

The resonant frequencies of the atomic nuclei within a sample are dependent on the location of each nucleus within the magnetic field. The location of a nucleus, and therefore the corresponding resonant frequency, is the critical information gathered when a sample is subjected to a torque within a field<sup>116</sup>. The chemical environment, as well as other nuclei surrounding a particular nucleus, will affect which frequencies are absorbed<sup>115</sup>. Distance measurements between the nuclei in a sample are useful for the determination of a protein structure.

HSQC experiments relate nitrogen atoms and amide protons, which are characteristic of all amino acid peptide bonds excluding proline. Each amide in the backbone of a protein, and side chains containing protons bound to nitrogen atoms, generate a peak in an HSQC spectrum<sup>117</sup>. Hydrogen nuclei have the largest gyromagnetic ratios and are therefore the most sensitive atoms to use for NMR<sup>118</sup>. In an HSQC experiment, the hydrogen atom signal is detected in the first dimension, which is directly measured, and the chemical shift of <sup>15</sup>N is indirectly measured throughout the series of one experiment. The relaxation time associated with an experimental series is increased to obtain the most information out of a single experiment<sup>115</sup>.

NMR spectroscopy studies were conducted at 25 °C and the buffers and experimental conditions were modeled based on the paper by Duncan *et al.*<sup>79</sup>. The doubly-phosphorylated 2xP peptide was titrated into solutions of uniformly, isotopically labeled <sup>15</sup>N- wild type Pin1, until a final peptide concentration of 2 molar equivalents was reached. <sup>1</sup>H and <sup>15</sup>N chemical shift assignments for Pin1 were transferred from Jacobs *et al.*, BMRB 5305<sup>122</sup>.

Chemical shift changes are observed when Pin1 and 2xP are mixed in solution, at different ratios of protein to peptide, up to a ratio of 1:2. **Figure 9A** shows the HSQC spectrum of Pin1 protein depicted by black peaks (**Figure 9A** – left panel) and the final titration spectrum of Pin1 with 2xP peptide depicted by green peaks (**Figure 9A** – right panel). The spectra are overlaid (**Figure 9A** – bottom panel) and residues that display visible peak shifts are labeled. The unassigned side chain peaks visible in the spectra are circled and indicated. When comparing the <sup>1</sup>H-<sup>15</sup>N HSQC spectra for <sup>15</sup>N-labeled Pin1, with and without 2xP peptide, 91 total peaks corresponding to backbone amide bonds

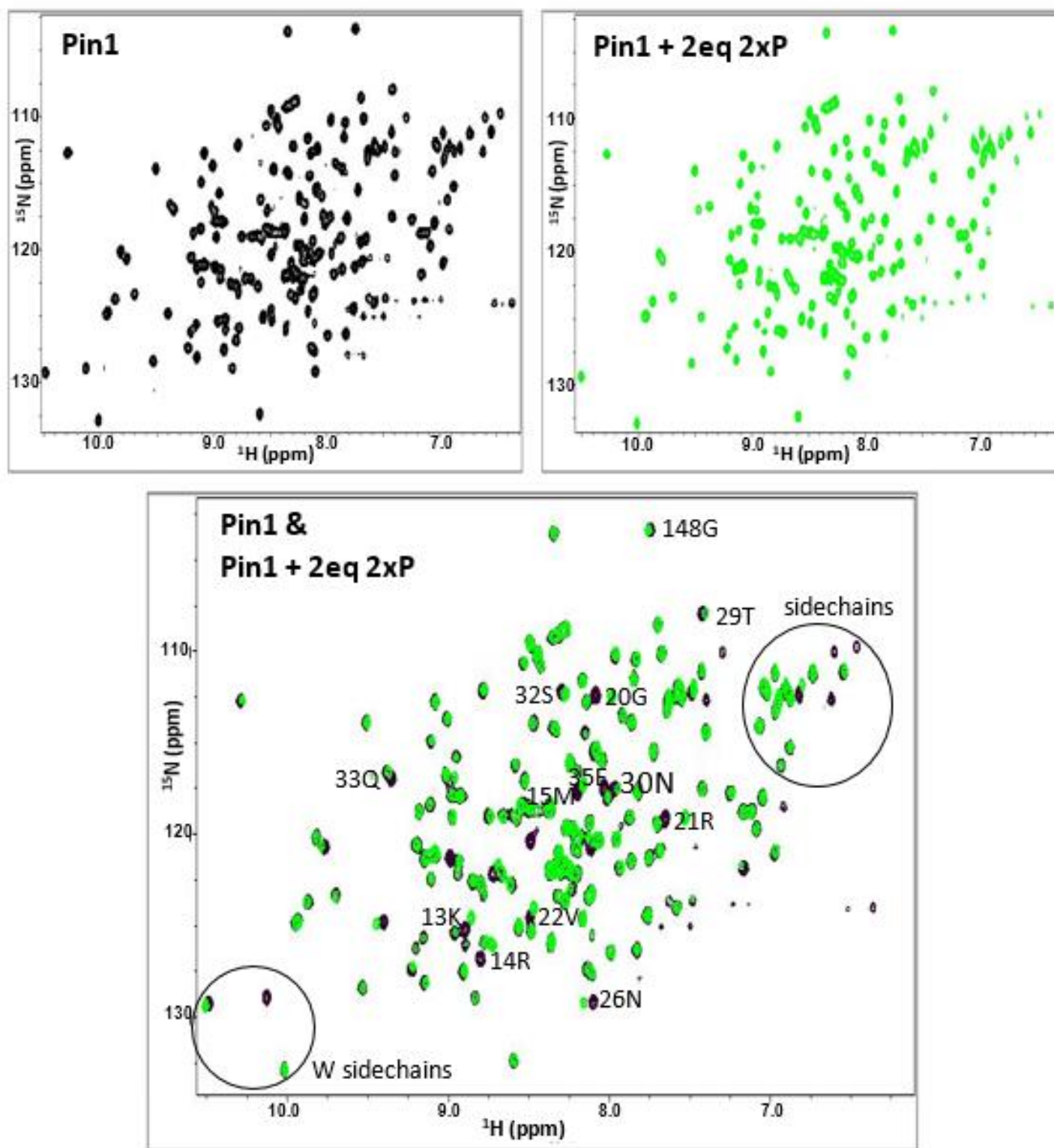


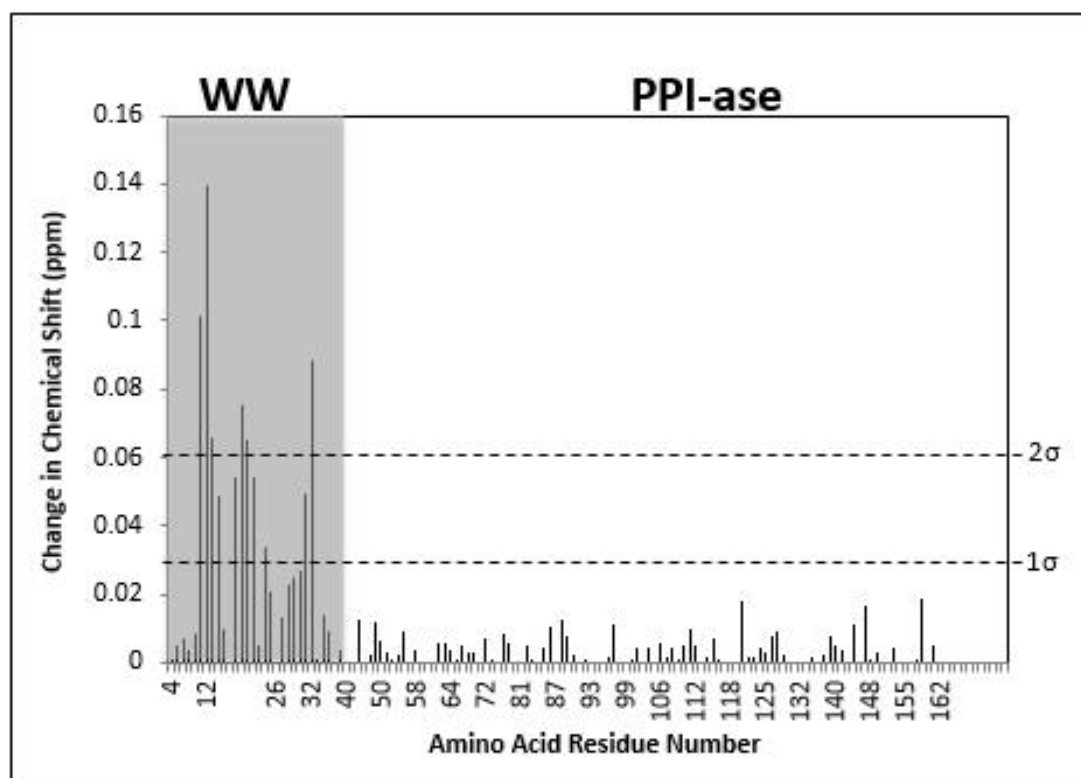
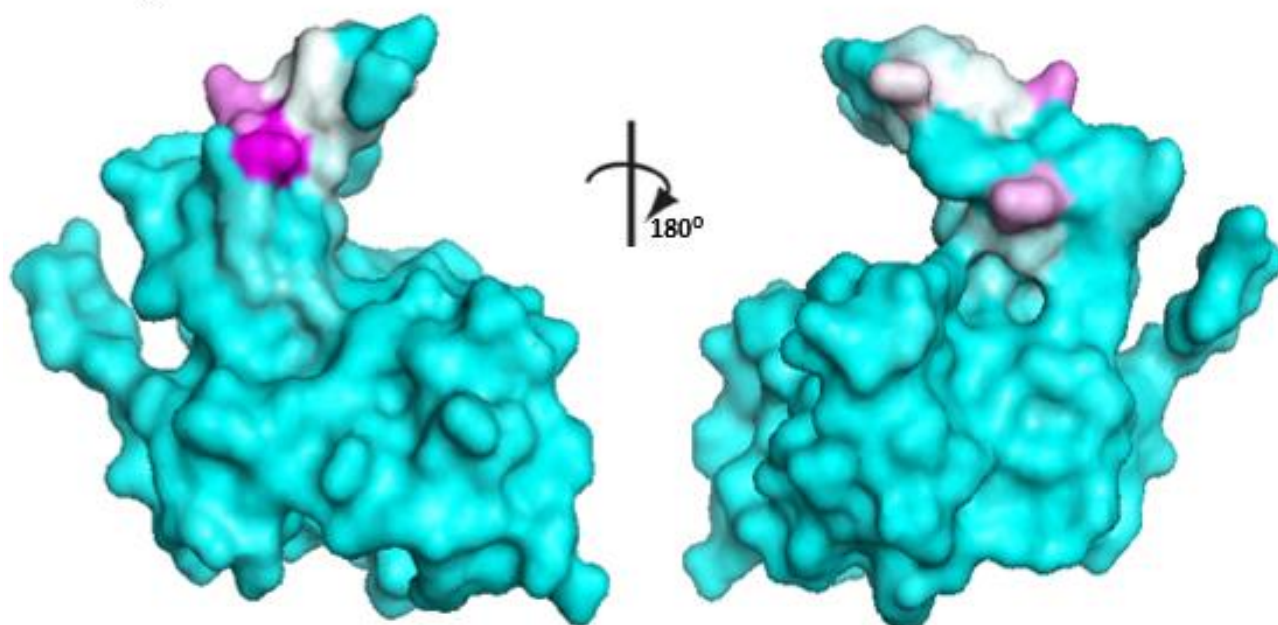
were revealed (**Figure 9B**). There are eleven peaks that shifted significantly in their position, indicative of a chemical shift greater than a  $1\sigma$  change, all of which are located in the WW domain of Pin1. Six of the aforementioned peaks show shifts greater than a  $2\sigma$  change. These peaks underwent fast exchange and could therefore be tracked throughout the titration experiments.

To appropriately define the main region of interaction between Pin1 and the doubly phosphorylated peptide, the chemical shift changes observed when 2xP peptide was bound to Pin1 were mapped to the three-dimensional (3D) structure of Pin1 according to their magnitudes (**Figure 9C**). Residues are coloured using a gradient from cyan, representing little or no chemical shift change, to white to magenta, representing the largest chemical shift change. This result confirms that the WW domain of Pin1 is in fact the dominant binding domain in the protein.

Notably, residue Arg14 exhibits the largest peak shift, through NMR experiments using wild type Pin1 protein, with a change greater than  $4\sigma$ , while the amino acids surrounding the arginine (Lys13, Met15 and Ser16) also show large changes. All peak shifts occurring after residue 35, which corresponds to the protein linker as well as the isomerase domain, exhibited less than a  $1\sigma$  chemical shift change (**Figure 9B**). The residues with the largest peak shifts are predominantly mapped to the WW domain.

A



**B****C**

**Figure 9**  $^1\text{H}$ - $^{15}\text{N}$  HSQC NMR spectra of Pin1 and Pin1-2xP complex with the changing residues plotted and mapped to the 3D structure of Pin1.

NMR spectroscopy titration experiments were conducted using wild type Pin1 and the doubly-phosphorylated 2xP peptide on a Varian Inova 600 MHz spectrometer with pulse field gradient triple resonance probes, at 25 °C. A spectrum of protein alone (322  $\mu\text{M}$ ) was taken before adding in peptide, at 0.25 molar equivalents, to a final concentration of 2 molar equivalents of protein. **(A)** The plots depict protein sample peaks in black (left panel) with the Pin1-2xP at a ratio of 1:2 in green (right panel). The two spectra are overlaid in the bottom panel and residues that display visible peak shifts are labeled by amino acid and number. The peak assignment was done previously and deposited into the BMRB as file 5305<sup>122</sup>. The unassigned side chains peaks are circled and indicated. **(B)** The graph presents the residues that exhibited chemical shift changes in Pin1 when 2xP peptide was added to the sample. The amount of peak shifting in both the  $^1\text{H}$  and  $^{15}\text{N}$  dimensions is depicted on the y-axis and the respective residue number on the x-axis. Dashed lines indicate standard deviations of 1 or 2. The WW domain residues are shaded grey and the chemical shift changes greater than  $1\sigma$  were limited to this domain. **(C)** Residues seen to have chemical shift changes, above 1 standard deviation, upon 2xP peptide addition to Pin1 were mapped to the surface of the full length protein. The residues are coloured according to the magnitude of chemical shift change with cyan depicting no change or little change, white showing some change and the darkest purple showing the largest changes.

Peak intensity changes were also observed in the  $^1\text{H}$ - $^{15}\text{N}$  HSQC spectra. In total, 36 peaks displayed intensity changes greater than a  $1\sigma$  change, with 14 of those peaks having a heightened intensity with increasing amounts of peptide (**Figure 10A**). All peaks exhibiting intensity changes are described to undergo slow or intermediate chemical exchange. These peaks were mapped to the structure of Pin1 (**Figure 10B**) and are visible on both faces of the protein. Many residues from Ser16 to Glu51, located in the WW domain as well as the linker between both Pin1 protein domains, showed peak intensity changes; with clusters of changes occurring from Ser16 to Arg21, Asn26 to Glu36 (both in the WW domain) and Gly39 to Glu51 (in the linker region of the protein). In the PPIase domain, from residue Lys95 to Ser126, there were also a large amount of peak intensity changes; with clusters of changes displayed from Glu100 to Ser105, Ala107 to Cys113 and Arg119 to Gly123. On the C-terminus of the protein, there is a cluster of peak intensity changes from residue Ile156 to Leu160. Of note are the intensity changes on the catalytic Cys113, involved in peptide bond isomerization by Pin1, and Lys122 which is one of the amino acids that binds to the side chain of a substrate Pro.

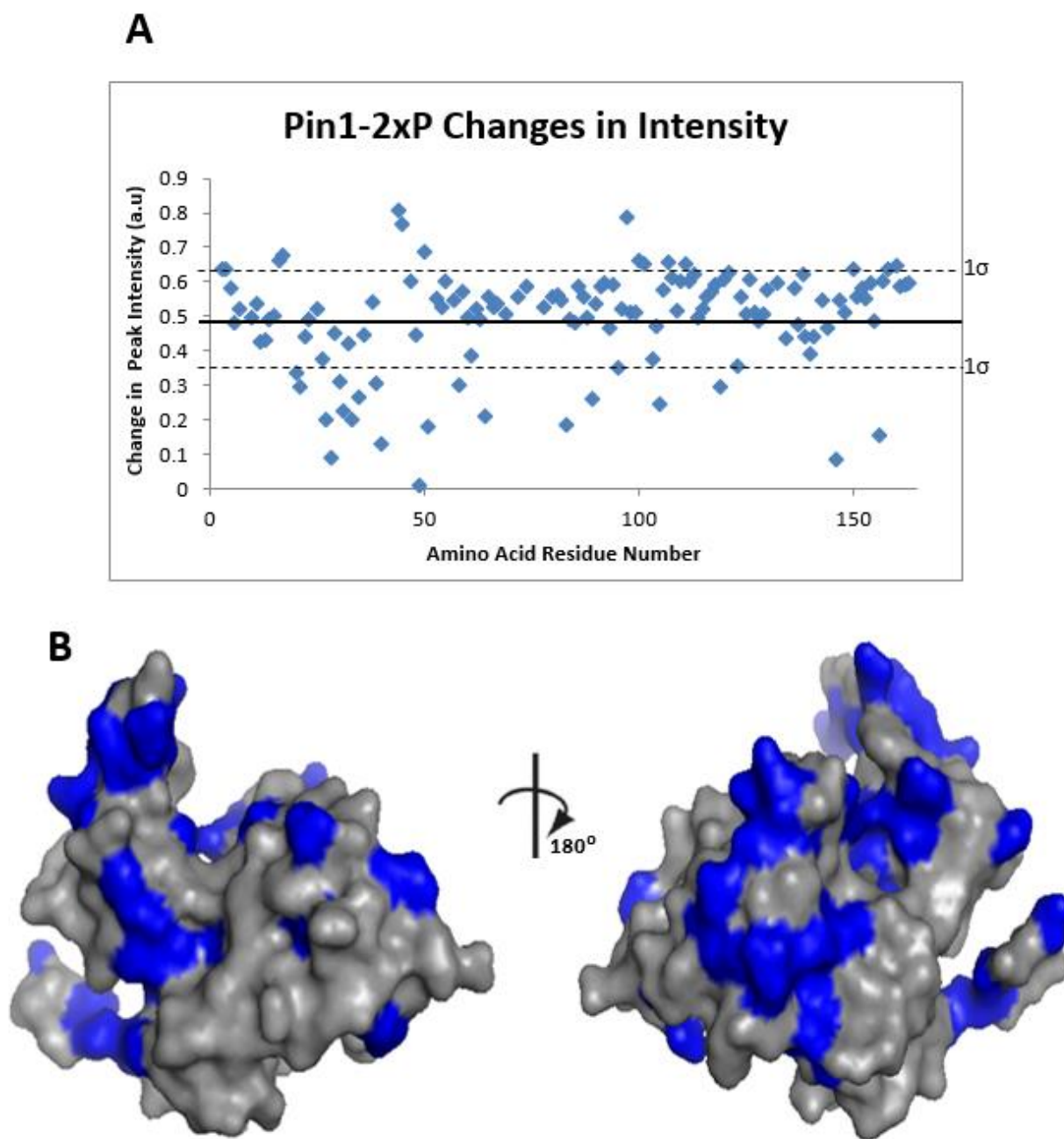


**Figure 10** Pin1-2xP complex intensity changes seen by NMR and their locations mapped to the surface of Pin1.

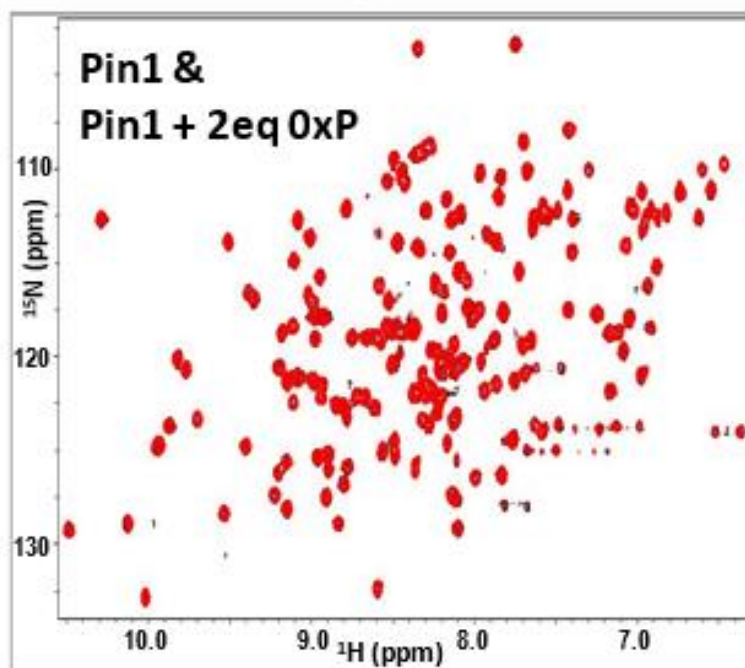
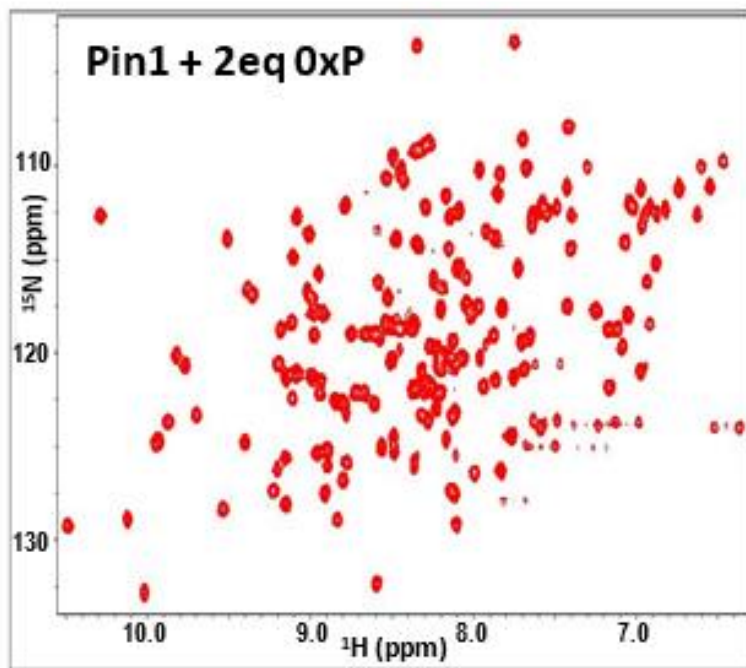
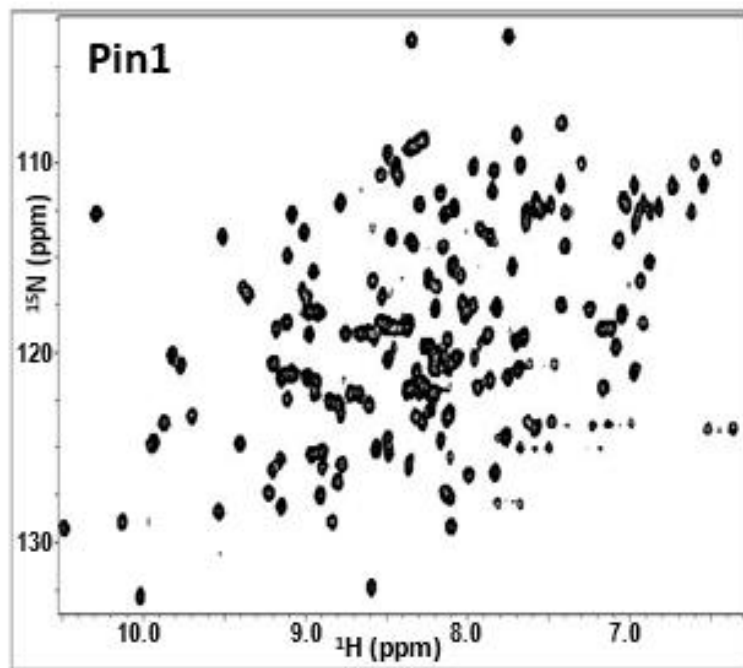
(A) The plot displays residues that underwent changes in intensity when the 2xP peptide was titrated into a solution of wild type full length Pin1. The dashed lines represent a  $1\sigma$  change from the mean, based on the standard deviation of the data. (B) Residues with intensity changes of  $\pm 1\sigma$ , upon 2xP peptide addition to Pin1, were mapped to the surface of the protein (grey). The residues are coloured in blue and are clustered throughout the protein. Both sides of Pin1 are shown.

In summary, binding of the doubly-phosphorylated 2xP peptide derived from human CDC25C brought about critical changes in the WW domain of Pin1, as well as many slow or intermediate exchanges occurring through intensity changes in both the WW and PPIase protein domains. Amino acid residues Gly20, Arg21 and Asn26 in the WW domain were further analyzed in the hopes of determining a binding constant. The plot shows binding curves for the selected residues with corresponding  $K_d$  values (**Appendix Figure A3**).

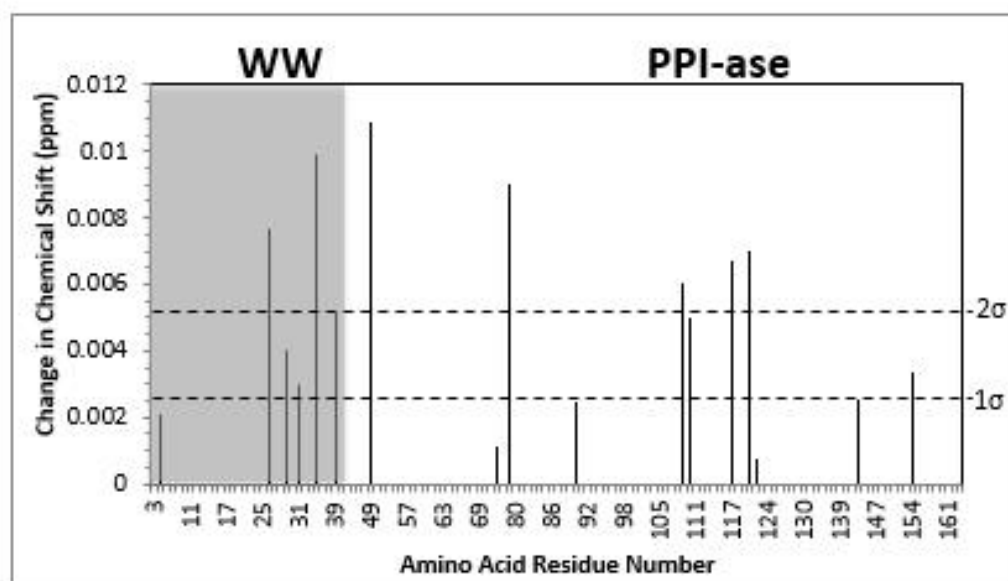
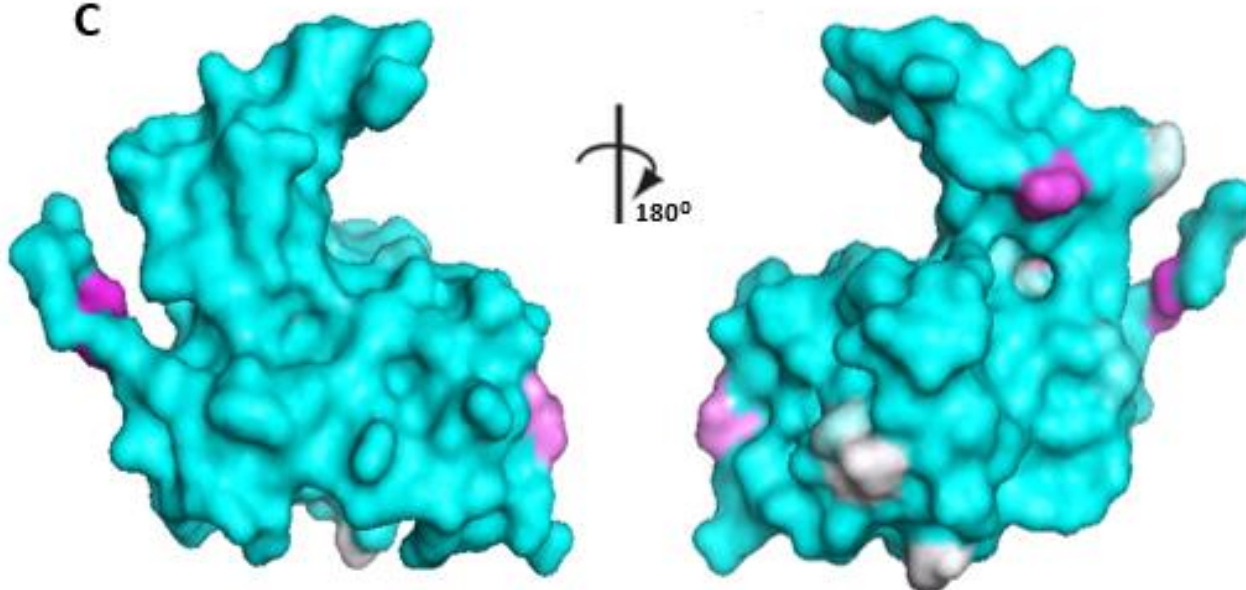
### *3.5 Pin1 does not bind to a non-phosphorylated peptide with high affinity*

Pin1 was also combined with the non-phosphorylated peptide (0xP) and  $^1\text{H}$ - $^{15}\text{N}$  HSQC NMR spectra were collected following each peptide addition. The HSQC spectrum of Pin1 protein is shown as black peaks (**Figure 11A** - left panel), while the final titration point of Pin1 with 2 molar equivalents of 0xP peptide is shown as red peaks (**Figure 11A** - right panel). The spectra are overlaid for comparison of  $^{15}\text{N}$ -labeled Pin1, with and without 0xP peptide (**Figure 11A** – bottom panel). Although little change can be seen, 17 peaks that shifted in position were revealed (**Figure 11B**). Five of the 17 peaks shifted less than a  $1\sigma$  change. Seven peaks shifted greater than a  $2\sigma$  change with residue Gln49 exhibiting the largest chemical shift change, a value greater than  $4\sigma$ . Residue Ser154, known to be involved in peptide bond isomerization, has a chemical shift perturbation of greater than  $1.25\sigma$ . The residues exhibiting chemical shift changes with the addition of 0xP were mapped to the 3D structure of Pin1 (**Figure 11C**), where the residues are coloured using a gradient from cyan, representing little or no chemical shift change, to white to magenta, representing the largest chemical shift change.



**A**



**B****C**

**Figure 11**  $^1\text{H}$ - $^{15}\text{N}$  HSQC NMR spectra and chemical shift data for Pin1 and the Pin1-0xP complex.

NMR spectroscopy titration experiments were conducted using wild type Pin1 and the non-phosphorylated 0xP peptide on a Varian Inova 600 MHz spectrometer with pulse field gradient triple resonance probes, at 25 °C. A spectrum of protein alone (322  $\mu\text{M}$ ) was taken before adding in peptide, at 0.25 molar equivalents, to a final concentration of 2 molar equivalents of protein. **(A)** The plots depict protein sample peaks in black (left panel) with the Pin1-0xP at a ratio of 1:2 in red (right panel). The two spectra are overlaid in the bottom panel, showing virtually no peak shifts. The peak assignment was done previously and deposited into the BMRB as file 5305<sup>122</sup>. **(B)** The graph presents the residues that exhibited chemical shift changes in Pin1 when 0xP peptide was added to the sample. The amount of peak shifting in both the  $^1\text{H}$  and  $^{15}\text{N}$  dimensions is depicted on the y-axis and the residue number is on the x-axis. Dashed lines indicate standard deviations of 1 or 2. The WW domain residues are shaded grey. Both domains have residues with chemical shift changes larger than  $1\sigma$ . **(C)** Residues seen to have chemical shift changes above 1 standard deviation, upon 0xP peptide addition to Pin1, were mapped to the surface of the full length protein. The residues are coloured according to the magnitude of chemical shift change with cyan depicting no change or little change, white showing some change and the darkest purple showing the largest changes.

An additional 24 peaks exhibited intensity changes larger than a  $1\sigma$  change, when 0xP peptide was mixed with the protein (**Figure 12A**). Notably, several of these residues are located in the linker between the WW and PPIase domains. These residues have been mapped to the structure of Pin1 (**Figure 12B**). The results indicate that the affinity of Pin1 to a non-phosphorylated substrate is weak, because few protein residues are heavily impacted by the addition of the 0xP peptide. The linker domain residues exhibit the largest peak intensity changes overall, but neither of the protein domains are affected. In summary, these results indicate that NMR, a commonly used method to detect protein interactions, cannot identify a change in any particular region of Pin1 upon 0xP binding.

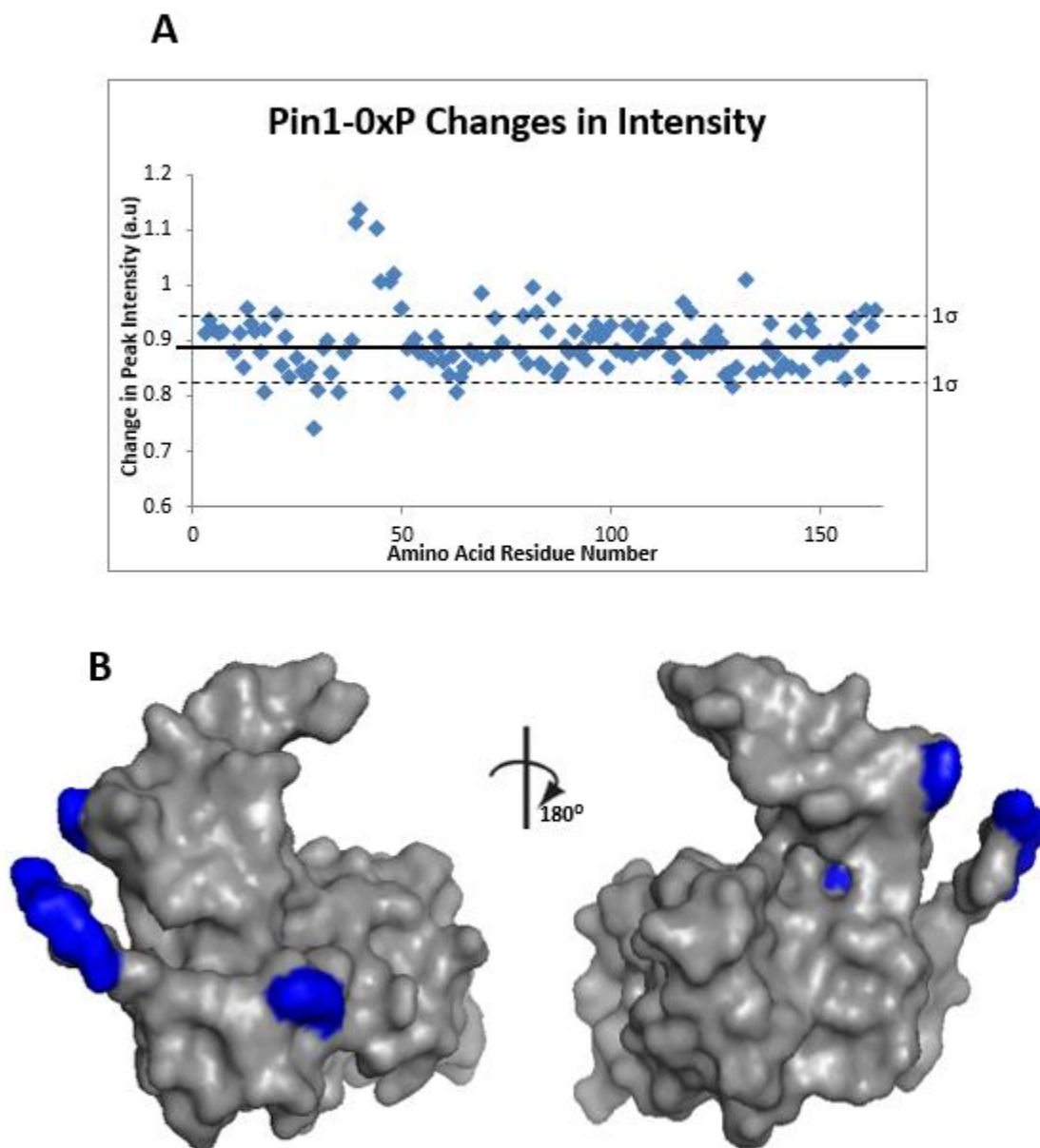


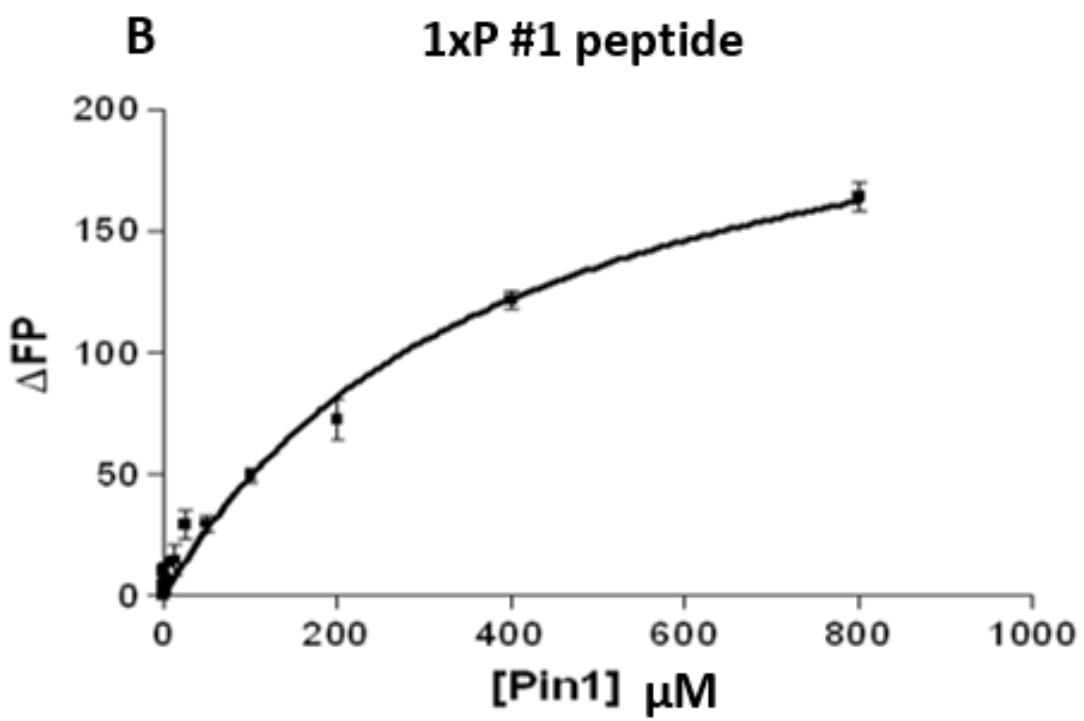
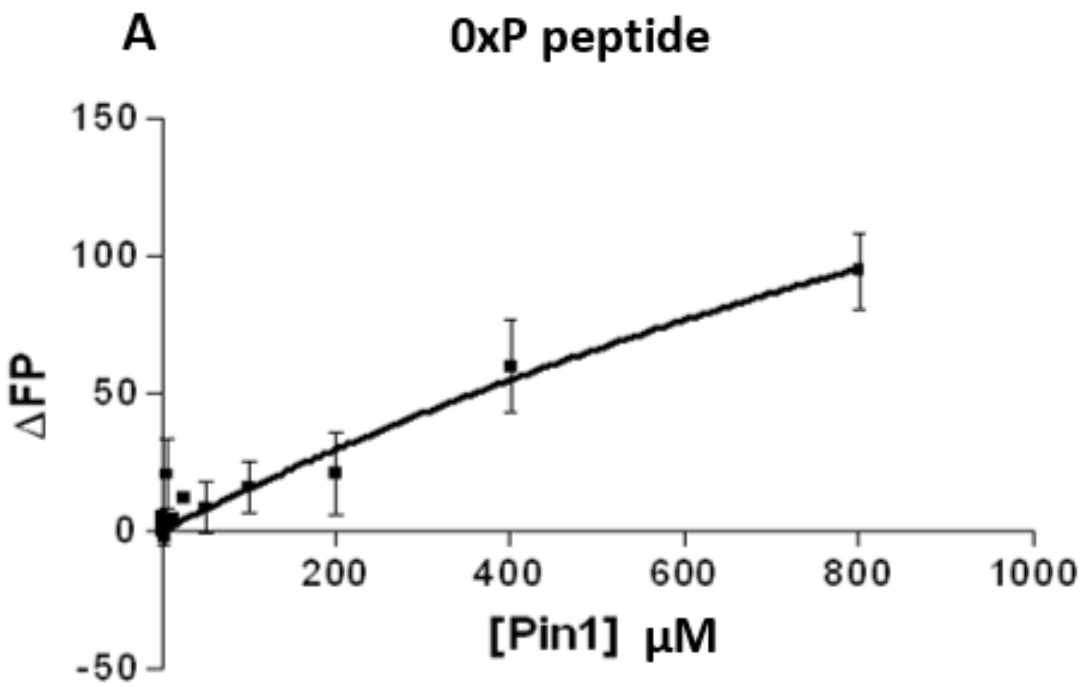
**Figure 12** Pin1-0xP complex intensity changes observed by  $^1\text{H}$ - $^{15}\text{N}$  HSQC NMR and their locations mapped to the surface of Pin1.

(A) The plot displays residues that underwent changes in intensity when the 0xP peptide was titrated into a solution of wild type full length Pin1. The dashed lines represent a  $1\sigma$  change from the mean, based on the standard deviation of the data. (B) Residues shown to have intensity changes  $\pm 1\sigma$ , upon 0xP peptide addition to Pin1, were mapped to the surface of the protein (grey). The residues are coloured in blue and are mostly clustered to the linker region of the protein, between the WW and PPIase domains. Both sides of Pin1 are shown.

### 3.6 *The number of phosphorylation sites affects Pin1-CDC25C peptide interactions*

Dissociation constants from Pin1 binding to CDC25C-derived peptides were calculated through *in vitro* fluorescence polarization assays, using fluorescein-labeled peptides. Fluorescence polarization is a biophysical method used to study protein-protein interactions. FP provides information regarding the binding of a tracer or dye to a protein, in solution. The light emitted by a fluorophore gives off a different intensity compared to excitation light<sup>119</sup>. The former light can be measured and quantified to determine binding of the labeled construct to a protein.

The affinities of labeled 0xP and 2xP are substantially different and can be seen visually as well as determined quantitatively using a curve for specific binding (**Figure 13**). The affinities calculated for both of the singly-phosphorylated 1xP peptides are similar. However, 1xP #2 does have a lower binding constant and therefore Pin1 has a higher binding affinity towards this peptide. The FP experiments for all of the peptides display specific one-site binding curves with the  $K_d$  values depicted in **Table 2**. The data illustrates that an increased number of phosphorylation sites, as well as the location of the site, does impact the interaction between full length Pin1 and the CDC25C-derived peptides.



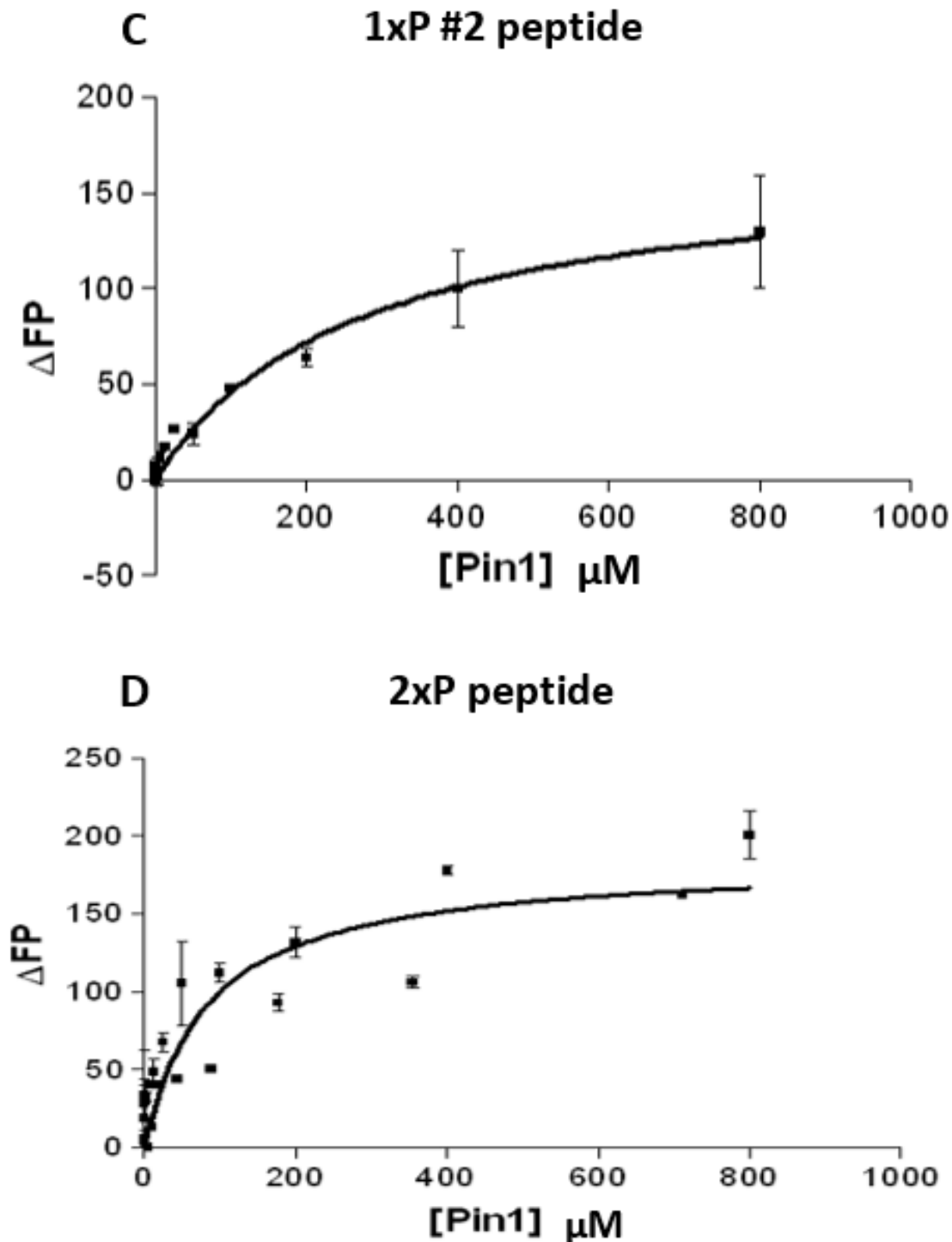


**Figure 13** Fluorescence polarization experiments of Pin1-peptide complexes.

NHS-fluorescein-labeled 0xP (A), 1xP #1 (B), 1xP #2 (C) and 2xP (D) CDC25C-derived peptides were combined with increasing amounts of wild type Pin1 protein to determine a binding constant. Wild type Pin1 was increased by a factor of two per titration point. Each curve is the average of three experiments, completed in duplicate, with error bars representing the standard deviation. Each graph was analyzed using a curve for specific one-site binding, as a function of protein concentration. **Table 2** shows the binding constants determined from analysis of the assays.

**Table 2 Fluorescence polarization experimental results of the human CDC25C-derived peptides synthesized to test binding affinities to Pin1 protein *in vitro*.**

The binding constant ( $K_d$ ) value for each of the Pin1-peptide interactions was tested with NHS-fluorescein labeled peptides, in duplicate for three separate reactions. Each data set was analyzed using a non-linear regression for single-site specific binding, based on the protein concentration.

| <b><u>Shorthand Peptide Notation</u></b> | <b><u><math>K_d</math> (<math>\mu\text{M}</math>)</u></b> |
|--|---|
| <b>0xP</b>                               | 2253  |
| <b>1xP #1</b>                            | 391.6   |
| <b>1xP #2</b>                            | 272.8   |
| <b>2xP</b>                               | 85.21   |



## 4. Discussion

Pin1 is characterized as a dual-domain isomerase, as it is composed of a WW binding domain and a peptidyl-prolyl isomerization domain. Both domains bind to similar pSer/Thr-Pro motifs, which increase the complexity of the system<sup>45,88</sup>. How Pin1 is capable of using this multi-site binding and substrate isomerization to regulate key signal transduction pathways is of utmost importance to aid in targeting diseases such as cancer.

Studies in the field of human Pin1 as a mitotic regulator began with the interaction of NIMA<sup>21</sup>, followed by interactions with CDC25<sup>23,24</sup>. Phosphorylation and Pin1 affect CDC25C, as the phosphatase is subjected to both positive and negative effects of phosphorylation<sup>24,98,129</sup>. Pin1 catalyzes the isomerization of CDC25C which promotes its dephosphorylation. CDC25C then becomes inhibited without the phosphate moiety and early entry into mitosis is stalled<sup>127</sup>. It has been demonstrated that full length Pin1 is necessary for the interaction with CDC25C<sup>95</sup>. Thus, in order to bind both phosphorylation motifs on the substrate at the same time, two sites on Pin1 would be required, potentially one on each domain.

Mitotic regulation by Pin1 can be explained in a two-step mechanism. First, a Ser/Thr-Pro motif becomes phosphorylated by the mitosis-specific activation of a protein kinase. Pin1 is next able to bind to the phosphorylation site and conduct isomerization, to promote a conformational change in the substrate<sup>24</sup>. This change in a phospho-protein can alter binding capabilities, enzymatic activity or function as observed for CDC25<sup>23,24</sup>. Not

only is Pin1 implicated in mitosis, but it has a role in cell proliferation and cancer as well as a role in the reversal of neurodegenerative disorders<sup>38</sup>.

#### 4.1 *Pin1-CDC25C interactions*

The Pin1-CDC25C interaction has been well characterized in the literature<sup>23,88,94,97,104,127</sup>. This association is important in the initiation of mitosis and if unregulated, the overexpression of both proteins separately can result in cancerous phenotypes<sup>8,38,130,131</sup>. The cellular concentrations of both proteins do not fluctuate during cell cycle progression<sup>23,132,133</sup>, in contrast with many proteins involved in the identical processes<sup>134-136</sup>. Preceding mitosis, the interaction is maximal and is mediated by the phosphorylation of CDC25, which activates the pathway. Following activation, the activity of CDC25 is inhibited to similar levels as observed for the phosphatase during interphase<sup>24</sup>. The aforementioned results implicate Pin1 as a regulatory protein in mitosis. Pin1 is suggested to disable the early entry into mitosis, induced by the NIMA kinase. In addition, overexpression of Pin1 generates a mitotic G2 phase arrest phenotype<sup>21</sup>. Not only does Pin1 negatively regulate mitosis, but it positively affects this process as well since it is required for progression through mitosis<sup>23</sup>.

The relationship between Pin1 and CDC25C was first identified through a study of Pin1 interactions with mitotic phospho-proteins<sup>23</sup>. The CDC25C-Pin1 interaction occurs in the presence of both Pin1 protein domains, with each domain in its entirety containing key residues for binding and catalysis. The CDC25C protein is phosphorylated at three Thr sites *in vivo*, Thr48, Thr67 and Thr130<sup>137</sup>, with the former two residues involved in Pin1 binding when phosphorylated<sup>88,127</sup>. A pThr peptide mimicking the human CDC25C sequence surrounding residue Thr48 specifically binds to

the WW domain of Pin1<sup>88</sup>. The peptides generated for the present study were derived using the known Pin1 binding motifs, taken from the protein sequence of human CDC25C surrounding Thr48 and Thr67 which are both pThr-Pro sites<sup>88,127</sup>.

#### *4.2 Effects of peptides on Pin1 global conformation*

As an initial step towards understanding the binding between Pin1 and CDC25C, the CDC25C-derived peptides were mixed with protein and the complexes were used to detect global changes within the protein. The overall conformation of Pin1 in solution did not change with the addition of peptide, measured based on the derived sedimentation coefficients for samples of protein alone and protein-peptide complexes, at molar ratios of 1:1 and 1:2 protein to peptide.

#### *4.3 Protein stability did not change when peptides were added*

The stability of Pin1 was neither increased nor decreased upon addition of the CDC25C-derived peptides, based on the secondary structural elements of the protein and its melting temperature. Of mention from the CD experiments was the noise visible in the spectra ranging from 180 to 210 nm. This noise is caused by a large high tension voltage on the spectropolarimeter, a value that increases as the wavelength being scanned decreases into the far ultra-violet range<sup>138</sup>. When the high tension voltage rapidly increases and the photo-multiplier tube reaches a saturation voltage, artifacts may be perceived in the sample<sup>139</sup>. These observations may impact the conclusion drawn from CD experiments, because the 180-200 nm spectral range shows differences between the examined samples. This may affect the secondary structure of Pin1, although the protein stability between samples remained the same. The hypothesis of two phosphorylated

binding sites increasing the binding affinity of Pin1 towards CDC25C-derived peptides remains plausible because the 2xP peptide does not decrease protein stability.

#### *4.4 Pin1 has a higher affinity for phosphorylated peptides*

The phosphorylation of Ser/Thr-Pro motifs impairs catalytic isomerization by cyclophilins and FKBP. In contrast, Tyr-Pro sequences are susceptible to this isomerization<sup>8</sup>. The novel parvulin-family PPIase Pin1 preferentially isomerizes Pro residues preceded by phosphorylated Ser or Thr with up to a 300-fold increase in  $k_{\text{cat}}/K_m$ , compared to its non-phosphorylated counterpart. Pin1 is therefore both a sequence-specific and phosphorylation-dependent enzyme<sup>8</sup>. For this reason, parvulins and Pin1 in particular, with specificity towards phosphorylated substrates, play important roles in cellular processes including the regulation of mitosis<sup>8</sup>. The results obtained by NMR using the doubly-phosphorylated CDC25C-derived peptide showed visible chemical shift changes indicative of peptide binding to Pin1. Residue Arg14 exhibited the largest peak shift when the 2xP peptide was bound. The amino acids Lys13, Met15 and Ser16 that surround the Arg also exhibited large peak shift changes (**Figure 9**). This is representative of the WW domain binding to the peptide with high affinity, consistent with a previous study where the WW domain was shown to have approximately a ten-fold stronger affinity for a substrate than the PPIase domain<sup>88</sup>.

Intensity changes are caused by slow or intermediate chemical exchange<sup>115</sup> when a substrate is added to Pin1. Peak intensity changes were displayed in each region of the protein with the addition of 2xP. This finding may relate to the binding of both phosphorylated motifs in the peptide, one to each of the Pin1 domains, as peak intensity reflects the speed at which molecules tumble in solution<sup>116</sup>. The central peptide residues

between the two binding motifs likely interact non-specifically with the protein linker. Through the use of both chemical shift and peak intensity data, local changes in Pin1 that occur on different time scales can be resolved<sup>115</sup>, as each residue in the protein will behave differently.

Experiments examining the binding of peptides to Pin1 were able to detect interactions, when protein concentrations of up to 800  $\mu$ M were used. Each peptide was labeled with NHS-fluorescein, to display a fluorescein tag on the N-terminus that could be visualized at the appropriate wavelength. This tag is unlikely to interfere with the protein-peptide interaction due to its location on the N-terminus of the peptide, which is seven residues away from the first binding site, and the cyclic nature of the label has little mobility.

Singly-phosphorylated peptides, containing the same CDC25C-derived sequence as the 2xP peptide, were designed to test the binding affinities of full length Pin1. Literature on the topic of Pin1 describes other singly-phosphorylated CDC25C peptides which yield diverse affinities towards the protein. The altering affinities are likely a result of amino acids surrounding the phosphorylated residue<sup>104</sup>. The peptide sequence VPRpTPV (CDC25C-Thr48)<sup>104</sup> has a binding affinity of 80-fold higher than that of the 1xP #1 peptide, also surrounding the Thr48 site. Both peptide-protein affinities are comparable due to being measured by fluorescence polarization. The VPRpTPV peptide is six residues in length, shorter than the 32 residue 1xP #1 peptide. The shorter peptide and one Pin1 protein domain are likely to bind, as the WW domain recognizes up to five amino acids<sup>104</sup> and the PPIase domain binds strongly to five residue peptides<sup>106</sup>. Due to the small size of the VPRpTPV peptide, it can remain inflexible and tightly bound to

Pin1, increasing the polarization of light in a fluorescence polarization experiment. Conversely, the binding of either Pin1 domain to the pThr site on either the 1xP #1 or 1xP #2 peptide may not be able to stabilize the extra 25 unbound peptide residues to polarize light sufficiently. For this reason, the binding affinities for the 1xP-Pin1 interactions would appear to decrease in comparison to the previously reported values by Verdecia *et al.* for the VPRpTPV peptide<sup>104</sup>.

The studies presented here analyzing the binding curves, and therefore binding affinities, of Pin1 towards a common CDC25C-derived peptide with varying amounts of phosphorylation indicated that an increase in the number of phosphorylation sites correlates with a decrease in  $K_d$  values. An increase in peptide phosphorylation from zero to one correlates with an increase in binding affinity, based on a decrease in  $K_d$  values from 2253  $\mu\text{M}$  to approximately 330  $\mu\text{M}$  (averaged from both singly-phosphorylated peptides). This is indicative of phosphorylation-dependent binding between Pin1 and the peptides. A study using mutations of CDC25C residues Thr48 and Thr67 to Val, an amino acid that cannot be phosphorylated, has shown that binding to full length Pin1 is abolished<sup>127</sup>.

Interestingly, the singly-phosphorylated CDC25C-derived peptides used in the present study exhibited different binding affinities based on the location of their phosphorylation site (see **Table 1** for the peptide sequences). With the phosphate moiety located at site #2 on the peptide, the  $K_d$  value was decreased by more than 100  $\mu\text{M}$ , indicative of a higher affinity. This result is likely due to the chemical environment surrounding the phosphate. Two small Gly residues are preceding the pThr, which could enable binding due to a lack of steric clashes, compared to the Arg residue preceding the

site #1 phosphate. The residues that appear after the pThr-Pro motif also differ at site #1 and site #2, as they are a Val and a Lys, respectively. This difference in hydrophobicity as well as charge may impact binding.

There is weak binding of full length Pin1 to the non-phosphorylated CDC25C-derived peptide, depicted by a dissociation constant of 2253  $\mu\text{M}$  measured by fluorescence polarization. This binding may be attributed to the promiscuity of the WW domain of Pin1, as this domain is the main binding domain of the protein and may be responsible for nonspecific interactions<sup>140</sup>.

Residues impacted by the addition of peptides to Pin1 are seen to localize to different regions of the protein based on the number of phosphorylation motifs available (**Figures 9 and 11**). Upon binding of the non-phosphorylated peptide, the linker region of the protein showed several peak intensity changes. This observation is feasible because the linker of Pin1 is flexible<sup>36</sup> and may enable nonspecific binding, while both of the protein domains are phosphorylation specific.

#### *4.5 Two phosphorylation sites further increase Pin1-peptide binding affinities*

Overall, the increase of phosphorylation sites on the CDC25C-derived peptides from zero to one and one to two increases the binding affinity towards Pin1. The dissociation constant measured in the present study for the Pin1-2xP interaction was 85.21  $\mu\text{M}$ , a smaller  $K_d$  value than those determined for the 0xP and 1xP peptides. This incremental increase in binding affinities is similar to the results observed in the literature from other known Pin1-interacting proteins. With the addition of a phosphate moiety to a

singly-phosphorylated sequence, peptides derived from the C-terminus of RNA polymerase II and from Tau exhibit an increased binding affinity<sup>90,104</sup>. An example of increased binding affinities towards doubly-phosphorylated substrates from the literature was shown using Tau-based peptides<sup>49</sup>.

The present study has determined dissociation constants for full length Pin1 with the CDC25C-derived peptides, but it would be beneficial to investigate the binding of each Pin1 domain to the peptides. The WW domain alone would likely bind to the peptides, because of its hydrophobic pocket that coordinates substrate binding<sup>88</sup>. It is difficult to conclude whether the PPIase domain alone would bind to the peptides, as there would be approximately 25 residues of free peptide tumbling in solution.

#### 4.6 *Peptide binding to individual Pin1 domains*

The PPIase domain of Pin1 is known for its catalytic function rather than substrate binding efficiency. *In vitro* studies have shown that this domain is usually unable to bind phospho-proteins<sup>88,95</sup>, although substrate specificity is required to bind a sequence for isomerization. Substrates may only have temporary interactions with the PPIase domain, upon bond catalysis. This is a probable option, as the Pin1 active site has been shown to be prepared for catalysis and amino acid exchange processes, even in the absence of a substrate<sup>141</sup>.

In contrast to the PPIase domain, the WW domain binds to peptides derived from substrates with dissociation constants in the low micromolar range, from approximately 1 to 150  $\mu\text{M}$ <sup>88,104,142</sup>. The large ranges of dissociation constants observed for interactions of peptides with full length Pin1 and each of the Pin1 domains suggests that binding



affinities are variable and depend on factors such as peptide length, sequence and phosphorylation states. In some cases, individual protein domains may be incapable of binding to a given peptide. Many Pin1 interacting proteins have been shown to require both the WW and PPIase domains to associate with Pin1 and successively perform their enzymatic or regulatory functions. Proteins that fall into this category include: protein kinases CK2<sup>143</sup> and PLK1<sup>32</sup>, the transcription factor c-Jun<sup>41</sup> and tumour suppressor p53<sup>144</sup>.

#### 4.7 *The WW domain of Pin1 acts as the main binding domain*

Residues Ser16, Arg17, Tyr23 and Trp34 on the surface of Pin1 form the hydrophobic binding pocket observed to enable the characteristic binding properties of the WW domain<sup>88</sup>. Through NMR experimentation using the changes in peak chemical shifts by <sup>1</sup>H-<sup>15</sup>N HSQC, the present study demonstrates that the doubly-phosphorylated peptide binding to Pin1 affects the WW domain only. However, the PPIase domain may exhibit much weaker affinities for the peptides which could be overlooked as the changes in peak chemical shifts are not the sole method to determine interactions by NMR. Studies from the literature have pointed out that the WW domain shows binding affinities of approximately ten-fold stronger than those of the PPIase domain, *in vitro*<sup>88,90</sup>. For this reason, the WW domain is thought to augment substrate specificity and function as the protein-targeting domain.

It is likely that binding of the second phosphorylation site in the CDC25C-derived peptide 2xP is too weak to detect through NMR, based on the protein and peptide concentrations used in the present work. Once the peak intensity changes from the NMR data have been taken into account, both domains display changes likely attributed to a

single phosphorylation site located in each of the two protein domains. Taken together, both the chemical shift changes and peak intensity data display the overall effects of Pin1-peptide binding.

#### 4.8 $K_d$ values compared to literature values

Dissociation constants for full length Pin1 binding to a variety of substrate peptides were measured previously, using fluorescence polarization, and the values ranged from 5 to approximately 80  $\mu\text{M}$ . These peptides were presented by Verdecia *et al.*, derived from known Pin1 interacting proteins of physiological relevance, were between six and eight amino acids in length and contained from zero to two phosphorylation sites<sup>104</sup>. One specific example was the examination of the binding affinity between Pin1 and an RNA polymerase II, C-terminal domain peptide, when the peptide contained two distinct phosphorylation sites separated by two amino acids (**Table 3**). The small separation between phospho-sites and the short total peptide length seem to impact binding, considering the  $K_d$  measured for this interaction was 10  $\mu\text{M}$ <sup>104</sup>. Of note are the examined pSer residues, as pSer-Pro motifs bind to Pin1 with lower affinity than pThr-Pro motifs<sup>145</sup>. However, the isomerase activity of Pin1 for pSer-Pro motifs is higher<sup>8</sup>. This may be a result of the conformations adopted by each of the phosphorylated residues<sup>146</sup>.

Another study looked at a 40 residue peptide, derived from the Pin1-interacting protein Tau, which contained three phosphorylation sites (**Table 3**). When tested for binding to Pin1, a dissociation constant of 70  $\mu\text{M}$  was measured for this interaction<sup>90</sup>. Two of the phosphorylated residues in this peptide sequence were spaced apart by 16

amino acids, suggesting that phosphorylated motifs are separated for a reason, potentially to improve substrate binding to Pin1.

An additional study looking into the binding of bivalent peptides to Pin1 was conducted in 2007, by Daum *et al.* These peptides were generated to target the Pin1 domains specifically (**Table 3**) and would only bind in a single orientation<sup>147</sup>. Using isothermal titration calorimetry, the dissociation constants determined for these peptides were all between 400 and 800 nM. These peptides contained a single Pin1 binding motif and a Pro-rich linker, with the latter not found in natural Pin1-binding proteins<sup>147</sup>. The optimally-designed peptides were generated for the purpose of specific domain binding. It is understandable why these peptides would bind to Pin1 with a higher affinity than other peptides, including those used in the present work.

In comparison to the aforementioned data by Daum *et al.* and Verdecia *et al.*, the  $K_d$  values obtained from the CDC25C-derived peptides in the present study were: 2253  $\mu\text{M}$  for the non-phosphorylated peptide, 391.6  $\mu\text{M}$  for 1xP #1, 272.8  $\mu\text{M}$  for 1xP #2 and 85.21  $\mu\text{M}$  for the doubly-phosphorylated peptide. These binding affinities are all lower than those observed in the literature, potentially due to the length of the peptide sequences. **Table 3** shows a peptide from each study, for direct comparison, and highlights the features of each. All the peptides, excluding the synthetic peptide, were derived from physiologically relevant Pin1-interacting proteins and contain multiple Pin1 binding motifs. The binding affinities measured for the three protein-derived peptides are all of the same order of magnitude. The CDC25C-derived peptide spans both Pin1 domains, similarly to the Tau peptide.

**Table 3 Peptides used in the literature compared to the 2xP peptide used in the present study.**

The peptide sequences are listed, with the phosphorylated residues in bold and red. The binding constant ( $K_d$ ) value for each of the full length Pin1-peptide interactions is also shown.

| <u>Peptide sequence</u>  | <u>Number of Residues in Peptide</u> | <u>Peptide Source</u>     | <u><math>K_d</math> (<math>\mu</math>M)</u> | <u>Citation</u>                  |
|--|--------------------------------------|---------------------------|---|----------------------------------|
| YpSPT <b>p</b> SPS   | 7                                    | RNA Pol II<br>(CTD-S2/S5) | 10  | Verdecia,<br>2000 <sup>104</sup> |
| GSPGTPGSRSR <b>pTPp</b> SLPTPPTREP<br>KVAVVR <b>pT</b> PPKSPSSAK             | 40                                   | Tau<br>(T212/S214/T231)   | 70  | Smet,<br>2005 <sup>90</sup>      |
| Ac-FE-Pip-Nal-Q(P) <sub>6</sub> A-Bth- <b>pTP</b> -<br>Cha-Q-NH <sub>2</sub> | 17                                   | Synthetic                 | 0.804                                       | Daum,<br>2007 <sup>147</sup>     |
| CPDVPR <b>pT</b> PVGKFLGDSANLSILSGG<br><b>pT</b> PKRSLD                      | 32                                   | CDC25C<br>(T48/T67)       | 85  | Present<br>study                 |

#### 4.9 *The distance between phosphorylated residues impacts binding*

Studies observing the effects of phosphorylated peptide binding to Pin1 have been described in the literature, containing shorter sequences as well as different spacing between phosphorylation sites<sup>49,90,104</sup>. The distance between the phosphorylation sites in a peptide seems to impact binding and substrate affinities towards Pin1. The peptides used in this study have a 19 amino acid separation between phosphorylation sites.

A protein containing 19 residues between Pin1 interaction sites, similarly to CDC25C, is the Tau protein involved in microtubule stabilization in neurons<sup>49</sup>. Tau and its interactions with Pin1 have been well studied in the literature for their involvement in Alzheimer's disease<sup>49,56,90,127</sup>. Residues Thr212 and Thr231 are both followed by a Pro residue and can be phosphorylated to be targeted by Pin1. As Tau-derived peptides have already been studied<sup>56</sup>, a logical next step would be to confirm the results *in vitro* using full length proteins and subsequently *in vivo*. It would be interesting to see whether the requirements for Tau binding to Pin1 are similar to those of CDC25C.

In 2007, Daum *et al.* used a bivalent peptide to study Pin1-substrate interactions. This peptide was shown to have up to a 350-fold increase in affinity towards Pin1, compared to a monovalent peptide<sup>147</sup>. Another key finding from this paper was the determination of an optimal linker length. Five Pro residues between the two Pin1 domains presented the highest affinity. Changing the linker length between the two binding motifs of a doubly-phosphorylated peptide, to obtain an increased affinity, could be elaborated as future work of the present study. In contrast to the present study, the peptides generated by Daum *et al.* only contained a single phosphorylation site. The use

of a doubly-phosphorylated human CDC25C-derived peptide is therefore unique and has given insight into a different form of bivalency.

Enhanced binding to Pin1 has been proposed as a result of cooperativity between phosphorylation sites, commonly spaced between 18 and 22 amino acids apart from one another in a sequence<sup>148</sup>. The peptides used in the present study have a spacing of 19 residues between binding motifs, which ideally promotes cooperative binding. In short, it seems improved Pin1 binding is determined by the number and positioning of phosphorylated residues.

#### *4.10 Pin1 binding to phosphate moieties*

Phosphate buffers were used in certain present study experiments in order to directly compare the results to previous studies<sup>79</sup>. The buffers used for NMR experiments were the same as those used in the Duncan *et al.*, 2011 paper, as the protein amide HSQC peaks had been previously assigned<sup>122</sup>. The phosphate concentration in the buffer was diluted for CD experiments to avoid background noise from excess phosphate, while the CD experiments were conducted to ensure the Pin1 protein was folded for the NMR experiments. As Pin1 is phosphorylation-dependent, the phosphate molecules in the buffer could have affected binding to the peptides. The peptide titration results do show Pin1-peptide interactions with affinities in the micromolar range, which indicates that binding still occurs in the presence of excess phosphate. This is likely due to the absence of the proper Pin1 binding motif in the buffer. With this in mind, the fluorescence polarization experiments were conducted in a HEPES buffer to avoid the potential for excess phosphate binding to Pin1 and misrepresentations in the data.

### 4.11 *Effects of molecular crowding on Pin1 binding*

A recent study conducted by Luh *et al.* discussed the effects of molecular crowding on substrate binding by the WW domain of Pin1. The study examined Pin1 in *Xenopus laevis* oocytes and in oocyte extracts crowded with proteins, through in-cell NMR experiments. The substrate recognition motif on the surface of the N-terminal Pin1 domain is able to form weak, nonspecific interactions with endogenous cellular proteins<sup>140</sup>. The researchers used a Pin1 intracellular concentration of 150  $\mu\text{M}$ , which is higher than that of specific Pin1 substrates. NMR signal loss, resulting from a longer rotational correlation time, was seen when only the WW domain was inserted into the oocytes. This observation implicates the WW domain in non-specific interactions that push Pin1 into large *in vivo* complexes. The NMR line broadening results obtained were therefore concluded to be due to nonspecific interactions<sup>140</sup>. Additional proteins added into the oocyte samples, to act as crowding agents, revealed further weak and nonspecific interactions with Pin1, implicating permanent interplay between endogenous proteins<sup>140</sup>. Consequently, it is crucial to explore Pin1 binding to CDC25C and CDC25C-derived peptides *in vivo* as a method to understand the binding affinities when competing molecules are available.

### 4.12 *Pin1 binding model*

The interactions observed in the present study between the doubly-phosphorylated peptide and Pin1 require both protein domains to bind two separate motifs. This was suggested by NMR studies that revealed peak intensity changes in both Pin1 domains upon 2xP peptide titrations (**Figure 10**). Neither the catalysis-first binding model nor the multimeric binding model seem to fit this data (**Figure 3A-B**), because there is no

indication of the PPIase domain binding to the peptide first and these experiments were performed using purified components without excess cellular proteins with which to form complexes. The sequential binding model (**Figure 3C**), which accounts for differential binding affinities between both Pin1 domains, is plausible for Pin1 interactions with the singly-phosphorylated peptides, due to a single available site for binding by the WW domain and then once released, isomerization can occur at the same site. This same method also accounts for Pin1 substrates with multiple binding motifs, where the WW domain binds to a target sequence first and the PPIase domain is free to catalyze the isomerization of other sites in the same molecule<sup>19</sup>. However, the Pin1 domains individually were shown to be incapable of binding full length CDC25C<sup>95</sup>. This provides evidence against the sequential binding model, as CDC25C would need to be initially targeted by the Pin1 WW domain alone. The results of the present study promote the simultaneous model (**Figure 3D**) for binding of Pin1 to CDC25C-derived peptides, as was previously suggested by Innes *et al.* This model states that the binding of each pSer/Thr-Pro motif may be weak individually, but the binding of both sites at the same time can increase the overall affinity<sup>95</sup>.

In comparison with the CDC25C-derived peptides, the Tau peptides may interact with Pin1 using a different binding model. It would be of interest to compare the binding models of the peptides through binding studies using the individual Pin1 domains. To further advance the aforementioned study, one could characterize the binding of Pin1 to other known substrates. Determining the differences between protein substrate sequences and their corresponding protein domain interactions could give insights into Pin1-ligand binding modes, as this was described in previous work to affect binding<sup>36</sup>.



### *4.13 Future directions for the present work*

Testing the binding of the CDC25C-derived peptides with each individual Pin1 domain would be a logical next step to understand how Pin1 interacts with a substrate. This can be accomplished by applying the same FP experiments as discussed in section 2.8, using the WW and PPIase domains individually instead of wild type full length Pin1. Studies from the literature have presented the idea of Pin1 domain-specific peptide binding where both domains can bind a peptide but exhibit differing affinities<sup>104</sup>. Several peptides had no detectable binding to the PPIase domain, while the peptides that did bind to this domain had dissociation constant values ranging from approximately 85 to greater than 500  $\mu\text{M}$ <sup>104</sup>. Some X-ray crystallographic data has also presented structures with peptides bound to the PPIase protein domain of Pin1<sup>45,107</sup>.

Not only could the individual domains of Pin1 be tested for binding to the peptides, but domains containing mutations that render them binding-deficient could also be examined. A Tyr23Ala mutation affects the hydrophobic patch on the WW domain that impacts binding<sup>88</sup>, while mutations Arg68/69Ala affect the basic cluster of the PPIase domain, also shown to impact binding<sup>23</sup>. These mutations could be generated on a full length Pin1 construct to test binding of the CDC25C peptide set used in the present study. It is reasonable to hypothesize that the domain mutants would each bind to a singly-phosphorylated peptide with a similar affinity to that exhibited by wild type protein, because only one domain of the wild type would be involved in the interaction. The doubly-phosphorylated peptide would expectantly bind to the mutant protein at a single site, leaving a large portion of the peptide mobile in solution. Through fluorescence polarization, the polarization of light could remain minimal and this may

affect assay results. With two functional domains, the protein will have a better chance of binding the 2xP peptide and increasing its binding affinity.

Another future study should look into a preferential sequence of substrate residues to increase binding to Pin1. In 1997, Yaffe *et al.* discovered that peptides with an Arg residue at the Pro + 1 position were more efficient, as their  $k_{\text{cat}} / K_m$  values increased up to 1300 times those of their non-phosphorylated equivalents<sup>8</sup>. A thorough analysis of amino acid residues located between the Pin1 binding motifs should therefore be performed, using a peptide walking series, to determine optimal residues at each position.

Binding affinities could also be determined using isothermal titration calorimetry (ITC). This technique was explored in the early stages of the present study, but the protein and peptide concentrations used did not generate a saturated binding curve. ITC requires high protein and ligand concentrations as well as a large volume of sample in the syringe if binding is in the high micromolar range. For the aforementioned reasons, this technique was not a feasible option.

As previously mentioned, one interesting future direction for the present work would be to generate peptides of different linker lengths between the two binding sites. Although, in a few known Pin1 substrates the distance between the two phosphorylated motifs is 19 amino acids, the linear peptide may not have the ability to generate any structural folds to aid in binding. Using a Pro linker was seen to optimize bivalent peptide binding, as proline residues are known to impact structure<sup>147</sup>. Varying the linker length of peptides may be useful to increase the protein-peptide binding affinity<sup>147</sup>.

Using shorter peptides to study Pin1 interactions may be useful, because a short peptide length could decrease flexibility upon Pin1 binding and could provide a different affinity for the binding outcome. The total peptide length and the length of the peptide sequence between Pin1 binding motifs are both important factors when generating peptides that bind optimally to the protein. Peptides of varying sizes could be generated and tested for binding to Pin1.

CDC25C is one of many Pin1-interacting proteins that contain multiple Pin1 binding motifs. Finally, it would be valuable to take a subset of such proteins and examine their sequences between binding sites, lengths and potential modes of binding. These key features will be useful in the generation of optimal Pin1-binding peptides that could act as specific protein inhibitors.

#### *4.14 Summary*

The present study aimed to determine any changes within the protein Pin1 when interacting with peptides derived from the phosphatase CDC25C, as well as the binding affinities associated with each Pin1-peptide complex. Pin1 did not exhibit global conformational changes when bound to any of the CDC25C-derived peptides, nor did the stability of the protein alter upon binding of the non-phosphorylated or doubly-phosphorylated peptides. An increased affinity was observed, by two separate biochemical techniques, when the peptides contained a phosphorylation site. This result is consistent with findings from the literature stating that Pin1 is phosphorylation-dependent<sup>8,149,150</sup>. To further this conclusion, Pin1 was seen to bind to a doubly-phosphorylated substrate with a higher affinity than either of the 1xP peptides. The binding of the 2xP peptide was presented as bound to the WW domain predominantly,

through NMR peak chemical shifts changes, yet peak intensity data implicated the WW domain, linker region and PPIase domain of Pin1 in binding. It is therefore likely that the doubly-phosphorylated peptide bound simultaneously to the two Pin1 domains, as the binding affinity was increased with two pThr-Pro motifs on a single peptide.

Multiple binding models for Pin1 interactions with substrates have been previously proposed<sup>94,95</sup>. This work has promoted the simultaneous model for Pin1 binding with CDC25C-derived peptides, although other models may still apply. Considering the dual-domain binding nature of Pin1, it is reasonable to assume that substrate proteins comprised of varying numbers of binding sites would bind to Pin1 differently, potentially through diverse binding models. The use of binding models could lead to an additional mode of classification for known Pin1-interacting proteins.

## References

1. Karve TM, Cheema AK. Small changes huge impact: the role of protein posttranslational modifications in cellular homeostasis and disease. *J Amino Acids*. 2011;2011:207691.
2. Schmid FX, Baldwin RL. Acid catalysis of the formation of the slow-folding species of RNase A: evidence that the reaction is proline isomerization. *Proc Natl Acad Sci U S A*. 1978;75(10):4764-4768.
3. Odefey C, Mayr LM, Schmid FX. Non-prolyl cis-trans peptide bond isomerization as a rate-determining step in protein unfolding and refolding. *J Mol Biol*. 1995;245(1):69-78.
4. Weiss MS, Jabs A, Hilgenfeld R. Peptide bonds revisited. *Nat Struct Biol*. 1998;5(8):676.
5. Tchaicheeyan O. Is peptide bond cis/trans isomerization a key stage in the chemo-mechanical cycle of motor proteins? *FASEB J*. 2004;18(7):783-789.
6. Schmid FX. Prolyl isomerases. *Adv Protein Chem*. 2001;59:243-282.
7. Schmid FX. Prolyl isomerase: enzymatic catalysis of slow protein-folding reactions. *Annu Rev Biophys Biomol Struct*. 1993;22:123-142.
8. Yaffe MB, Schutkowski M, Shen M, et al. Sequence-specific and phosphorylation-dependent proline isomerization: a potential mitotic regulatory mechanism. *Science*. 1997;278(5345):1957-1960.
9. Latham JA, Dent SY. Cross-regulation of histone modifications. *Nat Struct Mol Biol*. 2007;14(11):1017-1024.
10. Lu KP, Finn G, Lee TH, Nicholson LK. Prolyl cis-trans isomerization as a molecular timer. *Nat Chem Biol*. 2007;3(10):619-629.
11. Zimmerman SS, Scheraga HA. Stability of cis, trans, and nonplanar peptide groups. *Macromolecules*. 1976;9(3):408-416.
12. Brandts JF, Halvorson HR, Brennan M. Consideration of the Possibility that the slow step in protein denaturation reactions is due to cis-trans isomerism of proline residues. *Biochemistry*. 1975;14(22):4953-4963.
13. Stewart DE, Sarkar A, Wampler JE. Occurrence and role of cis peptide bonds in protein structures. *J Mol Biol*. 1990;214(1):253-260.

14. Fischer G, Wittmann-Liebold B, Lang K, Kiefhaber T, Schmid FX. Cyclophilin and peptidyl-prolyl cis-trans isomerase are probably identical proteins. *Nature*. 1989;337(6206):476-478.
15. Van Duyne GD, Standaert RF, Karplus PA, Schreiber SL, Clardy J. Atomic structure of FKBP-FK506, an immunophilin-immunosuppressant complex. *Science*. 1991;252(5007):839-842.
16. Trandinh CC, Pao GM, Saier MH. Structural and evolutionary relationships among the immunophilins: two ubiquitous families of peptidyl-prolyl cis-trans isomerases. *FASEB J*. 1992;6(15):3410-3420.
17. Rahfeld JU, Rücknagel KP, Schelbert B, et al. Confirmation of the existence of a third family among peptidyl-prolyl cis/trans isomerases. Amino acid sequence and recombinant production of parvulin. *FEBS Lett*. 1994;352(2):180-184.
18. Piotukh K, Gu W, Kofler M, Labudde D, Helms V, Freund C. Cyclophilin A binds to linear peptide motifs containing a consensus that is present in many human proteins. *J Biol Chem*. 2005;280(25):23668-23674.
19. Lu KP, Liou YC, Zhou XZ. Pinning down proline-directed phosphorylation signaling. *Trends Cell Biol*. 2002;12(4):164-172.
20. Velazquez HA, Hamelberg D. Conformation-directed catalysis and coupled enzyme-substrate dynamics in Pin1 phosphorylation-dependent cis-trans isomerase. *J Phys Chem B*. 2013;117(39):11509-11517.
21. Lu KP, Hanes SD, Hunter T. A human peptidyl-prolyl isomerase essential for regulation of mitosis. *Nature*. 1996;380(6574):544-547.
22. Hanes SD, Shank PR, Bostian KA. Sequence and mutational analysis of ESS1, a gene essential for growth in *Saccharomyces cerevisiae*. *Yeast*. 1989;5(1):55-72.
23. Shen M, Stukenberg PT, Kirschner MW, Lu KP. The essential mitotic peptidyl-prolyl isomerase Pin1 binds and regulates mitosis-specific phosphoproteins. *Genes Dev*. 1998;12(5):706-720.
24. Stukenberg PT, Kirschner MW. Pin1 acts catalytically to promote a conformational change in Cdc25. *Mol Cell*. 2001;7(5):1071-1083.
25. Mantovani F, Gostissa M, Collavin L, Del Sal G. KeePin' the p53 family in good shape. *Cell Cycle*. 2004;3(7):905-911.
26. Lu KP, Zhou XZ. The prolyl isomerase PIN1: a pivotal new twist in phosphorylation signalling and disease. *Nat Rev Mol Cell Biol*. 2007;8(11):904-916.

27. Shaw PE. Peptidyl-prolyl cis/trans isomerases and transcription: is there a twist in the tail? *EMBO Rep.* 2007;8(1):40-45.
28. Behrens MI, Lendon C, Roe CM. A common biological mechanism in cancer and Alzheimer's disease? *Curr Alzheimer Res.* 2009;6(3):196-204.
29. Xu GG, Etkorn FA. Pin1 as an anticancer drug target. *Drug News Perspect.* 2009;22(7):399-407.
30. Lu Z, Hunter T. Prolyl isomerase Pin1 in cancer. *Cell Res.* 2014;24(9):1033-1049.
31. Butterfield DA, Abdul HM, Opii W, et al. Pin1 in Alzheimer's disease. *J Neurochem.* 2006;98(6):1697-1706.
32. Eckerdt F, Yuan J, Saxena K, et al. Polo-like kinase 1-mediated phosphorylation stabilizes Pin1 by inhibiting its ubiquitination in human cells. *J Biol Chem.* 2005;280(44):36575-36583.
33. Ryo A, Nakamura M, Wulf G, Liou YC, Lu KP. Pin1 regulates turnover and subcellular localization of beta-catenin by inhibiting its interaction with APC. *Nat Cell Biol.* 2001;3(9):793-801.
34. Finn G, Lu KP. Phosphorylation-specific prolyl isomerase Pin1 as a new diagnostic and therapeutic target for cancer. *Curr Cancer Drug Targets.* 2008;8(3):223-229.
35. Zhou XZ, Lu PJ, Wulf G, Lu KP. Phosphorylation-dependent prolyl isomerization: a novel signaling regulatory mechanism. *Cell Mol Life Sci.* 1999;56(9-10):788-806.
36. Jacobs DM, Saxena K, Vogtherr M, Bernado P, Pons M, Fiebig KM. Peptide binding induces large scale changes in inter-domain mobility in human Pin1. *J Biol Chem.* 2003;278(28):26174-26182.
37. Joseph JD, Yeh ES, Swenson KI, Means AR, Winkler. The peptidyl-prolyl isomerase Pin1. *Prog Cell Cycle Res.* 2003;5:477-487.
38. Lee TH, Pastorino L, Lu KP. Peptidyl-prolyl cis-trans isomerase Pin1 in ageing, cancer and Alzheimer disease. *Expert Rev Mol Med.* 2011;13:e21.
39. Theuerkorn M, Fischer G, Schiene-Fischer C. Prolyl cis/trans isomerase signalling pathways in cancer. *Curr Opin Pharmacol.* 2011;11(4):281-287.
40. Alao JP. The regulation of cyclin D1 degradation: roles in cancer development and the potential for therapeutic invention. *Mol Cancer.* 2007;6:24.

41. Wulf GM, Ryo A, Wulf GG, et al. Pin1 is overexpressed in breast cancer and cooperates with Ras signaling in increasing the transcriptional activity of c-Jun towards cyclin D1. *EMBO J*. 2001;20(13):3459-3472.
42. Saegusa M, Hashimura M, Kuwata T. Pin1 acts as a modulator of cell proliferation through alteration in NF- $\kappa$ B but not  $\beta$ -catenin/TCF4 signalling in a subset of endometrial carcinoma cells. *J Pathol*. 2010;222(4):410-420.
43. Ao R, Zhang DR, Du YQ, Wang Y. Expression and significance of Pin1,  $\beta$ -catenin and cyclin D1 in hepatocellular carcinoma. *Mol Med Rep*. 2014;10(4):1893-1898.
44. Ryo A, Liou YC, Wulf G, Nakamura M, Lee SW, Lu KP. PIN1 is an E2F target gene essential for Neu/Ras-induced transformation of mammary epithelial cells. *Mol Cell Biol*. 2002;22(15):5281-5295.
45. Ranganathan R, Lu KP, Hunter T, Noel JP. Structural and functional analysis of the mitotic rotamase Pin1 suggests substrate recognition is phosphorylation dependent. *Cell*. 1997;89(6):875-886.
46. Liao Y, Wei Y, Zhou X, et al. Peptidyl-prolyl cis/trans isomerase Pin1 is critical for the regulation of PKB/Akt stability and activation phosphorylation. *Oncogene*. 2009;28(26):2436-2445.
47. Kang C, Bharatham N, Chia J, Mu Y, Baek K, Yoon HS. The natively disordered loop of Bcl-2 undergoes phosphorylation-dependent conformational change and interacts with Pin1. *PLoS One*. 2012;7(12):e52047.
48. Ryo A, Liou YC, Lu KP, Wulf G. Prolyl isomerase Pin1: a catalyst for oncogenesis and a potential therapeutic target in cancer. *J Cell Sci*. 2003;116(Pt 5):773-783.
49. Smet C, Sambo AV, Wieruszeski JM, et al. The peptidyl prolyl cis/trans-isomerase Pin1 recognizes the phospho-Thr212-Pro213 site on Tau. *Biochemistry*. 2004;43(7):2032-2040.
50. Nakamura K, Kosugi I, Lee DY, et al. Prolyl isomerase Pin1 regulates neuronal differentiation via  $\beta$ -catenin. *Mol Cell Biol*. 2012;32(15):2966-2978.
51. Huang GL, Qiu JH, Li BB, et al. Prolyl isomerase Pin1 regulated signaling pathway revealed by Pin1  $+/+$  and Pin1  $-/-$  mouse embryonic fibroblast cells. *Pathol Oncol Res*. 2013;19(4):667-675.
52. Driver JA, Zhou XZ, Lu KP. Regulation of protein conformation by Pin1 offers novel disease mechanisms and therapeutic approaches in Alzheimer's disease. *Discov Med*. 2014;17(92):93-99.



53. Landrieu I, Smet-Nocca C, Amniai L, et al. Molecular implication of PP2A and Pin1 in the Alzheimer's disease specific hyperphosphorylation of Tau. *PLoS One*. 2011;6(6):e21521.
54. Pastorino L, Sun A, Lu PJ, et al. The prolyl isomerase Pin1 regulates amyloid precursor protein processing and amyloid-beta production. *Nature*. 2006;440(7083):528-534.
55. Akiyama H, Shin RW, Uchida C, Kitamoto T, Uchida T. Pin1 promotes production of Alzheimer's amyloid beta from beta-cleaved amyloid precursor protein. *Biochem Biophys Res Commun*. 2005;336(2):521-529.
56. Lu PJ, Wulf G, Zhou XZ, Davies P, Lu KP. The prolyl isomerase Pin1 restores the function of Alzheimer-associated phosphorylated tau protein. *Nature*. 1999;399(6738):784-788.
57. Girardini JE, Napoli M, Piazza S, et al. A Pin1/mutant p53 axis promotes aggressiveness in breast cancer. *Cancer Cell*. 2011;20(1):79-91.
58. Li H, Wang S, Zhu T, et al. Pin1 contributes to cervical tumorigenesis by regulating cyclin D1 expression. *Oncol Rep*. 2006;16(3):491-496.
59. Kim CJ, Cho YG, Park YG, et al. Pin1 overexpression in colorectal cancer and its correlation with aberrant beta-catenin expression. *World J Gastroenterol*. 2005;11(32):5006-5009.
60. Yang JW, Hien TT, Lim SC, et al. Pin1 induction in the fibrotic liver and its roles in TGF- $\beta$ 1 expression and Smad2/3 phosphorylation. *J Hepatol*. 2014;60(6):1235-1241.
61. Tan X, Zhou F, Wan J, et al. Pin1 expression contributes to lung cancer: Prognosis and carcinogenesis. *Cancer Biol Ther*. 2010;9(2):111-119.
62. Miyashita H, Mori S, Motegi K, Fukumoto M, Uchida T. Pin1 is overexpressed in oral squamous cell carcinoma and its levels correlate with cyclin D1 overexpression. *Oncol Rep*. 2003;10(2):455-461.
63. Wiegand S, Dakic B, Rath AF, et al. The rotamase Pin1 is up-regulated, hypophosphorylated and required for cell cycle progression in head and neck squamous cell carcinomas. *Oral Oncol*. 2009;45(10):e140-149.
64. Ayala G, Wang D, Wulf G, et al. The prolyl isomerase Pin1 is a novel prognostic marker in human prostate cancer. *Cancer Res*. 2003;63(19):6244-6251.
65. Bao L, Kimzey A, Sauter G, Sowadski JM, Lu KP, Wang DG. Prevalent overexpression of prolyl isomerase Pin1 in human cancers. *Am J Pathol*. 2004;164(5):1727-1737.

66. Lam PB, Burga LN, Wu BP, Hofstatter EW, Lu KP, Wulf GM. Prolyl isomerase Pin1 is highly expressed in Her2-positive breast cancer and regulates erbB2 protein stability. *Mol Cancer*. 2008;7:91.
67. Khanal P, Namgoong GM, Kang BS, Woo ER, Choi HS. The prolyl isomerase Pin1 enhances HER-2 expression and cellular transformation via its interaction with mitogen-activated protein kinase/extracellular signal-regulated kinase kinase 1. *Mol Cancer Ther*. 2010;9(3):606-616.
68. Lee RJ, Albanese C, Fu M, et al. Cyclin D1 is required for transformation by activated Neu and is induced through an E2F-dependent signaling pathway. *Mol Cell Biol*. 2000;20(2):672-683.
69. Li C, Chang DL, Yang Z, et al. Pin1 modulates p63 $\alpha$  protein stability in regulation of cell survival, proliferation and tumor formation. *Cell Death Dis*. 2013;4:e943.
70. Krishnan N, Titus MA, Thapar R. The prolyl isomerase pin1 regulates mRNA levels of genes with short half-lives by targeting specific RNA binding proteins. *PLoS One*. 2014;9(1):e85427.
71. Takahashi K, Uchida C, Shin RW, Shimazaki K, Uchida T. Prolyl isomerase, Pin1: new findings of post-translational modifications and physiological substrates in cancer, asthma and Alzheimer's disease. *Cell Mol Life Sci*. 2008;65(3):359-375.
72. Marsolier J, Weitzman JB. [Pin1: a multi-talented peptidyl prolyl cis-trans isomerase and a promising therapeutic target for human cancers]. *Med Sci (Paris)*. 2014;30(8-9):772-778.
73. Rudrabhatla P, Pant HC. Phosphorylation-specific peptidyl-prolyl isomerization of neuronal cytoskeletal proteins by Pin1: implications for therapeutics in neurodegeneration. *J Alzheimers Dis*. 2010;19(2):389-403.
74. Takahashi N, Hayano T, Suzuki M. Peptidyl-prolyl cis-trans isomerase is the cyclosporin A-binding protein cyclophilin. *Nature*. 1989;337(6206):473-475.
75. März AM, Fabian AK, Kozany C, Bracher A, Hausch F. Large FK506-binding proteins shape the pharmacology of rapamycin. *Mol Cell Biol*. 2013;33(7):1357-1367.
76. Wang XJ, Etzkorn FA. Peptidyl-prolyl isomerase inhibitors. *Biopolymers*. 2006;84(2):125-146.
77. Behrsin CD, Bailey ML, Bateman KS, et al. Functionally important residues in the peptidyl-prolyl isomerase Pin1 revealed by unigenic evolution. *J Mol Biol*. 2007;365(4):1143-1162.

78. Guo C, Hou X, Dong L, et al. Structure-based design of novel human Pin1 inhibitors (III): optimizing affinity beyond the phosphate recognition pocket. *Bioorg Med Chem Lett*. 2014;24(17):4187-4191.
79. Duncan KE, Dempsey BR, Killip LE, et al. Discovery and characterization of a nonphosphorylated cyclic peptide inhibitor of the peptidylprolyl isomerase, Pin1. *J Med Chem*. 2011;54(11):3854-3865.
80. Macias MJ, Wiesner S, Sudol M. WW and SH3 domains, two different scaffolds to recognize proline-rich ligands. *FEBS Lett*. 2002;513(1):30-37.
81. Bayer E, Goettsch S, Mueller JW, et al. Structural analysis of the mitotic regulator hPin1 in solution: insights into domain architecture and substrate binding. *J Biol Chem*. 2003;278(28):26183-26193.
82. Lippens G, Landrieu I, Smet C. Molecular mechanisms of the phospho-dependent prolyl cis/trans isomerase Pin1. *FEBS J*. 2007;274(20):5211-5222.
83. Lu KP. Phosphorylation-dependent prolyl isomerization: a novel cell cycle regulatory mechanism. *Prog Cell Cycle Res*. 2000;4:83-96.
84. Landrieu I, Smet C, Wieruszkeski JM, et al. Exploring the molecular function of PIN1 by nuclear magnetic resonance. *Curr Protein Pept Sci*. 2006;7(3):179-194.
85. Fischer G, Tradler T, Zarnt T. The mode of action of peptidyl prolyl cis/trans isomerases in vivo: binding vs. catalysis. *FEBS Lett*. 1998;426(1):17-20.
86. Bailey ML, Shilton BH, Brandl CJ, Litchfield DW. The dual histidine motif in the active site of Pin1 has a structural rather than catalytic role. *Biochemistry*. 2008;47(44):11481-11489.
87. Xu N, Tochio N, Wang J, et al. The C113D mutation in human Pin1 causes allosteric structural changes in the phosphate binding pocket of the PPIase domain through the tug of war in the dual-histidine motif. *Biochemistry*. 2014;53(34):5568-5578.
88. Lu PJ, Zhou XZ, Shen M, Lu KP. Function of WW domains as phosphoserine- or phosphothreonine-binding modules. *Science*. 1999;283(5406):1325-1328.
89. Zarnt T, Lang K, Burtscher H, Fischer G. Time-dependent inhibition of peptidylprolyl cis-trans-isomerases by FK506 is probably due to cis-trans isomerization of the inhibitor's imide bond. *Biochem J*. 1995;305 ( Pt 1):159-164.
90. Smet C, Wieruszkeski JM, Buée L, Landrieu I, Lippens G. Regulation of Pin1 peptidyl-prolyl cis/trans isomerase activity by its WW binding module on a multi-phosphorylated peptide of Tau protein. *FEBS Lett*. 2005;579(19):4159-4164.

91. Landrieu I, De Veylder L, Fruchart JS, et al. The Arabidopsis thaliana PIN1At gene encodes a single-domain phosphorylation-dependent peptidyl prolyl cis/trans isomerase. *J Biol Chem.* 2000;275(14):10577-10581.
92. Fanghänel J, Fischer G. Insights into the catalytic mechanism of peptidyl prolyl cis/trans isomerases. *Front Biosci.* 2004;9:3453-3478.
93. Park ST, Aldape RA, Futer O, DeCenzo MT, Livingston DJ. PPIase catalysis by human FK506-binding protein proceeds through a conformational twist mechanism. *J Biol Chem.* 1992;267(5):3316-3324.
94. Wintjens R, Wieruszeski JM, Drobecq H, et al. 1H NMR study on the binding of Pin1 Trp-Trp domain with phosphothreonine peptides. *J Biol Chem.* 2001;276(27):25150-25156.
95. Innes BT, Bailey ML, Brandl CJ, Shilton BH, Litchfield DW. Non-catalytic participation of the Pin1 peptidyl-prolyl isomerase domain in target binding. *Front Physiol.* 2013;4:18.
96. Lee TH, Chen CH, Suizu F, et al. Death-associated protein kinase 1 phosphorylates Pin1 and inhibits its prolyl isomerase activity and cellular function. *Mol Cell.* 2011;42(2):147-159.
97. Crenshaw DG, Yang J, Means AR, Kornbluth S. The mitotic peptidyl-prolyl isomerase, Pin1, interacts with Cdc25 and Plx1. *EMBO J.* 1998;17(5):1315-1327.
98. Hoffmann I, Clarke PR, Marcote MJ, Karsenti E, Draetta G. Phosphorylation and activation of human cdc25-C by cdc2--cyclin B and its involvement in the self-amplification of MPF at mitosis. *EMBO J.* 1993;12(1):53-63.
99. Nakamura K, Zhou XZ, Lu KP. Distinct functions of cis and trans phosphorylated tau in Alzheimer's disease and their therapeutic implications. *Curr Mol Med.* 2013;13(7):1098-1109.
100. Fukuchi M, Fukai Y, Kimura H, et al. Prolyl isomerase Pin1 expression predicts prognosis in patients with esophageal squamous cell carcinoma and correlates with cyclinD1 expression. *Int J Oncol.* 2006;29(2):329-334.
101. Wang JZ, Zhu WD, Xu ZX, et al. Pin1, endothelial nitric oxide synthase, and amyloid- $\beta$  form a feedback signaling loop involved in the pathogenesis of Alzheimer's disease, hypertension, and cerebral amyloid angiopathy. *Med Hypotheses.* 2014;82(2):145-150.
102. Ryo A, Suizu F, Yoshida Y, et al. Regulation of NF-kappaB signaling by Pin1-dependent prolyl isomerization and ubiquitin-mediated proteolysis of p65/RelA. *Mol Cell.* 2003;12(6):1413-1426.

103. Thanasoula M, Escandell JM, Suwaki N, Tarsounas M. ATM/ATR checkpoint activation downregulates CDC25C to prevent mitotic entry with uncapped telomeres. *EMBO J.* 2012;31(16):3398-3410.
104. Verdecia MA, Bowman ME, Lu KP, Hunter T, Noel JP. Structural basis for phosphoserine-proline recognition by group IV WW domains. *Nat Struct Biol.* 2000;7(8):639-643.
105. Onica D. *Characterizing the domain- and phosphorylation-requirements of the interaction between peptidyl prolyl isomerase pin1 and mitotic phosphatase cdc25c*, University of Western Ontario; 2014.
106. Zhang Y, Füssel S, Reimer U, Schutkowski M, Fischer G. Substrate-based design of reversible Pin1 inhibitors. *Biochemistry.* 2002;41(39):11868-11877.
107. Zhang Y, Daum S, Wildemann D, et al. Structural basis for high-affinity peptide inhibition of human Pin1. *ACS Chem Biol.* 2007;2(5):320-328.
108. Lebowitz J, Lewis MS, Schuck P. Modern analytical ultracentrifugation in protein science: a tutorial review. *Protein Sci.* 2002;11(9):2067-2079.
109. Brown PH, Schuck P. Macromolecular size-and-shape distributions by sedimentation velocity analytical ultracentrifugation. *Biophys J.* 2006;90(12):4651-4661.
110. Beychok S. Circular dichroism of biological macromolecules. *Science.* 1966;154(3754):1288-1299.
111. Greenfield NJ. Using circular dichroism spectra to estimate protein secondary structure. *Nat Protoc.* 2006;1(6):2876-2890.
112. Sreerama N, Venyaminov SY, Woody RW. Estimation of protein secondary structure from circular dichroism spectra: inclusion of denatured proteins with native proteins in the analysis. *Anal Biochem.* 2000;287(2):243-251.
113. Doty F. Magnetism in high-resolution NMR probe design. I: General methods. *Concepts in Magnetic Resonance.* 1998;10(3):133--156.
114. Malz F, Jancke H. Validation of quantitative NMR. *J Pharm Biomed Anal.* 2005;38(5):813-823.
115. Edwards JC. Principles of NMR. 87 A Sand Pit Rd, Danbury CT 06810: Process NMR Associates LLC; 1998.
116. James TL. Fundamentals of NMR. Nuclear Magnetic Resonance. San Francisco, CA: Department of Pharmaceutical Chemistry, University of California; 1998.

117. Wu PS, Ozawa K, Jergic S, Su XC, Dixon NE, Otting G. Amino-acid type identification in <sup>15</sup>N-HSQC spectra by combinatorial selective <sup>15</sup>N-labelling. *J Biomol NMR*. 2006;34(1):13-21.
118. Freude D. Spectroscopy for Physicists: Nuclear Magnetic Resonance. 2006.
119. Halfman CJ, Schneider AS. Direct measurement of fluorescence polarization or anisotropy. *Analytical Chemistry*. 1982;54(12):2009-2011.
120. Tanford C. 'Cohn and Edsall': physical chemistry conclusively supports a protein model. *Biophys Chem*. 2003;100(1-3):81-90.
121. Philo JS. An improved function for fitting sedimentation velocity data for low-molecular-weight solutes. *Biophys J*. 1997;72(1):435-444.
122. Jacobs DM, Saxena K, Grimme S, et al. <sup>1</sup>H, <sup>13</sup>C and <sup>15</sup>N backbone resonance assignment of the peptidyl-prolyl cis-trans isomerase Pin1. *J Biomol NMR*. 2002;23(2):163-164.
123. Leslie AG. The integration of macromolecular diffraction data. *Acta Crystallogr D Biol Crystallogr*. 2006;62(Pt 1):48-57.
124. Evans P. Scaling and assessment of data quality. *Acta Crystallogr D Biol Crystallogr*. 2006;62(Pt 1):72-82.
125. Adams PD, Afonine PV, Bunkóczi G, et al. PHENIX: a comprehensive Python-based system for macromolecular structure solution. *Acta Crystallogr D Biol Crystallogr*. 2010;66(Pt 2):213-221.
126. Innes BT, Sowole MA, Konermann L, Litchfield DW, Brandl CJ, Shilton BH. Oxidation-Mediated Inhibition of the Peptidyl-Prolyl Isomerase Pin1. *J Biol Chem*. 2014;289(12):8121-8131.
127. Zhou XZ, Kops O, Werner A, et al. Pin1-dependent prolyl isomerization regulates dephosphorylation of Cdc25C and tau proteins. *Mol Cell*. 2000;6(4):873-883.
128. Wüthrich K. The way to NMR structures of proteins. *Nat Struct Biol*. 2001;8(11):923-925.
129. Peng CY, Graves PR, Thoma RS, Wu Z, Shaw AS, Piwnicka-Worms H. Mitotic and G2 checkpoint control: regulation of 14-3-3 protein binding by phosphorylation of Cdc25C on serine-216. *Science*. 1997;277(5331):1501-1505.
130. Kristjánisdóttir K, Rudolph J. Cdc25 phosphatases and cancer. *Chem Biol*. 2004;11(8):1043-1051.
131. Boutros R, Lobjois V, Ducommun B. CDC25 phosphatases in cancer cells: key players? Good targets? *Nat Rev Cancer*. 2007;7(7):495-507.

132. Kumagai A, Dunphy WG. Regulation of the cdc25 protein during the cell cycle in *Xenopus* extracts. *Cell*. 1992;70(1):139-151.
133. Hoffmann I, Karsenti E. The role of cdc25 in checkpoints and feedback controls in the eukaryotic cell cycle. *J Cell Sci Suppl*. 1994;18:75-79.
134. Hunt T. Maturation promoting factor, cyclin and the control of M-phase. *Curr Opin Cell Biol*. 1989;1(2):268-274.
135. Dorée M. Control of M-phase by maturation-promoting factor. *Curr Opin Cell Biol*. 1990;2(2):269-273.
136. Bürger C, Wick M, Müller R. Lineage-specific regulation of cell cycle gene expression in differentiating myeloid cells. *J Cell Sci*. 1994;107 ( Pt 7):2047-2054.
137. Franckhauser C, Mamaeva D, Heron-Milhavet L, Fernandez A, Lamb NJ. Distinct pools of cdc25C are phosphorylated on specific TP sites and differentially localized in human mitotic cells. *PLoS One*. 2010;5(7):e11798.
138. DiNitto JM, Kenney JM. Noise characterization in circular dichroism spectroscopy. *Appl Spectrosc*. 2012;66(2):180-187.
139. Kelly SM, Jess TJ, Price NC. How to study proteins by circular dichroism. *Biochimica et Biophysica Acta (BBA) - Proteins and Proteomics*. 2005;1751(2):119-139.
140. Luh LM, Hänsel R, Löhr F, et al. Molecular crowding drives active Pin1 into nonspecific complexes with endogenous proteins prior to substrate recognition. *J Am Chem Soc*. 2013;135(37):13796-13803.
141. Labeikovsky W, Eisenmesser EZ, Bosco DA, Kern D. Structure and dynamics of pin1 during catalysis by NMR. *J Mol Biol*. 2007;367(5):1370-1381.
142. Mercedes-Camacho AY, Etzkorn FA. Enzyme-linked enzyme-binding assay for Pin1 WW domain ligands. *Anal Biochem*. 2010;402(1):77-82.
143. Messenger MM, Saulnier RB, Gilchrist AD, Diamond P, Gorbsky GJ, Litchfield DW. Interactions between protein kinase CK2 and Pin1. Evidence for phosphorylation-dependent interactions. *J Biol Chem*. 2002;277(25):23054-23064.
144. Zheng H, You H, Zhou XZ, et al. The prolyl isomerase Pin1 is a regulator of p53 in genotoxic response. *Nature*. 2002;419(6909):849-853.
145. Zhou W, Yang Q, Low CB, et al. Pin1 catalyzes conformational changes of Thr-187 in p27Kip1 and mediates its stability through a polyubiquitination process. *J Biol Chem*. 2009;284(36):23980-23988.

146. Velazquez HA, Hamelberg D. Conformational selection in the recognition of phosphorylated substrates by the catalytic domain of human Pin1. *Biochemistry*. 2011;50(44):9605-9615.
147. Daum S, Lücke C, Wildemann D, Schiene-Fischer C. On the benefit of bivalency in peptide ligand/pin1 interactions. *J Mol Biol*. 2007;374(1):147-161.
148. Nishi H, Shaytan A, Panchenko AR. Physicochemical mechanisms of protein regulation by phosphorylation. *Front Genet*. 2014;5:270.
149. Rippmann JF, Hobbie S, Daiber C, et al. Phosphorylation-dependent proline isomerization catalyzed by Pin1 is essential for tumor cell survival and entry into mitosis. *Cell Growth Differ*. 2000;11(7):409-416.
150. Wulf G, Finn G, Suizu F, Lu KP. Phosphorylation-specific prolyl isomerization: is there an underlying theme? *Nat Cell Biol*. 2005;7(5):435-441.

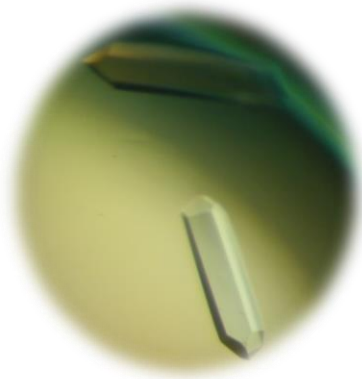


## Appendices

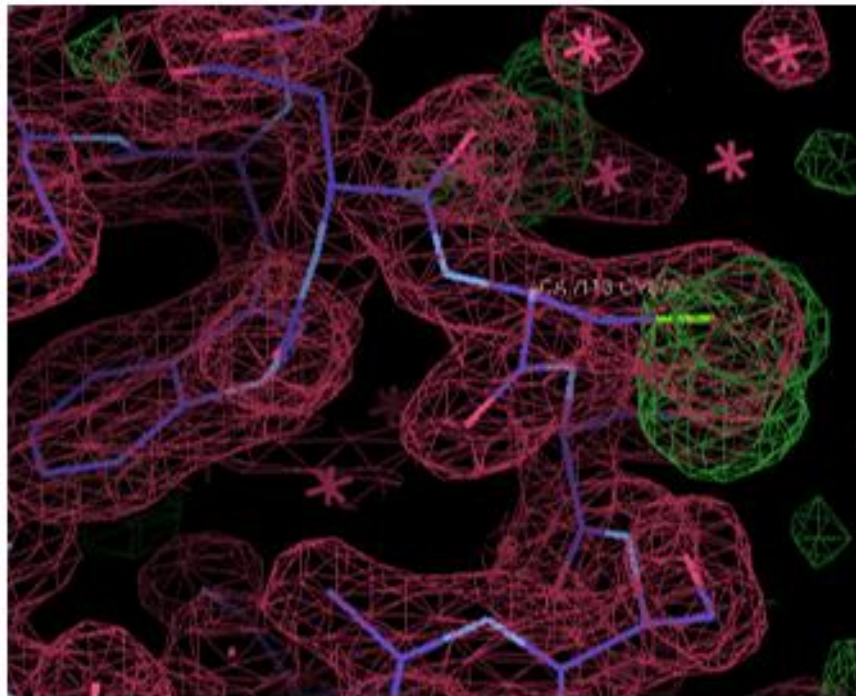
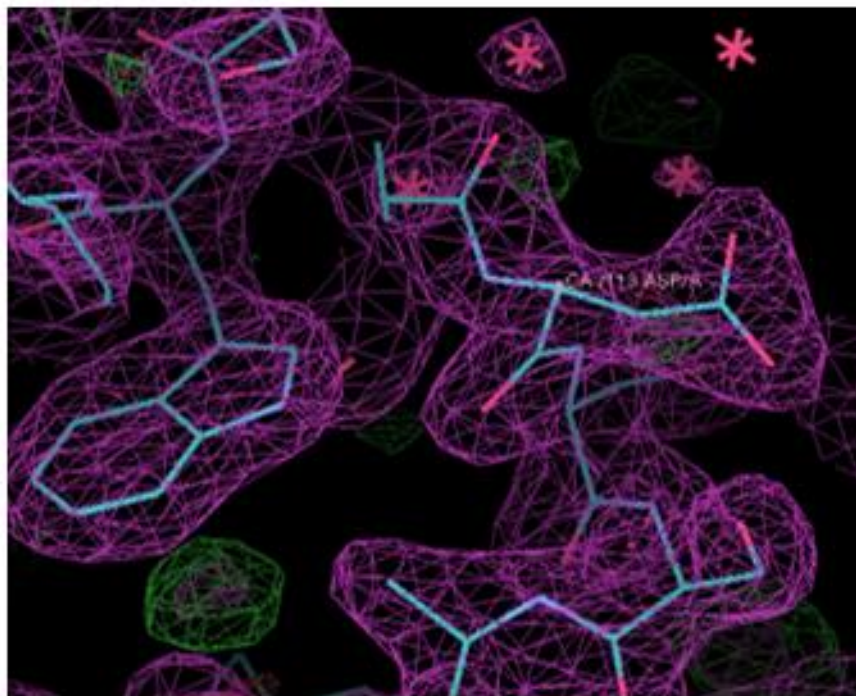
### *Appendix A: Crystal structure of Cys113Asp Pin1 construct shows a residue change in the active site*

Crystals of purified Pin1 protein were generated using the R14A C113D construct (courtesy of Dr. Brian Shilton), which has the six N-terminal residues deleted to decrease protein flexibility as well as the characteristic Arg to Ala mutation at residue 14. Residue Cys113 is located within the active site of the protein and has been reported to impact the catalysis of substrate isomerization<sup>77</sup>. Crystals were made by sitting drop method using 1  $\mu$ l of 18 mg protein mixed with 1  $\mu$ l of the mother liquor precipitant solution from the well below, comprised of 2.4 M ammonium sulphate in 100 mM HEPES buffer pH 7.8 and 1% *polyethylene glycol* 400 (**Figure A2**). R14A construct crystals have been previously described in the literature under similar conditions<sup>45</sup>, but the Cys113Asp mutation has yet to be presented in a high resolution 3D structure. The crystallographic data collection and refinement information is listed in **Table A1**. **Figure A2-A** shows the electron density contour maps of 2Fo-Fc (blue) and Fo-Fc (green and red representing positive and negative densities, respectively) surrounding the Cys113 residue, before changing the residue in the software to an Asp. The two green electron density blobs are associated with the Asp side chain and fit into the contour map once the structure has been refined with Asp113 (**Figure A2-B**).

**Table A1 Pin1 R14A C113D crystallographic data collection and refinement parameters.**



|  |  |                              |         |
|--|--|------------------------------|---------|
| <b>R14A C113D Pin1</b>                   |  | <b>Number of atoms</b>       | 1497    |
|  |  | <b>macromolecules</b>        | 1228    |
| <b>Resolution Range (Å)</b>              | 27.791 - 1.865<br>(1.8901 - 1.8645)        | <b>ligands</b>               | 49      |
| <b>Space group</b>                       | P3 <sub>1</sub> 21                         | <b>water</b>                 | 220     |
| <b>unit cell</b>                         | 68.530 68.530 79.270<br>90.00 90.00 120.00 | <b>Protein residues</b>      | 145     |
| <b>Total reflections</b>                 | 34415                                      | <b>RMS (bonds)</b>           | 0.006   |
| <b>Total reflections (non-anomalous)</b> | 18281                                      | <b>RMS (angles)</b>          | 1.055   |
| <b>Multiplicity</b>                      | 5.8 (5.4)                                  | <b>Ramachandran favored</b>  | 98.58 % |
| <b>Completeness (%)</b>                  | 98.5 (89.9)                                | <b>Ramachandran allowed</b>  | 1.42 %  |
| <b>Mean I / sigma (I)</b>                | 24.3 (8.6)                                 | <b>Ramachandran outliers</b> | 0.00 %  |
| <b>Wilson B-factor</b>                   | 20.412                                     | <b>Clash score</b>           | 5.10 %  |
| <b>R-merge</b>                           | 0.045 (0.179)                              | <b>Average B-factor</b>      | 22.3833 |
| <b>R-meas</b>                            | 0.050                                      | <b>macromolecules</b>        | 20.4619 |
| <b>R-work</b>                            | 0.1829 (0.2674)                            | <b>ligands</b>               | 31.2879 |
| <b>R-free</b>                            | 0.2179 (0.3076)                            | <b>solvent</b>               | 31.6173 |

**A****B**

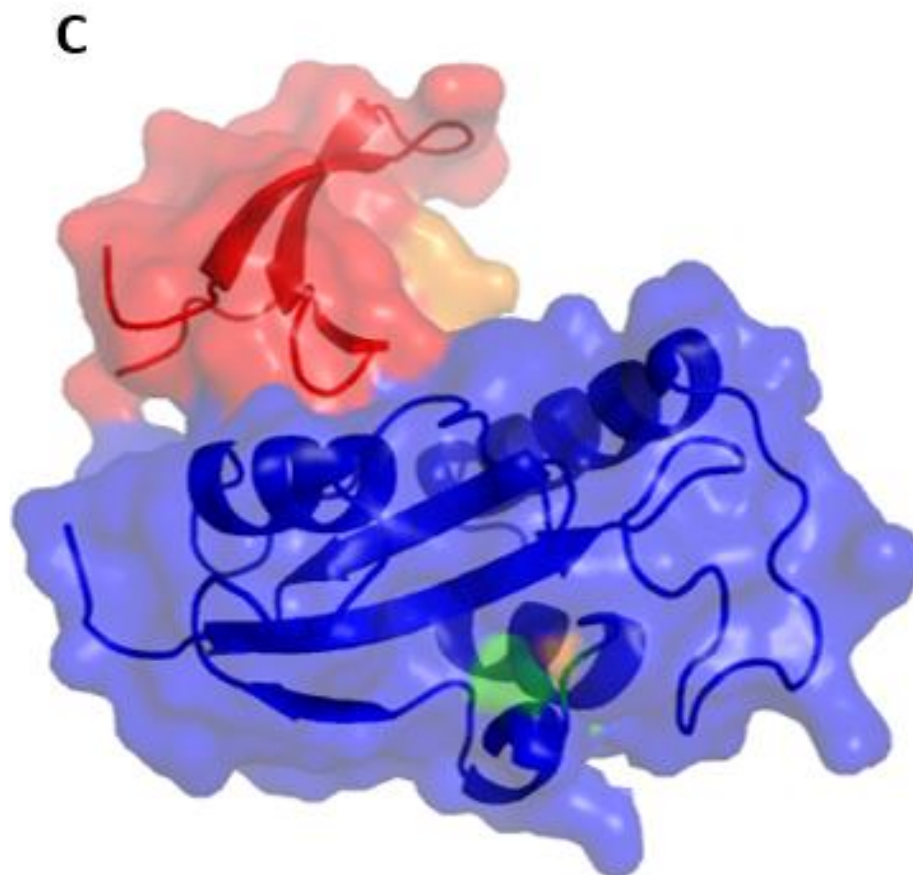


**Figure A2 Pin1 C113D refined crystal structure.**

Zoomed in portion of R14A C113D Pin1 crystal structure showing residue C113 with additional positive electron density (shown in green) (**A**) and D113 with no additional electron density (**B**) at 1.865 Å, illustrating difference maps with a  $2|F_o|-|F_c|$  contour map (blue) at 1.0  $\sigma$  and a  $|F_o|-|F_c|$  contour map (green/red) at 3.0  $\sigma$ . (**C**) Three dimensional structure of R14A Pin1 C113D showing the WW domain (red), the PPIase domain (blue), the sulphate, PEG molecule and glycerol atoms (orange) and the catalytic Cys residue mutated to an Asp (green).

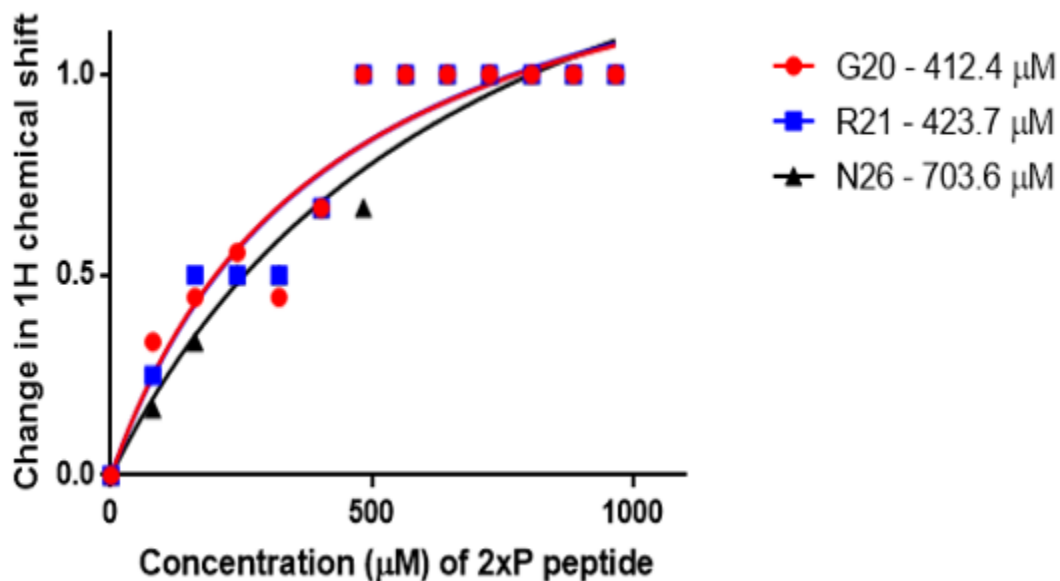


**Figure A3** Plot of select WW domain residues displaying peak chemical shift changes.

Select residues in the WW domain were further analyzed in the hopes of determining a binding constant. Only the  $^1\text{H}$  dimensional chemical shift changes were used for this analysis. The plots show binding curves for the selected residues: Gly20, Arg21 and Asn26, with corresponding  $K_d$  values listed in the legend to the right. WW domain residues were plotted based on their changes in chemical shift as a function of peptide concentration.

# Curriculum Vitae

**Michelle K. Dubinsky**

## **Education**

*The University of Western Ontario; London, Ontario, 2012-2015*

Master of Science candidate in Biochemistry

Poster Presentations:

London Health Research Day, 2014.

Harold Stewart Research Day, The University of Western Ontario, 2013.

*McMaster University; Hamilton, Ontario, 2008-2012*

Honours Bachelor of Science in Biochemistry with a Specialization in Biomedical Sciences

## **Awards and Honours**

Poster Presentation Award at the CIHR – Strategic Training Program in Cancer Research & Technology Transfer (CaRTT) & The Department of Oncology's 10<sup>th</sup> Annual Oncology Research and Education Day, 2013.

## **Research Experience**

*M.Sc. Thesis:* Biochemistry, The University of Western Ontario; London, Ontario, 2012-2015. Supervisor: Dr. David Litchfield.

*Summer Research Student:* Biochemistry, The University of Western Ontario; London, Ontario, 2012. Research Advisor: Dr. Megan Davey.

*Undergraduate Honours Thesis:* Biochemistry, McMaster University; Hamilton, Ontario, 2011-2012. Supervisor: Dr. Alba Guarné.

*Research Student:* Biochemistry, McMaster University; Hamilton, Ontario, 2011. Research Advisor: Dr. Alba Guarné.

## **Related Work Experience**

*Teaching Assistant:* Biochemistry, The University of Western Ontario; London, Ontario, 2012-2014.

## **Publications**

Pillon MC, Dubinsky M, Johnston RN, Liu SL, Guarné A. Characterization of the defects in the ATP lid of E. coli MutL that cause transient hypermutability. *DNA Repair (Amst)*. 2013;12(10):864-9.

Innes BT, Sowole MA, Gyenis L, Dubinsky M, et al. Peroxide-Mediated Oxidation and Inhibition of the Peptidyl-Prolyl Isomerase Pin1. (Accepted).